High functionalization of titanium oxide-based materials and their application

(酸化チタン系材料の高機能化とその応用)

by

Hideya Hattori

Submitted to Hiroshima University

In partial fulfillment of the requirements for the degree of

Philosophy of Doctor

Supervisor：Professor Dr. Tsuneji Sano

Department of Applied Chemistry,

Graduate School of Engineering,

Hiroshima University

September 2018

Referee in Chief : Professor Tsuneji sano

Referees : Professor Takeshi Shiono

Professor Kei Inumaru

Associate Professor Masahiro Sadakane

Department of Applied Chemistry,

Graduate School of Engineering,

Hiroshima University

Chapter 1

Overview

1-1. Titanium oxide as photocatalyst

Titanium oxide is abundant, non-toxic, and stable. It is a semiconductor; thus, it is expected to have various applications in solar power generation, as a photocatalyst, and in sunscreen. Furthermore, since its characteristics as a photocatalyst were first discovered by Honda and Fujishima[1], it has drawn attention for use in energy conversion. In this chapter, I discuss the use of titanium oxide as photocatalyst and as a UV absorber.

1-1-1. What is a photocatalyst?

A photocatalyst is a substance that acts as a catalyst by absorbing light. Like other catalysts, the material itself does not change but promotes chemical reactions. Currently, the most widely studied photocatalytic material is titanium oxide, but, in the 1960's, zinc oxide was also reported to be a photocatalyst. However, since Honda and Fujishima et al. reported the photocatalytic activity of titanium oxide in 1972 (Fig. 1-1) [1], significant research into titanium oxide has been carried out. In addition, they reported that TiO_2 was stable to light irradiation, putting this new material in the limelight. By the end of the 1970's, numerous applications of TiO_2 photocatalysis had been reported. For example, the photodetoxification of HCN [2], ammonia synthesis from N_2 and water [3], the reduction of CO_2 [4], and H_2 production from carbohydrates and water [5].

In the photocatalytic reaction, the photocatalyst absorbs the ultraviolet light in sunlight or that produced by a fluorescent lamp, generating active compounds from oxygen and water. By using these active substances, photocatalysts can decompose odorous substances and inactivate bacteria and viruses. The features of the photocatalyst are (1) semi-permanent functioning because the photocatalyst itself does not change; (2) decomposition of organic substances, as well as larger particles; and (3), as mentioned above for titanium oxide, high safety as a food additive. However, there is a problem: the decomposition is non-selective and any organic matter is decomposed in the presence of the catalyst; thus, if titanium oxide is processed into cloth or paper, the fabric will be damaged. In addition, even when used as an inorganic semiconductor alone, only 3% of the sunlight can be used because the catalyst is only responsive to ultraviolet light (as a result of the band gap). In the following chapter, I discuss research into combating these drawbacks while utilizing or extending the above characteristics.

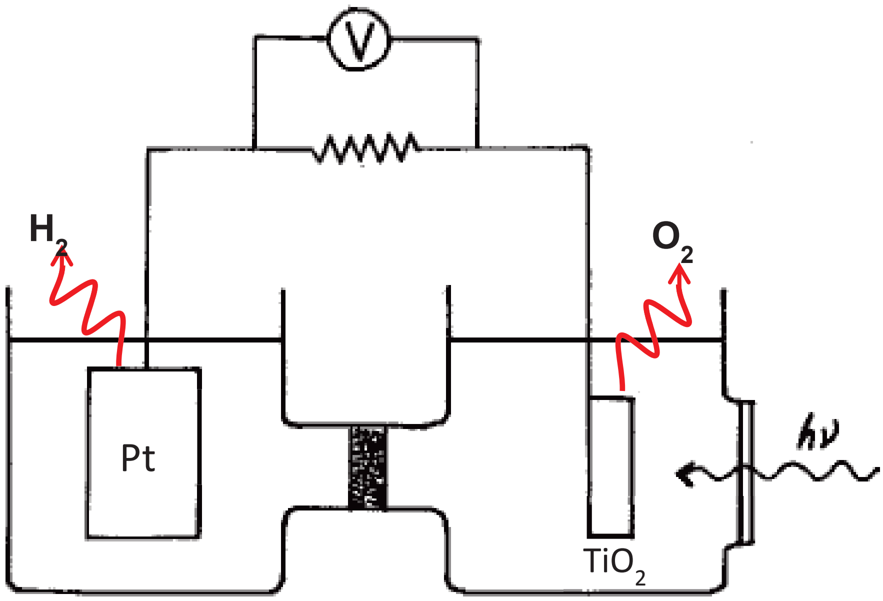

Nature, **1972**, *238*, 37.

Fig. 1-1 The photocatalytic activity of TiO_2 for the decomposition of water.

1-1-2. A brief history of TiO_2 photocatalysts and problems affecting applications

As described above, in 1972, Honda and Fujishima reported water decomposition in an electrolytic system consisting of water, a platinum electrode, and a titanium oxide electrode. The reaction proceeded on the irradiation of the titanium oxide electrode with ultraviolet light in the presence of a slight electric field [1]. After this discovery, it was found that water decomposition proceeds under ultraviolet light irradiation with platinum-nanoparticle-supported titanium oxide in the absence of an electric field. Since these discoveries, the conversion of light energy to chemical energy by semiconductor photocatalysts has been recognized.

Titanium oxide is thus expected to be an inorganic semiconductor based on the above properties. It has been extensively studied as a photocatalyst for the complete oxidation of compounds, as discussed below. However, recently, the production of clean and inexpensive fuels and simple chemicals using solar energy has drawn attention as an economical and environmentally friendly synthetic method, and the application of titanium oxide to this field is also expected. However, although titanium oxide has the usefulness mentioned above, there are some problems that must be solved before it can be used for these applications. For example, when titanium oxide is applied as a photocatalyst for the synthesis of simple chemicals, it lacks oxidative selectivity. In reactions in an organic solvent, the desired partially oxidized product is nonselectively sequentially and completely oxidized by the photoexcited radical species. In aqueous reactions, OH radicals, which are strong oxidizing agents, are generated, and the oxidation selectivity further decreases. Therefore, in the case of using titanium oxide, the desired partial oxidation product is easily sequentially and completely oxidized in both reaction systems, and the product yield and selectivity are low. Thus, the development of novel catalysts for improving the yield and selectivity of partial oxides has been heavily investigated.

On the other hand, studies of photocatalysts for the decomposition and removal of harmful organic compounds have been actively conducted since the 1980's. Many degradation mechanisms using titanium oxide have also been reported in studies of water quality and organic soil pollutants, and basic research into titanium oxide has advanced worldwide [6]. The decomposition or removal of harmful organic compounds by a photocatalyst is effective for green chemistry because titanium oxide show catalytic activity on irradiation with the ultraviolet (UV) light in sunlight, as well as from artificial light sources. Another advantage is that no toxic by-products are formed during the decomposition process. However, titanium oxide only responds to UV light, which represents a mere 3% of the light in sunlight. Therefore, its activity is poor and only low concentrations of contaminants can be removed in the presence of weak indoor visible light and under sunlight. Similarly, even for atmospheric purification, because titanium oxide responds only to UV light, volatile organic compounds such as formaldehyde and toluene can only be removed at low concentrations. Therefore, it is important to improve the UV photoactivity and to impart visible-light-responsiveness to enable the decomposition of organic pollutants in high concentrations. In the following chapters, I introduce representative remedial methods.

1-1-3. Improvement of photocatalytic activity: (1) Visible light responsiveness

For the decomposition/removal of harmful organic compounds, titanium oxide can be doped with heteroatoms or loaded with precious metals; these methods improve the UV photoactivity and impart visible light responsiveness. The amount of solar energy that falls on the earth is enormous, but most is unusable. When titanium oxide absorbs light of energy coincident with the band gap, electron excitation occurs, and electrons move from the valence band to the conduction band. Then, holes and electrons are formed, inducing various photocatalytic reactions. Therefore, the band gap is the factor that controls reactivity. The band gap can be reduced by doping titanium oxide with heteroatoms. Initially, doping with transition metals was reported. However, in this method, the absorption in the visible light region is dependent on the impurity level of the doping element generated in the band gap, so that the recombination of photogenerated electrons and holes tends to occur and the catalytic activity is low. In 2001, the substitution of nitrogen and sulfur for oxygen (anionic site) in titanium oxide was found to reduce the band gap and allow visible-light-induced photocatalytic reactions [7]. Research into visible light operation type photocatalyst has since increased. However, even with nitrogen doping, although the absorption capacity in the visible light region improves, the absorption intensity is significantly lower than that for ultraviolet light. On the other hand, sulfur-doped titanium oxide, in which sulfur is exchanged with titanium as a cation instead of an anion, has a relatively high absorption intensity for visible light. Furthermore, in the decomposition of methylene blue, the photocatalytic activity is higher under visible light or ultraviolet light irradiation than that of pure titanium oxide. Sulfur-doped titanium oxide showed about 65% of ultraviolet light activity, even under visible light irradiation [8].

In addition to the application of visible light responsiveness, studies have been actively carried out using precious metals. Among the noble metal nanoparticles, in particular, gold nanoparticles can be strongly fixed on the surface of the titanium oxide. When gold nanoparticles are supported on titanium oxide, gold captures the electrons photoexcited in titanium oxide by ultraviolet light irradiation within femtoseconds and prevents recombination with the holes; as a result, the separation of photoexcited holes and electrons on titanium oxide occurs efficiently. Another advantage of gold nanoparticles for the development of visible-light-responsive photocatalysts is that gold nanoparticles themselves are visible-light-responsive photocatalysts (Fig. 1-2) [9]. The strong absorption of visible light by the collective excitation of the surface of gold nanoparticles has been reported. Silva et al. reported that water decomposition by gold nanoparticle-supported titanium oxide is activated by irradiation with visible light (monochromatic 532-nm light) [10]. In this reaction, gold nanoparticles absorb visible light by surface plasmon resonance and electrons are injected into the conduction band of titanium oxide; thus, holes are formed in the gold nanoparticles and electrons are formed in the conduction band of the semiconductor, and these act as active sites. In addition, radical species, such as superoxide anions, are generated by the reaction of photogenerated electrons with O_2 and hydroxyl radicals are generated by the reaction of photogenerated holes with OH^-. These highly oxidizing compounds are the active species in the photocatalytic reaction. Based on the above mechanism, photocatalytic activity is imparted under visible light irradiation. On the other hand, it is known that gold-nanoparticle-supported titanium oxide exhibits high activity as a photocatalyst for the synthesis of simple molecules [11, 12].

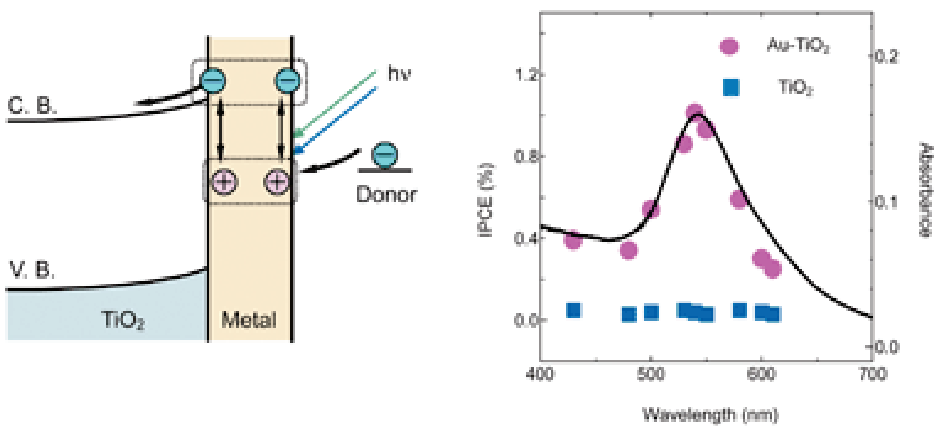

Chem. Commun., **2004**, 1810

Fig. 1-2 Mechanism of visible light absorbing and visible light activity of TiO_2 and Au-TiO_2.

1-1-4. Improvement of photocatalytic activity: (2) Structural design

By using a porous material as a support, it is also possible to incorporate the unique properties of the porous material, such as adsorption concentration effects, into the photocatalytic process. Among the porous materials, novel photocatalysts consisting of ultrafine titanium oxide fixed in the pores of a zeolite or mesoporous silica, or titanium oxide species with highly coordinated tetra-coordinated structure of molecular size incorporated in a framework have been reported to be useful. A nanostructured titanium oxide photocatalyst is also a useful technique for functional design. For example, Shiraishi et al. reported the selective oxidation of benzene to phenol using mesoporous titanium oxide (Fig. 1-3) [13]. It was concluded that benzene (the substrate) is adsorbed on the catalyst and the sequential and complete oxidation of the product (phenol) is suppressed by preventing its adsorption, thus promoting selective oxidation. Likewise, structural design using layered titanates has also been reported. Layered titanates take in substances between layers by intercalation, and these materials have a specific structure and function depending on the type and number of functional units between the taken-in layers; therefore, selective organic synthesis is also possible. Normally, layered titanate responds only to ultraviolet light, but it can also be applied as a photocatalyst with visible light activity by incorporating a substance having visible light absorption. For example, Choy et al. reported the efficient decomposition of organic compounds on a cluster of chromium oxide having visible light absorption between layers of layered titanate in water under visible light irradiation [14].

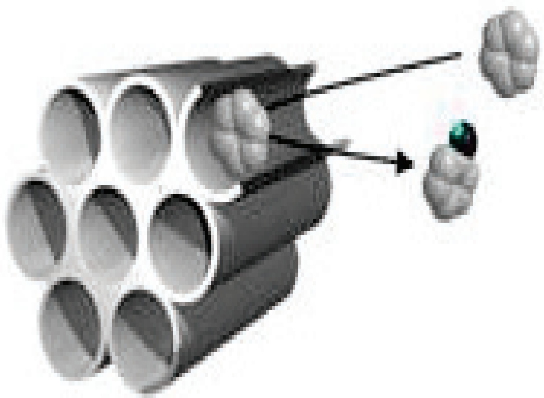

J. Am. Chem. Soc., **2005**, *127*, 12820.

Fig. 1-3 Selective oxidation of benzene on mesoporous TiO_2.

1-1-5. Improvement of photocatalytic activity: (3) Covering the titanium oxide surface

By covering the surface of titanium oxide with another inorganic semiconductor material, improvements, such as imparting visible light responsiveness and improving the selectivity for the target product, can be made. For example, the product selectivity was improved by coating the surface of titanium oxide with other inorganic oxides. Tanaka and colleagues achieved the selective oxidation of benzyl alcohol under visible light irradiation by coating the surface of titanium oxide with a layer of niobium oxide (Fig. 1-4) [15]. By combining semiconductors with different band gaps, ozonide ions which are strong oxidizing agents, are formed on titanium oxide, whereas ozonide ions are not formed by completely covering the titanium oxide surface with niobium oxide; therefore, sequential/complete oxidation is suppressed. In addition, Shiraishi et al. achieved the selective oxidation of benzyl alcohol upon irradiation with light having a wavelength of 350 nm by modifying the titanium oxide surface with tungsten oxide [16]. They reported that the selective partial oxidation reaction progressed after the modification of tungsten oxide because the reaction between the titanium oxide holes, which are strongly oxidizing, and benzaldehyde, the desired partial oxidation product, was suppressed.

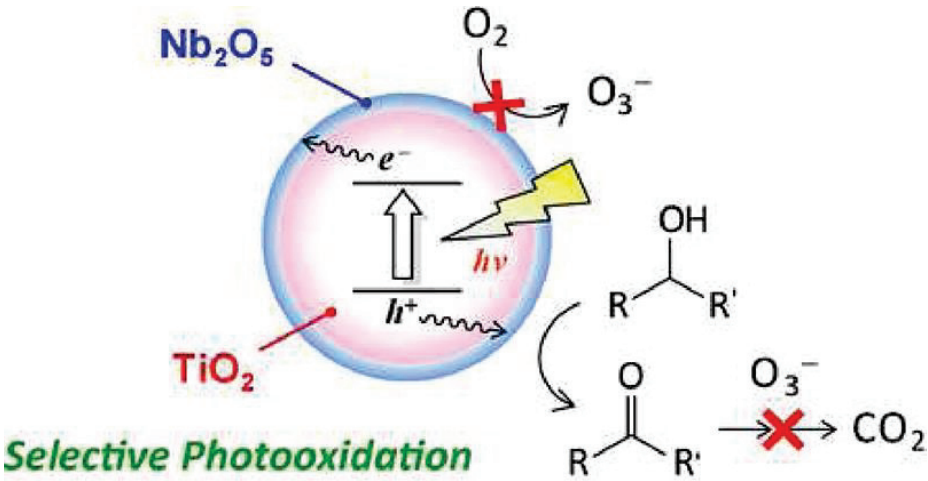

ACS Catal., **2012**, *2*, 175.

Fig. 1-4 Selective oxidation by coating the surface of titanium oxide with a layer of niobium oxide.

1-1-6. Improvement of photocatalytic activity: (4) Designing the reaction environment

Improvements in the reaction efficiency and product selectivity for the organic synthesis and decomposition removal of organic compounds by heterogeneous catalysis under sunlight irradiation are crucial.

The reaction efficiency can be improved and the product selectivity can be controlled by careful design of the reaction environment. However, because of the mild reaction conditions, improvements to the photocatalytic activity by reaction environment design are rarely reported. Tabata et al. found that water decomposition on a platinum-loaded titanium oxide was improved by about 800 times for hydrogen generation and about 1500 times for oxygen generation when UV light was irradiated from the top of the reaction mixture rather than the bottom [17]. Arakawa et al. added sodium carbonate to the reaction system for the decomposition of water using TiO_2-supported platinum as a catalyst. In this system, Pt is covered with carbonate, so the reverse reaction (formation of water) on Pt is suppressed; as a result, the hydrogen and oxygen generation efficiency hydrogen and oxygen is doubled [18].

Naya et al. reported that when a cationic surfactant was added to the solution used for the visible-light photocatalytic oxidation of primary alcohols to carbonyls on Au/TiO_2, the yield improved by 30 times [19]. In this system, the surfactant covers the surface of the catalyst, resulting in a hydrophobic surface; thus, the reaction intermediate ions easily move from the surface of the catalyst to the aqueous solution. Ide et al. reported that the efficiency and selectivity for visible-light benzene oxidation using a pillared gold catalyst with layered titanate was increased by adding phenol as a product before the reaction (Fig. 1-5) [20]. Thus, the efficiency of catalytic activity can be improved not only by improving the catalyst but also by designing the reaction environment.

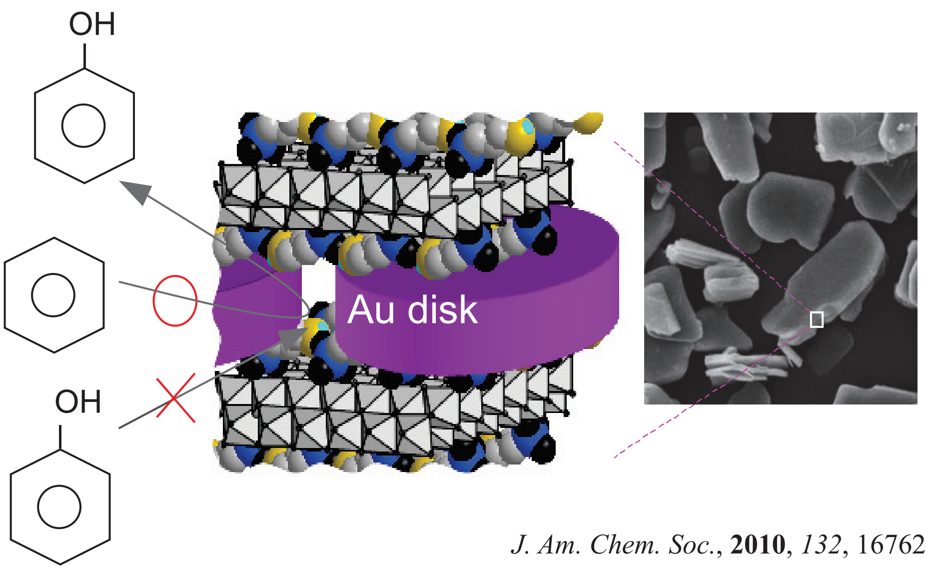

J. Am. Chem. Soc., **2010**, *132*, 16762.

Fig. 1-5 Selective oxidation of benzene to phenol using a catalyst in which gold is pillared between layered titanate.

1-2. Application as a sunscreen

1-2-1. What is a sunscreen?

An ultraviolet absorber is a substance that can absorb sunlight and ultraviolet rays, resulting in fluorescence, while remaining structurally stable. This prevents damage to surrounding compounds by converting high energy ultraviolet light into thermal energy or longer wavelength light. Ultraviolet absorbers are mainly used as stabilizers for plastics, rubber, paints, and dyes to prevent photodegradation caused by long-term exposure to sunlight. Ultraviolet absorbers must be non-colored and show excellent coalescence, heat resistance, and chemical stability, as well as have low volatility. Ultraviolet rays with a wavelength of 290 nm or less are completely absorbed by the ozone layer before reaching the ground, but ultraviolet light with a wavelength of 290 to 400 nm reaches the ground and is related to polymer aging. An ultraviolet absorber selectively absorbs these high-energy ultraviolet rays, converting them into harmless energy by energy conversion, either releasing or consuming the converted energy. Although organic ultraviolet light absorbers have drawn attention, inorganic ultraviolet screening agents have attracted more attention because of concerns about the safety of organic compounds to the human body. To absorb ultraviolet rays with an inorganic compound, the band excitation of a semiconductor can be utilized, and a semiconductor having a band gap energy of about 3 eV is necessary to remove ultraviolet light with a wavelength of 400 nm or less. In addition, to enhance the transparency of the material, it is necessary to use fine particles to prevent light scattering. Titanium oxide and zinc oxide nanoparticles have already been widely used as ultraviolet screening agents, and the use of nanoparticles of cerium oxide is also being studied. On the other hand, titanium oxide and zinc oxide are also representative photocatalysts, and it is known that active oxygen species are generated by light irradiation, promptly oxidizing organic compounds and inactivating bacteria. However, in recent years, oxidative DNA damage caused by the active oxygen species generated by the photoexcitation of semiconductors such as titanium has been reported, and, when semiconductor nanoparticles are incorporated into cosmetic products for skin application, the generation of active oxygen by the photoexcitation of semiconductor nanoparticles must be considered. Therefore, taking into consideration the influence on the human body, the development of materials without photocatalytic activity is required. The ultraviolet absorber must (1) strongly absorb ultraviolet light (especially ultraviolet light having a wavelength of 290 to 400 nm); (2) be thermally stable, especially during high-temperature processing, and have low volatility; (3) be chemically stable and not react with other components in the material; (4) have excellent coalescence and be easily dispersed uniformly in the material, for example, phenomena such as blooming and exudation should not occur; (5) not be absorbed, decomposed, or discolored; (6) be colorless, nontoxic, and odorless; (7) tolerate immersion and washing; and (8) be low cost and easy to obtain. Titanium-oxide-based ultraviolet light absorbers having these necessary properties have been developed and are introduced in the next chapter.

1-2-2. A brief history of TiO_2-based absorber and problems for application

Titanium oxide is expected to be a UV-absorbing coating material that can be dispersed in a versatile polymer. Irradiation with UV light not only destroys DNA, suppresses the immune system, and causes skin aging, but also decomposes and degrades plastics, pigments, dyes, and organic compounds, such as wood and paper, used in general purpose equipment. Thus, protection against UV radiation has received attention from science and industry. Organic UV-light-absorbing materials dispersed in a polymer have been used as UV-light-protecting layers for organic materials because they convert the absorbed light energy into thermal energy through a photophysical process, preventing damage (Fig. 1-6) [21, 22]. However, the polymer may be decomposed by the excited state of the absorbing material when exposed to UV radiation. Therefore, application of these materials has been limited [23]. The high refractive index and high UV photoactivity of titanium oxide are major problems when it is applied as a UV-absorbing coating material. Because of the high refractive index, the polymer matrix whitens and loses permeability, and the high UV photoactivity causes degradation and decomposition of the polymer. To solve these problems, the use of fine particles of titanium oxide, doping of elements with less electron localization than O^{2-}, and complexation with other inorganic materials have been reported. For example, Tressaud et al. prepared a new UV-absorbing coating material by fluorine doping (Fig. 1-7) [24]. This material exhibited light absorption similar to that of anatase, but the photocatalytic activity was low, and the refractive index of visible light was 1.9. In addition, Cui et al. prepared, via a sol-gel method, a UV-absorbing coating material composed of titanium oxide and cerium oxide or silicon oxide [25]. These materials strongly absorb UV light, and the transmission of visible light was high. Under mild conditions, crystalline material was obtained, which efficiently absorbed UV light. Because of these properties, we conclude that even organic materials that are sensitive to heat can be protected.

Chem. Soc. Rev., **2007**, *36*, 1270.

Fig. 1-6 An organic UV absorber.

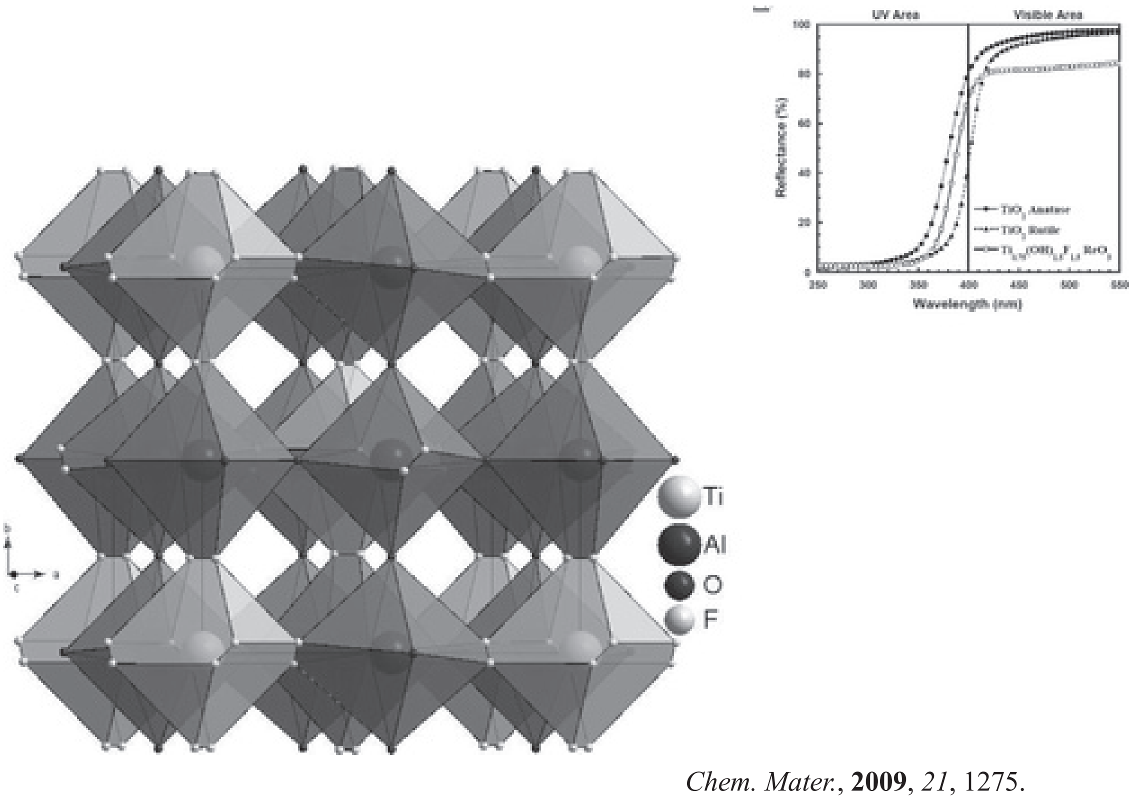

Chem. Mater., **2009**, *21*, 1275.

Fig. 1-7 A new UV-absorbing coating material prepared by fluorine doping.

1-3. Objectives of this research

Based on the above background, titanium oxide has been applied as a photocatalyst for the synthesis of simple chemicals and for environmental purification, and UV light absorber. Titanium oxide, which is a promising photocatalyst, was prepared, and I attempted to achieve visible light responsiveness using inexpensive materials, as well as to promote the catalytic reaction by controlling the reaction environment. In addition, I have attempted to prepare new titanium-oxide-based materials for various applications. I report the preparation method and the applications of this material. This paper consists of eight chapters.

In Chapter 1, I introduced the utility and problems in applying titanium oxide as a photocatalyst or UV-light-absorbing material and described the significance of this paper.

In Chapters 2 and 3, I describe the selective synthesis of simple chemicals and the removal of harmful substances in water by controlling the reaction environment. In Chapter 2, the selective synthesis of industrially important simple chemicals is reported. This was achieved on Fe-grafted titanium oxide with sunlight irradiation under a CO_2 atmosphere [26, 27]. The effects of CO_2 addition are discussed from various viewpoints. As reported in Chapter 3, even when using titanium oxide (P25, anatase, and rutile), efficient decomposition and the removal of harmful organic compounds under sunlight irradiation was achieved under an Ar atmosphere [28]. Under an argon atmosphere, the decomposition efficiency was significantly improved compared to other gas atmospheres, and this is also discussed.

In Chapters 4–6, I describe the reaction efficiency of the new photocatalyst, which was tuned by design and combination with existing catalysts. In Chapter 4, a novel titanium-oxide-based photocatalyst co-modified with three components (gold, iron, and nickel), all of which increase the photocatalytic reaction efficiency of titanium oxide, is reported. This catalyst was efficient for the selective synthesis of simple chemicals synthesis under sunlight irradiation [29]. In Chapter 5, layered titanate, which is a layered crystal of titanium oxide composition and a zeolite-like photocatalyst modified with iron between the interlayers, was designed to achieve efficient and selective chemical synthesis on irradiation with sunlight [30]. By conducting the reaction under a CO_2 atmosphere, as described in Chapter 2, the catalytic activity was further improved. As reported in Chapter 6, mixing the layered titanate and the titanium-oxide-based photocatalyst in water resulted in improved reaction efficiency. In addition, in this chapter, the differences resulting from the different combinations of material types, as well as the mechanism for the increased efficiency, are discussed [31].

In Chapter 7, I report the successful synthesis of a novel microporous titanium oxide by the hydrothermal treatment of layered titanates [32]. Because of its unique nanostructure, it shows little photocatalytic activity and has a considerably lower refractive index than conventional titanium oxide; thus, it was applied as UV-absorbing transparent coating material dispersed in a general purpose polymer.

Finally, in Chapter 8, I summarize my findings.

1-4. References

[1] A. Fujishima and K. Honda, *Nature*, **1972**, *238*, 37.

[2] S. N. Frank and A. J. Bard, *J. Am. Chem. Soc.*, **1977**, *99*, 303.

[3] G. N. Schrauzer and T. D. Guth, *J. Am. Chem. Soc.*, **1977**, *99*, 7189.

[4] T. Inoue, A. Fujishima, S. Konishi, and K. Honda, *Nature*, **1979**, *277*, 637.

[5] T. Kawai and T. Sakata, *Nature*, **1980**, *286*, 474.

[6] I. Matryanov and J. Klabunde, *Environ. Sci. Technol.*, **2003**, *37*, 3448.

[7] R. Asahi, T. Morikawa, T. Ohwaki, K. Aoki and Y. Taga, *Science*, **2001**, *293*, 269.

[8] T. Ohno, T. Mitsui and M. Matsumura, *Chem. Lett.*, **2003**, *32*, 364.

[9] Y. Tian and T. Tatsuma, *Chem. Commun.*, **2004**, 1810.

[10] C. G. Silva, R. Juarez, T. Marino, R. Molinari and H. Garcia, *J. Am. Chem. Soc.*, **2011**, *133*, 595.

[11] D. I. Enache, J. K. Edwards, P. Landon, B. Solsona-Espriu, A. F. Carley, A. A. Herzing, M. Watanabe, C. J. Kiely, D. W. Knight and G. J. Hutchings, *Science.*, **2006**, *311*, 362.

[12] J. T. Carneiro, C. - C. Yang, J. A. Moma, J. A. Moulijn and G. Mul, *Catal Lett.*, **2009**, *129*, 12.

[13] Y. Shiraishi, N. Saito and T. Hirai, *J. Am. Chem. Soc.,* **2005**, *127*, 12820.

[14] T. Kim, S. G. Hur, S.-J. Hwang, H. Park, W. Choi and J.-H. Choy, *Adv. Funct. Mater.,* **2007**, *17*, 307.

[15] S. Furukawa, T. Shishido, K. Teramura and T. Tanaka, *ACS Catal.*, **2012**, *2*, 175.

[16] D. Tsukamoto, M. Ikeda, Y. Shiraishi, T. Hara, N. Ichikuni, S. Tanaka and T. Hirai, *Chem. Eur. J.*, **2011**, *17*, 9816.

[17] S. Tabata, H. Nishida, Y. Masaki and K. Tabata, *Catal. Lett.*, **1995**, *34*, 245.

[18] K. Sayama and H. Arakawa, *Chem. Commun*., **1992**, 150.

[19] S. Naya, M. Teranishi, T. Isobe and H. Tada, *Chem. Commun*., **2010**, *46*, 815.

[20] Y. Ide, M. Matsuoka and M. Ogawa, *J. Am. Chem. Soc.,* **2010**, *132,* 16762

[21] J. Keck, M. Roessler, C. Schroeder, G. J. Stueber, F. Waiblinger, M. Stein, D. LeGourriérec, H. E. Kramer, H. Hoier, S. Henkel, P. Fischer, H. Port, T. Hirsch, G. Rytz and P. Hayoz, *J. Phys. Chem. B*, **1998**, *102*, 6975.

[22] M. Zayat, P. Garcia-Parejo and D. Levy, *Chem. Soc. Rev.*, **2007**, *36*, 1270.

[23] P. Garcia-Parejo, M. Zayat and D. Levy, *J. Mater. Chem.*, **2006**, *16*, 2165.

[24] A. Demourgues, N. Penin, E. Durand, F. Weill, D. Dambournet, N. Viadere and A. Tressaud, *Chem. Mater.*, **2009**, *21*, 1275.

[25] Z. Wang, Y. Pan, Y. Song and H. Cui, *J. Sol-Gel Sci. Technol.*, **2009**, *50*, 261.

[26] Y. Ide, N. Nakamura, H. Hattori, R. Ogino, M. Ogawa, M. Sadakane and T. Sano, *Chem. Commun*., **2011**, *47*, 11531.

[27] Y. Ide, H. Hattori, M. Sadakane and T. Sano, *Green Chem*., **2012**, *14*, 1264.

[28] Y. Ide, H. Hattori and T. Sano, *Phys. Chem. Chem. Phys.*, **2014**, *16*, 7913.

[29] Y. Ide, N. Kawamoto, Y. Bando, H. Hattori, M. Sadakane and T. Sano, *Chem. Commun.*, **2013**, *49*, 3652.

[30] H. Hattori, Y. Ide, S. Ogo, K. Inumaru, M. Sadakane and T. Sano, *ACS Catal*., **2012**, *2*, 1910.

[31] H. Hattori, M. Eguchi, Y. Ide and T. Sano, *Bull. Chem. Soc. Jpn.,* **2017**, *90*, 1276.

[32] H. Hattori, Y. Ide and T. Sano, *J. Mater. Chem. A*, **2014**, *2*, 16381.

Chapter 2

Highly efficient and selective sunlight-induced photocatalytic oxidation of cyclohexane on an eco-catalyst under a CO_2 atmosphere

2-1. Introduction

Heterogeneous photocatalysis driven by sunlight is a possible way to produce chemical, medical commodity and fuels in an economically and environmentally favorable manner. An improvement of the reaction efficiency and selectivity is required and, accordingly, much effort has been made to design the structure, composition and morphology of photocatalysts. Titanium dioxide is a promising material for the purpose due to availability, low toxicity, and chemical stability; however, it responds only to UV light, occupying 3–4% of sunlight, and tends to be nonselective for synthetic reactions. After Fujishima et al. reported photocatalytic ability of TiO_2 [1], great endeavors are continuously being done to modify TiO_2 by doping with metal [2] and nonmetal elements [3] or hybridization with organic dyes[4] and nanoparticles,[5] as well as to design novel catalysts such as molecular-sieve-like TiO_2 [6–9] and non-TiO_2 materials,[10–14] to achieve efficient and selective photocatalysis under sunlight. Besides catalyst design, there have been several studies on the influence of reaction environments on heterogeneous photocatalysis.

TiO_2-supported gold nanoparticles are well known as visible light responsive photocatalysts. When gold nanoparticles are supported on TiO_2, gold nanoparticle captures photoexcited electrons on TiO_2 under UV light irradiation with the speed of fs and suppresses returning to holes, so separation of holes and electrons of TiO_2 is efficient. Also, since it has been reported that gold nanoparticles strongly absorb visible light due to surface plasmon resonance caused by collective excitation of electrons [15], it has been widely studied as a visible light responsive photocatalyst. On the other hand, catalyst combining an inexpensive base metal and TiO_2 has also been developed. Among them, iron is nontoxic and is a metal abundantly present as a resource. However, doping iron into defects of TiO_2 improves visible light activity but reduces ultraviolet light activity. [16] It is thought that this is because the energy level formed by doping becomes the site of recombination of electrons and hole. In order to solve this problem, Tada et al. developed a catalyst which improves not only visible light but also UV light activity by using a method to modify the surface of TiO_2 with iron oxide [17, 18].

Selective oxidation of cyclohexane to cyclohexanone and cyclohexanol is one of the most important synthetic reactions, since the partially oxidized products are an important intermediate in ε-caprolactam synthesis, which is used in the manufacture of nylon polymers. Nonetheless, in the oxidation of cyclohexane which is currently used industrially, despite the severe reaction conditions of reaction temperature 140 to 160 ° C, and pressure 1 to 1.5 MPa, cyclohexane conversion is 4 to 10%, selectivity of partial oxide is about 80% [19]. Therefore, an efficient oxidation of cyclohexane with high conversion and selectivity is required. Oxidation of cyclohexane over TiO_2 has been widely carried out by Herrmann group[20] and Mul group.[21] Some of them report that partialoxidation of cyclohexane is promoted with high selectivity (> 98%). However, in these studies, ultraviolet light irradiation is necessary for catalytic activation. On the other hand, oxidation of cyclohexane using a catalyst activated under visible light irradiation has also been reported. Shiraishi et al. reported selective cyclohexane oxidation using molecular oxygen as an oxidizing agent under irradiation with visible light, using Cr / Ti / Si composite oxide as a catalyst [22]. The selectivity of the partial oxide is 99%, and the reaction mechanism is also mentioned.

As described above, in the synthesis of basic chemicals using heterogeneous catalysts under sunlight irradiation, new catalysts are actively designed to improve reaction efficiency and product selectivity. On the other hand, there are some reports that the reaction efficiency can be improved and the product selectivity can be controlled by controlling the reaction environment. For example, Arakawa and colleagues added sodium carbonate to the reaction system of the decomposition of water using TiO_2-supported platinum as a catalyst in order to cover Pt with carbonate, the reverse reaction of hydrogen and oxygen generated on Pt was suppressed, as a result, the generation efficiency of hydrogen and oxygen was improved by about 2 times [23]. It was also reported by Naya and colleagues that when cationic surfactant was added to the solution in the photocatalytic oxidation reaction of the primary alcohol to carbonyl compound under visible light irradiation on Au/TiO_2, the yield was improved up to about 30 times [24]. It is proposed that the surfactant covers the surface of the catalyst and becomes hydrophobic, as a result, the reaction intermediates easily move from the catalyst surface to the aqueous solution. Ide and colleagues reported that efficiently and selectively of benzene oxidation using a catalyst in which gold is pillared between layers of layered titanate under irradiation with visible light by adding phenol as a product before the reaction. [25] In addition, Ide et al. proposed that partial oxidation phenol is achieved by preliminarily adding CO_2 generated by complete oxidation in the oxidation reaction of benzene under visible light irradiation using gold fine particle-supported titanium oxide as a catalyst. [26]

Therefore, in this research, I tried to design a new reaction field in which efficient and selective reactions proceed on known photocatalysts. Partial oxidation reaction of cyclohexane to cyclohexanone and cyclohexanol, which is an industrially important reaction, was carried out under simulated sunlight irradiation. Iron-modified TiO_2 was used as a catalyst and the reaction was carried out under a CO_2 atmosphere which is a complete oxidation product.

2-2. Experimental

Reagents and materials

P25 was supplied by Nippon Aerosil. Fe(Ⅲ)acetylacetonate ($Fe(acac)_3$), ethanol and hexane were purchased from Wako Pure Chemical Industries, Ltd. Toluene was purchased from Kanto Chemical Industry Co., Ltd. Cyclohexane and acetonitrile were purchased from Nacalai tesque Ltd. All reagents and materials were used as received.

Synthesis of TiO_2 supported iron oxide

FeO@P25 was synthesized according to the literature:[17, 18] P25 (1.0 g, Nippon Aerosil) was added to 6.5×10^{-4} mol L^{-1} of iron(III) acetylacetonate in a mixed solvent (100 mL, ethanol/hexane = 3 : 17 v/v) and the mixture was stirred at room temperature for 24 h. The product was separated by centrifugation (3000 rpm, 20 min), washed repeatedly with the same solvent, and calcined at 500 °C for 1 h. The reaction was repeated three times.

Oxidation of cyclohexane

Photocatalytic conversions were carried out by photoirradiation with solar simulator (San-Ei Electric Co., Ltd) to a mixture of catalyst (30 mg), O_2-saturated acetonitrile (18 mL) solution of cyclohexane (2 mL) and CO_2 (dry ice) in a stainless-made closed container equipped with Pyrex glass (75 mL) under controlled atmosphere at 42 °C, with shaking. After analyzing gas phase, the irradiation was started. The container was placed by ca. 30 cm away from the light source to irradiate 1 solar (1000 W m^{-2})-power light to the mixture. CO_2 was quantitatively analyzed by GC-TCD (the measurement accuracy was within 1.0%) and organic compounds recovered by filtration, and the resulting supernatant was analyzed by GC-FID (Shimazu GC-2014). Toluene was used as internal standard for GC-FID. Only three products, cyclohexanone, cyclohexanol, and CO_2, were detected in the present study. The intermediates, such as cyclohexyl hydroperoxide, were not detected.

Adsorption test of cyclohexanone

Adsorption tests were done in a similar way that conducted in photocatalytic conversions except that 10 mg of the catalyst and a solution of cyclohexanone (2 mL) in acetonitrile (18 mL), which was not bubbled with O_2, were mixed.

Measurement of action spectrum

For action spectra measurement, the full arc from a 500W-Xe lamp (Ushio) was monochromated using SM-25 (Bunkokeiki) and then irradiated a mixture of catalyst (60 mg), O_2^-saturated acetonitrile (18 mL) solution of cyclohexane (2 mL) and 40 mg of CO_2 (dry ice) in a stainless-made closed container equipped with Pyrex glass (75 mL).

Analytical equipments and evaluation condition

Apparatus using for characterization of synthesis catalysts and quantification of substrate and products of photocatalytic test were shown below. Diffused reflectance UV-vis spectra were measured with ultraviolet-visible near-infrared spectrophotometer (Nihonbunko, JASCO V-570). Measurement wavelength range were 200 - 800 nm, and $BaSO_4$ used for baseline. Transmission electron microscopic (TEM) images were obtained with a JEOL JEM-2011.

2-3. Results and discussion

2-3-1. Characterization of catalysts

In the XRD pattern and TEM image of FeO@P25, diffraction peaks only due to TiO_2 were detected and particles other than P25 were not observed, respectively (data were not shown). These results imply the presence of molecular-level iron oxide adjacent to the P25 surface.[17, 18] The adsorption spectrum of FeO@P25 showed a shoulder centered at 500 nm (Fig. 2-1). These results imply the presence of molecular-level iron oxide adjacent to the P25 surface. An iron(III) acetylacetonate complex has been reported to irreversibly react with surface titanol groups to form Ti–O–Fe covalent bond via ligand exchange reaction. The amount of the immobilized iron oxide in FeO@P25 was estimated to be 0.81 Fe^{3+} ions nm^{-2}. Taking the amount (more than 4 groups nm^{-2}) of titanol on P25 into account, iron oxide on P25 is thought to exist as patchy molecular-level particles, rather than a contentious ultrathin layer.

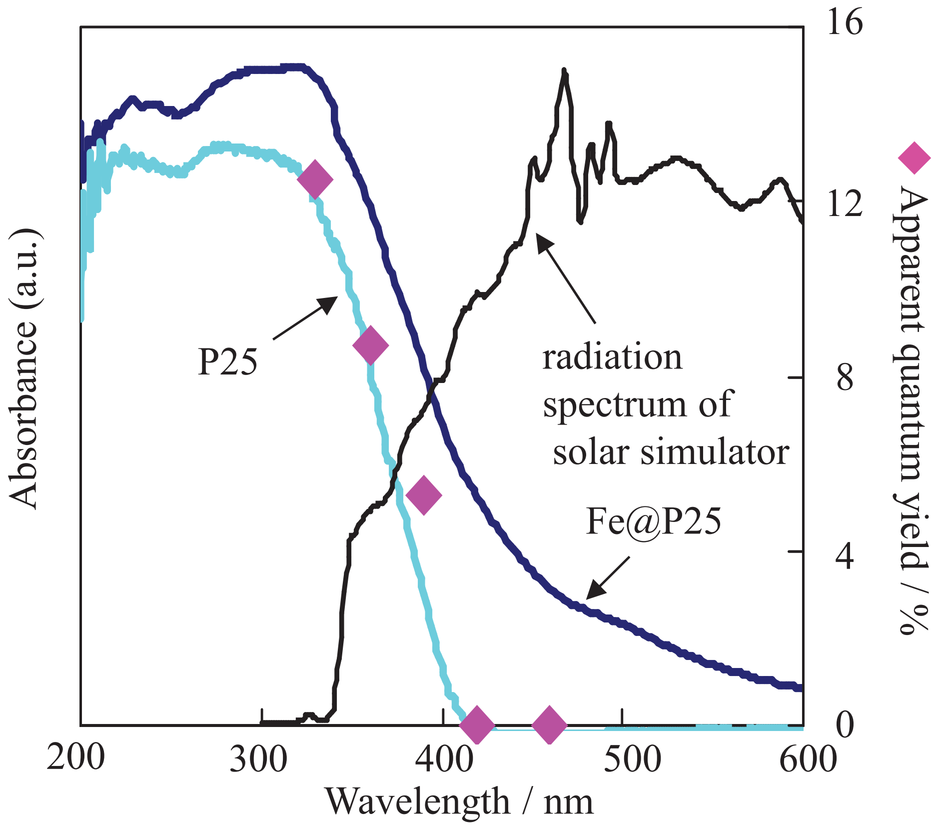

Fig. 2-1 Diffused reflectance UV-vis spectra of P25 and FeO@P25, (◆) action spectrum in cyclohexanone formation on FeO@P25, and radiation spectrum of solar simulator used in this study.

2-3-2. Oxidation of cyclohexane and adsorption of cyclohexanone

Oxidation of cyclohexane

Table 2-1 summarizes all the results and Fig. 2-2 shows the CO_2 pressure dependence of the yield and the selectivity for cyclohexanone formation on P25 (entry 1～6) and FeO@P25 (entry 7～16) under typical conditions. Cyclohexanone and cyclohexanol describe as CHA-one and CHA-ol. When the reaction was done on Fe@P25 under 51 kPa of a CO_2 atmosphere for 24 h, the best result, with a selectivity of ca. 100%, was attained (Table 2-1, entry 13). A notable finding is that even the reaction on FeO@P25 in air gives a selectivity of ca. 100%, and by conducting the reaction under 51 kPa of CO_2, even when the irradiation time was prolonged, the yield is substantially improved with a selectivity maintained at ca. 100% (Table 2-1, entries 7, 9, 12 and 13, and Fig. 2-2). To the best of our knowledge, 100% selectivity is the highest among those that had been reported for photocatalytic cyclohexanone production under visible light.[27,28] Also, the yield (more than 200 TON) was considerably higher than those obtained in other selective photocatalytic cyclohexane oxidations under visible light. For example, 68% selectivity and 2.5 TON for cyclohexanone production were obtained on Cr–Si binary oxide and 99% selectivity[29] and 22 TON for cyclohexanone and cyclohexanol production were attained on hydrophobically modified Cr–Si binary oxide[28]. In the present study, it is also worth mentioning that the photocatalytic performance of pristine P25 is improved to give a higher yield with a selectivity maintained to some extent by conducting the reaction under CO_2 (Table 2-1, entries 1 and 3, and Fig. 2-2). All of the results described above suggest that effective and selective sunlight-induced organic synthesis is possible even on cheap and abundant photocatalysts just by conducting the reaction under CO_2 atmosphere.

Interestingly, a high level of effective and selective cyclohexane oxidation was attained only when FeO@P25 was irradiated by sunlight including UV light (320 nm < λ) (Table 2-1). P25 produced much larger amount of CO_2 when irradiated by sunlight (excitation with UV light (λ < 420 nm), Fig. 2-1), resulting in much lower selectivity (Table 2-1, entries 1–6). It is well known that valence band holes possess strong oxidation power; therefore, highly selective cyclohexane oxidation is difficult on P25, even under CO_2. On the other hand, when FeO@P25 was irradiated by sunlight, only with a wavelength longer than 420 nm (only molecular iron oxide was excited, Table 2-1, entry 14), smaller amount of cyclohexanone formed on FeO@P25 if compared to that obtained by sunlight irradiation (320 nm < λ, Table 2-1, entry 9), although similar selectivity (ca. 100%) were attained. Also, no products were detected on FeO@SiO_2 under identical conditions (data is not shown), showing that the iron oxide functioned as the photocatalysis of cyclohexane oxidation only when it was adjacent to TiO_2. Moreover, no products were detected on FeO@P25 without any irradiation, which revealed that iron oxide did not work as a thermocatalyst. From these observations, we considered a possible role of iron oxide in the selective cyclohexane oxidation over FeO@P25 as follows: electrons, which transfer from both the TiO_2 valence band by UV excitation, and iron oxide by visible light excitation (possibly due to the d–d transition of molecular iron oxide) [17, 30] to the TiO_2 conduction band, effectively reduce adsorbed O_2 to generate O_2^-. The obtained superoxide anion plays an important role in the selective cyclohexane oxidation over FeO@P25. Lower amount of cyclohexanone formed on FeO@P25 when only the iron oxide was excited (Table 2-1, entries 9 and 14), which was explained by that smaller amount of electrons, which were necessary to generate O_2^-, were transferred to the conduction band of TiO_2. Fig.1 shows action spectrum on FeO@P25. The action spectrum (from 330 to 460 nm) in cyclohexanone formation on FeO@P25 was in good agreementwith the UV-vis spectrum of P25 rather than that of FeO@P25, supporting the above hypothesis. The mineralization of cyclohexane and the successive oxidation of cyclohexanone and cyclohexanol hardly occurred to give only trace amounts of CO_2 on FeO@P25 (especially under lower loading levels of CO_2), since iron oxide efficiently prevented the interactions between bulky molecules, cyclohexane and the partially oxidized products, with the valence band holes on the P25 surface. The coating of TiO_2 particles with silica and alumina layers is useful to suppress the photocatalytic decomposition activity of organic compounds[31, 32].

Table 2-1 Results of cyclohexane oxidation on P25 and FeO@P25 under simulated sunlight.

Entry	Catalyst	Added CO_2 / kPa	Yield / μmol			CHA-one+CHA-ol TON /- [c]	Selectivity / % [d]
			CHA-one [a]	CHA-ol [b]	CO_2		
1	P25	0 [e]	39.70	13.6	126.0	-	71.7
2		51	24.6	8.0	183.0	-	51.7
3		102	47.1	15.1	252.4	-	59.6
4		127	30.5	3.3	821.2	-	19.8
5		153	29.6	13.7	373.3	-	41.0
6		191	30.3	10.0	503.5	-	32.4
7	FeO@P25	0 [e]	3.6	trace	trace	5.3	> 99.9
8		26	2.5	trace	n.d.	3.7	> 99.9
9		51	6.3	trace	n.d.	9.3	> 99.9
10		102	5.4	trace	75.1	7.9	30.0
11		153	4.8	trace	50.6	7.1	36.2
12		51 [f]	18.8	7.0	n.d.	38	> 99.9
13		51 [g]	78.8	60.7	n.d.	206	> 99.9
14		51 [h]	4.3	trace	n.d.	6.3	> 99.9
15		51 [i]	6.2	trace	n.d.	9.2	> 99.9
16		0 [j]	9.2	trace	154.7	14	26.2

[a] Cyclohexanone. [b] Cyclohexanol.

[c] [formed CHone] + [formed CHnol]/[formed CHone] + [formed CHnol] + 1/6[formed CO_2]× 100.

[d] Estimated on the basis of Fe amount. [e] In air. [f] Irradiation time, 12 h. [g] Irradiation time, 24 h.

[h] Sunlight with a wavelength shorter than 420 nm was cut-off. [i] After the reaction (entry 9), the catalyst was recovered, washed with acetonitrile, and then used for reaction.

[j] Argon was purged.

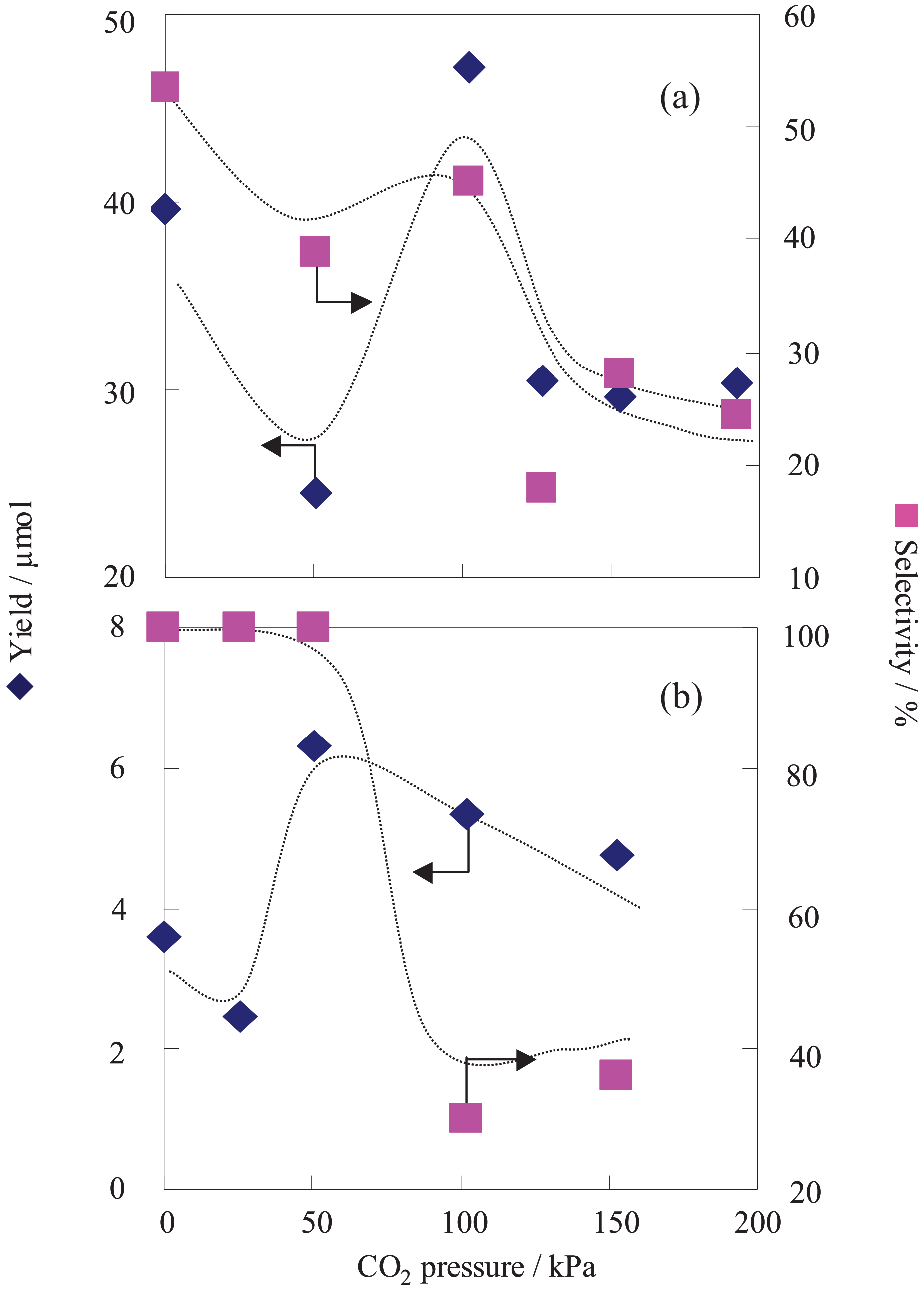

Fig. 2-2 CO_2 pressure-dependence of photocatalytic oxidation activity of cyclohexane to cyclohexanone on (a) P25 and (b) FeO@P25 under sunlight irradiation for 6 h.

Adsorption of cyclohexanone

As shown in Table 2-1 (entry 16), when the atmosphere was changed from CO_2 (or air) to Ar (purged), larger amounts of cyclohexanone and CO_2 formed on FeO@P25. Moreover, the yield and the selectivity for cyclohexanone and cyclohexanol formation on FeO@P25 and P25 varied with CO_2 pressure (Table 2-1 and Fig. 2-2). These results imply that CO_2 dissolves in the liquid phase and/or adsorbs on the catalyst surface depending on CO_2 pressure, affecting the present photocatalysis. CO_2 is known to adsorb on metal oxides,[33] so that the surface modification of P25 with CO_2 possibly promotes the desorption of the formed cyclohexanone and cyclohexanol to suppress the successive oxidation. It is also thought that dissolved CO_2 changes the polarity of the liquid phase to influence the adsorption or the desorption of the partially oxidized products, since it has been reported that the adsorption behavior of cyclohexanone on TiO_2 dramatically varies with solvents.[34] To confirm the hypothesis, the adsorption of cyclohexanone from acetonitrile on FeO@P25 and P25 was investigated under controlled CO_2 pressure. As shown in the Fig. 2-3, the amount of the adsorbed cyclohexanone on FeO@P25 and P25 varied with CO_2 pressure, and the curves almost mirrored the curves for CO_2 pressure dependence of the photocatalytic performance. Accordingly, it is plausible that under an appropriate CO_2 loading (ca. 50 and 100 kPa for FeO@P25 and P25, respectively) a balanced combination between the CO_2-modified surface properties of the catalysts and the polarity of the liquid phase makes the formed cyclohexanone and cyclohexanol promptly desorb from the catalysts surface, which prevents the successive oxidation of the partially oxidized products.

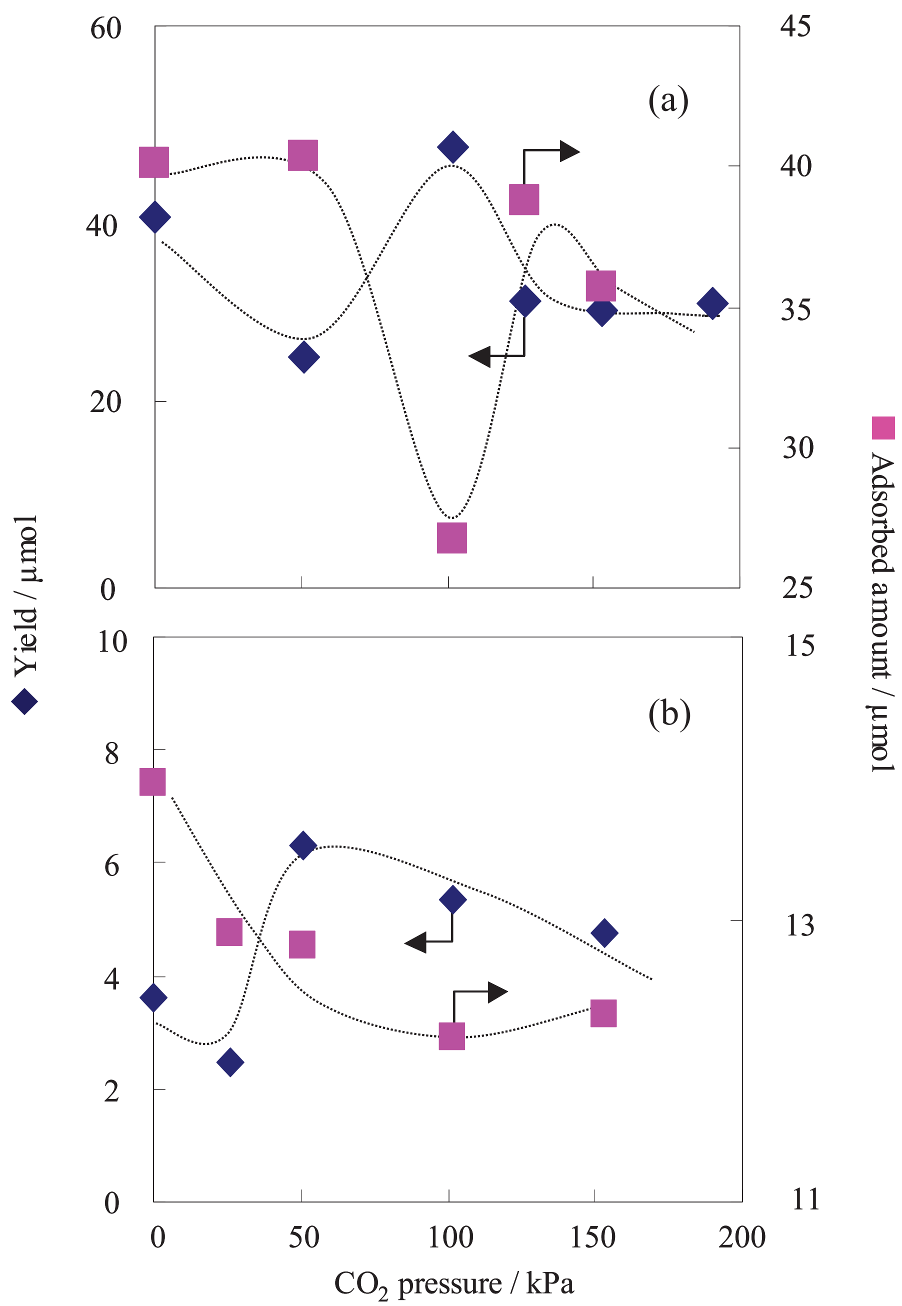

Fig. 2-3 Comparison between (◆) CO_2 pressure-dependence of cyclohexanone formation on (a) P25 and (b) FeO@P25 (plots same to those in Fig. 2-14) and (■) that of cyclohexanone adsorption from acetonitrile on (a) P25 and (b) FeO@P25.

2-4. Conclusion

From all of above results, I found a highly effective and selective sunlight-induced photocatalytic oxidation of cyclohexane, in acetonitrile, to cyclohexanone and cyclohexanol on TiO_2 (P25) modified with iron oxide under a CO_2 atmosphere. [35] In addition to the versatility, this idea is compelling in terms of CO_2 reduction, capture and storage. The present success opens up new opportunities to synthesize a wide variety of fine chemicals in an economically and environmentally favorable fashion.

2-5. References

[1] A. Fujishima and K. Honda, *Nature*, **1972**, *238*, 37.

[2] M. Anpo and M. Takeuchi, *J. Catal.*, **2003**, *216*, 505.

[3] R. Asahi, T. Morikawa, T. Ohwaki, K. Aoki and Y. Taga, *Science*, **2001**, *293*, 269.

[4] W.J. Youngblood, S.-H. A. Lee, K. Maeda and T. E. Mallouk, *Acc. Chem. Res.,* **2009**, *42*, 1966.

[5] A. Primo, A. Cormaand H. Garcia, *Phys. Chem. Chem. Phys.*, **2011**, *13*, 886.

[6] Y. Shiraishi, N. Saito and T. Hirai, *J. Am. Chem. Soc.*, **2005**, *127*, 12820.

[7] T. W. Kim, S. G. Hur, S.-J. Hwang, H. Park, W. Choi and J.-H. Choy, *Adv. Funct. Mater.*, **2007**, *17*, 307.

[8] Y. Ide, M. Matsuoka and M. Ogawa, *J. Am. Chem. Soc.*, **2010**, *132*, 16762.

[9] Y. Ide, Y. Nakasato and M. Ogawa, *J. Am. Chem. Soc.*, **2010**, *132*, 3601.

[10] K. Maeda and D. Domen, *J. Phys. Chem. Lett.*, **2010**, *1*, 2655.

[11] A. Kudo and T. Miseki, *Chem. Soc. Rev.*, **2009**, *38*, 253.

[12] F. E. Osterloh, *Chem. Mater.*, **2008**, *20*, 35.

[13] Y. Shiraishi and T. Hirai, *J. Photochem. Photobiol., C*, **2008**, *9*, 157.

[14] H. Kominami, A. Tanaka and K. Hashimoto, *Chem. Commun.*, **2010**, *46*, 1287.

[15] Y. Tian and T. Tatsuma, *Chem. Commun*., **2004**, 1810.

[16] K. Nagaveni, M. S. Hedge and G. Madras, *J. Phys. Chem. B*, **2004**, *108*, 20204.

[17] H. Tada, Q. Jin, H. Nishijima, H. Yamamoto, M. Fujishima, S. Okuoka, T. Hattori, Y. Sumida and H. Kobayashi, *Angew. Chem. Int. Ed.*, **2011**, *50*, 3501.

[18] Q. Jin, M. Fujishima and H. Tada, *J. Phys. Chem. C*, **2011**, *115*, 6478.

[19] Bart P. C. Hereijgers and Bert M. Weckhuysen, *J. Catal.*, **2010**, *270*, 16.

[20] J. M. Herrmann and A. Sclafani, *J. Phys. Chem.,* **1996**, *100*, 13655.

[21] A. R. Almeida, J. A. Moulijn and G. Mul, *J. Phys. Chem. C.,* **2008**, *112*, 1552.

[22] D. Tsukamoto, A. Shiro, Y. Shiraishi and T. Hirai, *J. Phys. Chem. C.,* **2011**, *115*, 19782.

[23] K. Sayama and H. Arakawa, *J. Chem. Soc. Chem. Commun.,* **1992**, 150.

[24] S. Naya, M. Teranishi, T. Isobe and H. Tada, *Chem. Commun*., **2010**, 46, 815.

[25] Y. Ide, M. Matsuoka and M. Ogawa, *J. Am. Chem. Soc.,* **2010**, *132*, 16762.

[26] Y. Ide, N. Nakamura, H. Hattori, R. Ogino, M. Ogawa, M. Sadakane and T. Sano, *Chem. Commun*., **2011**, *47*, 11531.

[27] H. Sun, F. Blatter and H. Frei, *J. Am. Chem. Soc*., *1996*, **118**, 6873.

[28] Y. Shiraishi, H. Ohara and T. Hirai, *New J. Chem*., **2010**, *34*, 2841.

[29] Y. Shiraishi, Y. Teshima and T. Hirai, *Chem. Commun*., **2005**, 4569.

[30] H. Yu, H. Irie, Y. Shimodaira, Y. Hosogi, Y. Kuroda, M. Miyauchi and K. Hashimoto, *J. Phys. Chem. C*, **2010**, *114*, 16481.

[31] O. K. Park, Y. S. Kang and B. G. Jo, *J. Ind. Eng. Chem*., **2004**, *10*, 733.

[32] R. Kato, N. Shimura and M. Ogawa, *Chem. Lett*., **2008**, *37*, 76.

[33] J.Baltrusaitis, J. Schuttlefield, E. Zeitler and V. H. Grassian., *Chem. Eng. J.* **2011**, *170*, 471.

[34] C.B.Almquist and P. Biswas., *Appl. Catal. A: General.* **2001**, *214*, 259.

[35] Y. Ide, H. Hattori, M. Sadakane and T. Sano, *Green Chem*., **2012**, *14*, 1264.

Chapter 3

Extraordinary effects of argon atmosphere on TiO_2 photocatalysis

3-1. Introduction

Recently, removal of toxic chemicals from wastewater is currently one of the most compelling objectives in pollution control. Solar-driven photocatalysis has been regarded to be a most effective and environmentally benign method for the purpose. TiO_2 is a promising photocatalyst due to its abundance, non-toxicity and high stability. However, TiO_2 responds only to the UV light, which takes only 3-4% of the incident solar light, and the solar photocatalytic activity is insufficient for practical use. Accordingly, as shown in Chapter 2, designing novel photocatalysts has been extensively investigated in recent years. [1-5]

In this Chapter, when used under a unique environment, Ar atmosphere, even TiO_2 exhibits a high solar photocatalytic activity toward the decomposition (mineralization) of known organic contaminants in water.

3-2. Experimental

Reagents and materials

P25 and rutile (JRC-TIO-06) were supplied by Nippon Aerosil and Catalysis Society of Japan, respectively. Anatase, NaOH and $Ba(OH)_2$was purchased from Wako Pure Chemical Industries, Ltd. Cationic organic dyes, crystal violet (CV) and basic violet 4 (BV), were purchased from Tokyo Chemical Industry Co., Ltd. All reagents and materials were used as received.

Photocatalytic test

A mixture of TiO_2 (60 mg) and a solution of CV or BV in water (25 mL, 50 or 250 ppm) in a stainless-made closed container (75 mL) equipped with Pyrex glass and gas inlet/outlet, was irradiated (λ > 320 nm) by a solar simulator (XES-155S1, San-Ei Electric Co., Ltd., 500 W Xe lamp,1000 W m^{-2}) at room temperature, under shaking. Gas flow rate was 0.1 mL min^{-1}. Prior to photoirradiation, the mixture was settled in dark for 15 min under each atmosphere. For the reaction at a higher pH, 0.1 M-NaOH aqueous solution was added into the starting mixture to adjust the pH to 9. After the reaction, the supernatant was separated by filtration and analyzed by UV-vis spectroscopy (V-570, JASCO Co.) to determine the amount of residual organic dye in the supernatant. The gas phase CO_2 was quantitatively analyzed by GC-TCD (GC-8A, the measurement accuracy was within 1.0%) before and after photocatalytic test. When the reaction was conducted under gas flow environments, a saturated $Ba(OH)_2$ solution was set up at the down stream of the flow to capture CO_2 formed as $BaCO_3$ and then the amount of Ba in the supernatant was determined with Inductively Coupled Plasma Atomic Emission Spectroscopy (ICP-AES, SPS7700, Seiko Instruments Inc.). The photocatalysis under an Ar or a N_2 atmosphere (150 kPa) was also conducted by the way similar to that conducted for the photocatalysis in other environments.

Adsorption of CV

Adsorption test was conducted by the way similar to that conducted for the photocatalysis except that the mixture of P25 and aqueous CV was shaken in dark under each atmosphere immediately after mixing. After the adsorption, the supernatant was separated by filtration and analyzed by UV-vis spectroscopy to determine the amount of residual organic dye in the supernatant.

Gas adsorption

The adsorption–desorption isotherms of O_2, N_2 or Ar on P25 were measured at 77 K with a BEL-Max (BEL Japan, Inc.). Prior to the measurements, P25 was evacuated at 353 K for 3 h.

Estimation of amounts of carbon deposits

The recovered P25 was washed sufficiently with water and ethanol to remove possibly adsorbed CV and analyzed by thermogravimetric-differential thermal analysis under air using a SSC/5200 (Seiko Instrument Inc.)

Contact angle measurement

Deionized water was bubbled with CO_2, N_2, O_2 or Ar gas for 15 min. Each droplet was positioned on a fluorocarbon polymer (PTFE) substrate and the contact angle values were measured in an ambient environment, at room temperature.

3-3. Results and discussion

Crystal violet (named as CV), whose molecular structure is shown in Fig. 3-1 a, is a cationic organic dye in wastewater coming from dyeing and finishing industry and known to be relatively stable under solar light. I also confirmed that no appreciable decomposition of CV was detected in the absence of catalyst under the present irradiation condition. Fig. 3-2 (a: CV decomposition, b: CO_2 evaluation) shows the time-course curves of photocatalytic reactions on TiO_2 (P25) in aqueous solutions of CV under simulated solar light irradiation in different atmospheres. In air (the reaction container was closed), CV was photocatalytically decomposed gradually, forming the completely oxidized products, CO_2 (black circles). [6-9] Surprisingly, when the photocatalytic reaction was conducted under Ar flow (the gas phase of the container was ventilated with pure Ar gas), CV decomposition and CO_2 evolution occurred much more rapidly (purple squares). The initial rate for photocatalytic CV decomposition under Ar flow was 2.7 μmol min^{-1}, which was about 12-times faster than that (0.22 μmol min^{-1}) observed in air. Almost all CV mineralized into CO_2 under Ar flow at the end of the irradiation; while, the degree of the mineralization was only about 50 % in air (complete mineralization of 1 mol of CV implies the evolution of the equivalent amount, 25 mol, of CO_2 as shown in Fig. 3-1 a). Just by using an inert and versatile Ar gas, namely, in an environmentally and economically benign fashion, the solar photocatalytic activity of P25 was substantially improved. It should be noted here that air flow (green squares) and N_2 flow (data not shown) were less effective in the photocatalytic reaction than Ar flow, showing an important role of Ar, not but N_2 and O_2, in the photocatalysis.

Most TiO_2 photocatalytic reactions for organic pollutants removal requires (dissolved) O_2 as both a conduction band electron scavenger and a reagent for mineralization; on the other hand, some photocatalytic reactions can be enhanced in the absence of O_2 when the reductive pathways are dominant. The present photocatalytic reaction under Ar flow is not the former cases, because CV decomposition rate in the absence of dissolved O_2 was slower than that in the presence of dissolved O_2 and CO_2 evolution was observed even without dissolved O_2 (Fig. 3-2 a and b, red triangles). Indeed, many organic dyes, like CV, are thought to be photocatalytically degraded and mineralized mainly with oxidizing species such as hydroxy radicals and superoxide radicals from water and dissolved O_2, respectively. [6-9] I measured the amount of dissolved O_2 in an aqueous CV solution after 15 min-Ar flow to be 5.01 mg L^{-1}, which was comparable to that (8.59 mg L^{-1}) in the original solution. Dissolved O_2 was thus not effectively removed from the reaction mixture during the present photocatalysis under Ar flow. Therefore, even under Ar flow, dissolved O_2 successfully acted as a conduction band electron scavenger and/or a reagent for CV mineralization. When the Ar flow rate was slowed down to half (0.05 mL min^{-1}) and accelerated twofold (0.2 mL min^{-1}), the amounts of dissolved O_2 in an aqueous CV solution after 15 min of the flows were 5.82 and 4.91 mg L^{-1}, respectively. The photocatalytic CV decomposition rate did not depend on the Ar flow rate (Fig. 3-2c). Therefore, a higher flow rate of Ar negatively affected the photocatalysis because a larger amount of O_2 was removed.

The usefulness of Ar flow was further confirmed by the photocatalytic reaction at a higher concentration of initial CV. As described above, dissolved O_2 is required for effective photocatalytic CV mineralization over P25. Therefore, at a higher concentration of initial CV, the amount of O_2 dissolved in water could strongly affect the activity for CV decomposition, namely, O_2 flow could accelerate photocatalytic CV decomposition more effectively than Ar flow did. However, as can be seen in Fig. 3-2 d, even at a much higher initial CV concentration, photocatalytic CV decomposition was considerably accelerated under Ar flow. On the other hand, O_2 flow substantially suppressed CV decomposition activity.

I investigated other photocatalytic oxidations under Ar flow to show the versatility of the strategy. As shown in Fig. 3-3, both the photocatalytic decomposition of another known cationic dye in wastewater, basic violet 4 (BV, Fig. 3-1 b) over P25 and that over anatase-phase-TiO_2 (while P25 is composed mainly of anatase and rutile crystallites[10,11]) were also considerably accelerated when the reactions were conducted under Ar flow. On the other hand, with rutile-phase-TiO_2, that showed no appreciable photocatalytic activity toward the decomposition of neither CV nor BV under the identical irradiation condition, the activity was not improved at all even under Ar flow (CO_2 hardly evolved). It should be noted here that Ar flow improved the adsorption ability of rutile for CV (Fig. 3-3c).

Although a number of factors should concern the highly improved photocatalytic decomposition of CV and BV under Ar flow, in this study, I propose three possible factors. The first of which is the pH of aqueous mixture. It is generally known that a larger amount of cationic species adsorb on TiO_2 surface in dark (without light irradiation) when the pH of aqueous mixtures is higher, because increasing the pH causes the de-protonation of neutral hydroxyl groups on TiO_2 surface into negatively charged ones.[12] Accordingly, the initial rate of photocatalytic reactions of cationic reactants on TiO_2 increases with increasing the pH of reaction mixtures.[13] Here I compared the adsorption of CV from water on P25 under Ar flow (Fig. 3-4 a, purple squares) to that under air flow (green squares). A larger amount of CV adsorbed on TiO_2 under Ar flow, which was explained by higher pH of the aqueous mixture all during the adsorption (Fig. 3-4 b). Difference in pH variation between the two aqueous mixtures was explained as follows. The pH of water decreases depending on the amount of dissolved CO_2, which is proportional to the concentration of CO_2 in gas phase according to Henry's law. Under air flow, the pH of aqueous CV mixture decreased by continuously supplied CO_2 in the gas phase and hardly increased afterward (Fig. 3-4 b, green squares). On the other hand, under Ar flow, CO_2 in the gas phase was removed with Ar and thus CO_2 evolved from aqueous CV mixture to be removed, which increased the pH gradually (Fig. 3-4 b, purple squares). Therefore, during the present photocatalytic reaction under Ar flow, CO_2 derived from CV mineralization was effectively removed from the reaction mixture to maintain the pH higher, which promoted CV adsorption and decomposition. In the case of the photocatalysis in air, CO_2 gas generated by CV decomposition remained in the closed reaction container. The estimated concentration of CO_2 was up to 3% (at 240 min-irradiation in Fig. 3-2 b) if the free space volume is the same as that of the solution and if all CO_2 go into the free space (gas phase).[14] This concentration is higher than that in air flow (ca. 0.04%). Accordingly, photocatalytic CV decomposition rate in air was slower than that under air flow and considerably slower than that under Ar flow. The solubility of Ar in water (3.37 cm^3/100 g, 20 ºC , 1 atm) is higher than those of N_2 (1.56 cm^3/100 g) and O_2 (3.10 cm^3/100 g), which might also contribute to remove CO_2 from aqueous CV mixture more effectively under Ar flow.

To confirm the speculation described above, photocatalytic CV decomposition on P25 under CO_2 flow and CV adsorption on P25 from CO_2-saturated water in air, namely, under much lower pH than that of aqueous CV mixture under air flow, were investigated. As expected, photocatalytic CV decomposition under CO_2 flow was suppressed if compared to that in air (Fig. 3-2a, gray circles). CV adsorption was also suppressed under such low pH and promoted immediately after applying Ar flow, namely, increasing pH (Fig. 3-4, gray circles). As described above (Fig. 3-3c), the amount of the adsorbed CV from the aqueous mixture on the photocatalytically inactive rutile during irradiation under Ar flow was larger than that in air, which was also due to the increase of the solution pH.

Judging from the above discussion, photocatalytic oxidations of CV or BV over TiO_2 in “buffered” water seems better choice for simple improvement of the activity since the pH control by adding some bases is very easy as compared to Ar flow. I conducted photocatalytic CV decomposition over P25 at an initial pH of 9 (the final one of 8) adjusted by an aqueous NaOH solution, revealing that the initial CV decomposition rate and the degree of CV mineralization were much lower than those observed under Ar flow (Fig. 3-2 a, black open circles vs purple squares). This result indicates again a merit of Ar flow to improve the activity of TiO_2 photocatalysis.

As the second possible factor for the improved TiO_2 photocatalysis depending on atmosphere gases, I considered the effects of gas adsorption on TiO_2 surface on the photocatalytic activity. Fig. 3-5 depicts the adsorption/desorption isotherms of N_2, O_2, or Ar on P25 at 77 K (at 298 K, all the gases hardly adsorbed). It was revealed that Ar adsorbed on P25 less effectively than did N_2 and O_2. Therefore, gases other than Ar might adsorb on TiO_2 to prevent organic dyes adsorption and decomposition. I cannot rule out the possibility that the adsorption behaviour of each gas on P25 from the gas phase is different from that from the aqueous solution.

Finally, I considered the possible deactivation of TiO_2 during the present reactions depending on atmospheres. It is well-known that the accumulation of carbon deposits on TiO_2 during the photocatalytic oxidation of organic compounds deactivates the photocatalytic activity.[15] Here I recovered TiO_2 after photocatalytic CV decomposition under different atmospheres at similar CV consumption (15, 120 and 240 min for Ar flow, air flow and air environments, respectively, in Fig. 3-2 a) and estimated the amounts of carbon deposits in these samples, giving the following sequence; in air (1.1 mass%) > under air flow (0.6 mass%) > under Ar flow (0.3 mass%) as shown in Fig. 3-6. This sequence was opposite to that of photocatalytic CV decomposition and CO_2 evolution rates. Therefore, the oxidized products of CV were removed (desorbed) more effectively from TiO_2 surface under Ar flow, which inhibited the accumulation of carbon deposits and thus preserved the original activity during the photocatalysis.

As to a possible reason for the improved desorption of the oxidized products of CV from TiO_2 under Ar flow, I consider that the nature of the reaction media plays an important role, because some literature have discussed the effects of natures, such as polarity and hydrophilicity/hydrophobicity, of reaction media for photocatalysts on the desorption of oxidized products and the photocatalytic activity.[16-20] As can be seen in Fig. 3-7, the hydrophilicity sequence of water saturated with CO_2, N_2, O_2 or Ar gas estimated as follows from the wettability on a fluorocarbon polymer (PTFE) substrate; $CO_2 > O_2 > Ar > N_2$. The change of UV-vis absorption spectra of CV during the photocatalysis over P25 in different environments showed that when CV consumption was low, e.g. in air or under O_2 flow, a new absorption band appeared at around 265 nm (Fig. 3-8), suggesting that the photocatalytic mechanism for CV degradation and decomposition under Ar flow is different to those in other environments (in such environments, larger amounts of intermediates which convert into carbon deposits are thought to be generated). Thus, aqueous CV mixture flowed with Ar, which has a well-balanced hydrophilic/hydrophobic nature, might be more compatible with the oxidized products of CV (or BV) having hydrophilic and hydrophobic functional groups, such as N-de-methylated intermediates and cleavage intermediates,[6, 7] than those flowed with the other gases.

As described above, photocatalytic CV decomposition over P25 did not depend on the Ar flow rate (Fig. 3-2 c), which suggests the importance of a balance of CO_2 removal and Ar dissolution. Also, pH control by NaOH was not effective to improve P25 photocatalysis (Fig. 3-2 a). Furthermore, when photocatalytic CV decomposition over P25 was conducted under an Ar atmosphere (150 kPa), but not Ar flow, the initial rate was slightly higher than that obtained in air (Fig. 3-9, purple pluses); on the other hand, a N_2 atmosphere (150 kPa) substantially lowered the activity (yellow pluses). These results strongly support our hypothesis that Ar acts not only to remove CO_2 (to control solution pH) but also to tune the hydrophilicity/hydrophobicity of solution and then to desorb the intermediate products of CV that convert into carbon deposits.

From all the results obtained, the present methodology, TiO_2 solar photocatalysis under Ar flow, seems be applicable to other photocatalytic reactions involving the adsorption of cationic reactants and the evolution of CO_2, such as the photocatalytic removal (recovery) of metals from water containing metal ions and hydrogen production from water which are often conducted in the presence of sacrificial reagents (e.g. alcohols, organic acids).

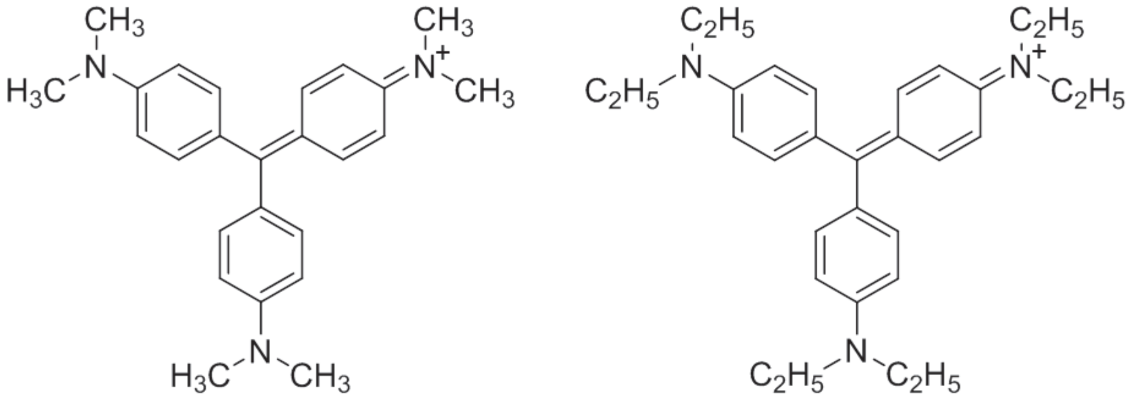

a *b*

Fig. 3-1 Structure of (a) crystal violet (CV) and (b) basic violet 4 (BV).

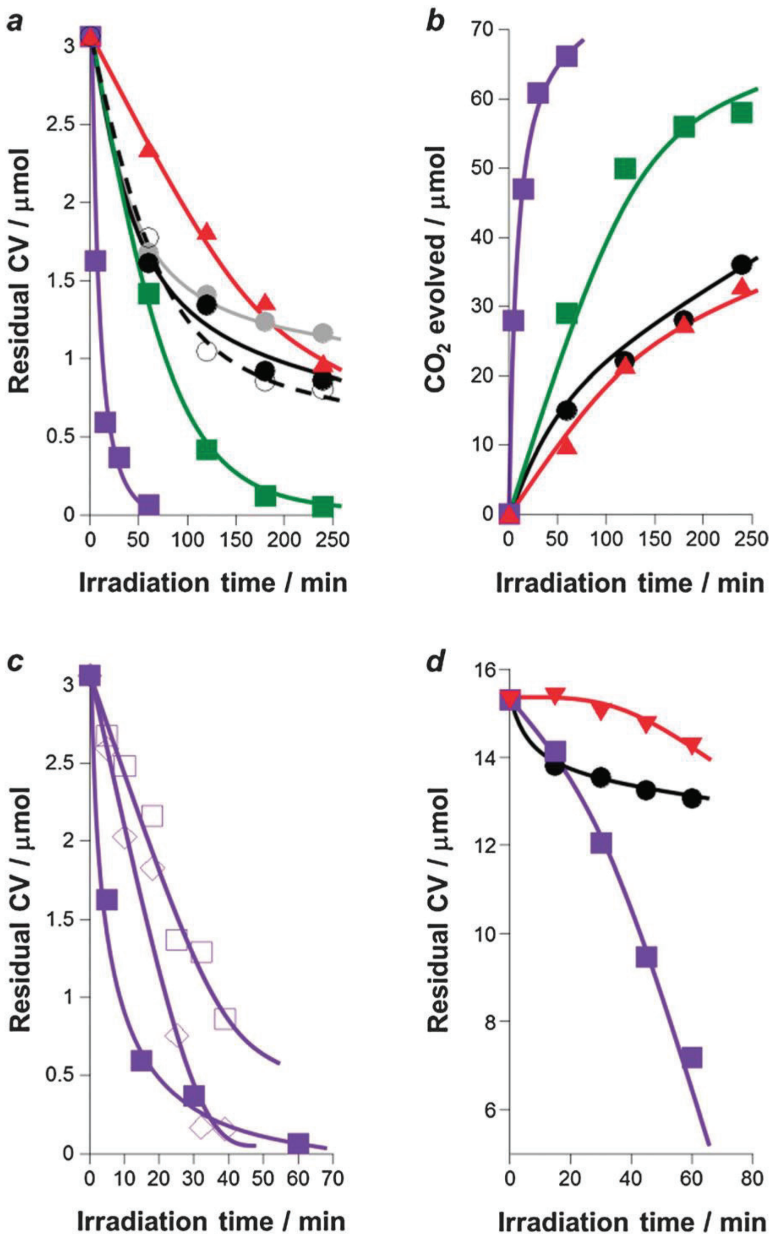

Fig. 3-2 a and b, time-course curves of photocatalytic decomposition of CV over P25 under various conditions (●) in air, (■) under air flow, (■) Ar flow, (▲) in air without dissolved O_2, (●) CO_2 flow, (○) in air at a higher pH and (▼) O_2 flow. (c) Time-course curves of CV decomposition over P25 under 0.05 (□), 0.1 (■) and (◇) 0.2 mL min^{-1} of Ar flow. d, time-course curves of photocatalytic decomposition of CV at a higher CVconcentration over P25 under various conditions (●) in air, (▼) O_2 flow and (■) Ar flow.

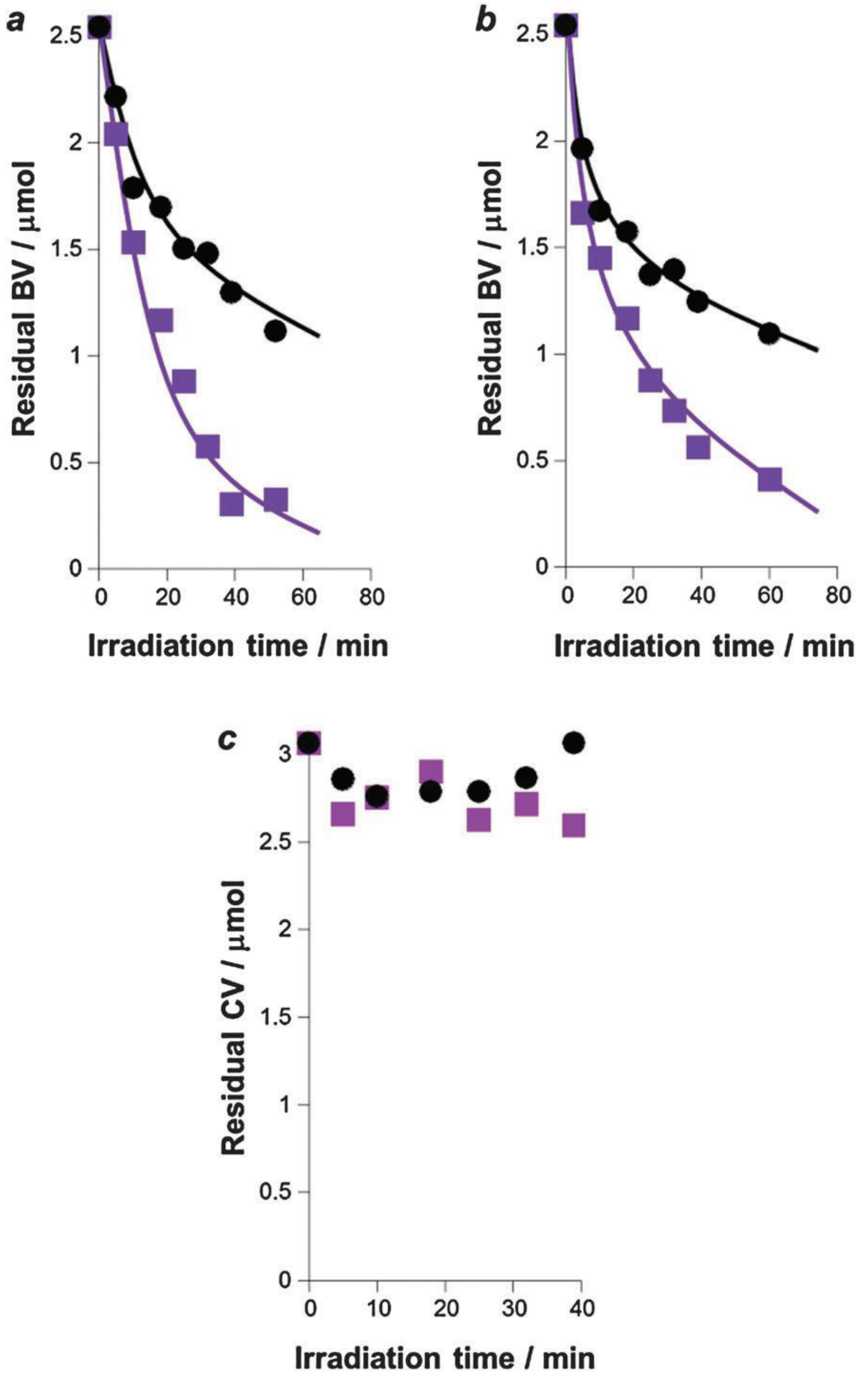

Fig. 3-3 Time course curves of BV decomposition over (a) P25 and (b) anatase in air (●) and under Ar flow (■). (c) Time-course curves of CV decomposition over rutile in air (●) and under Ar flow (■).

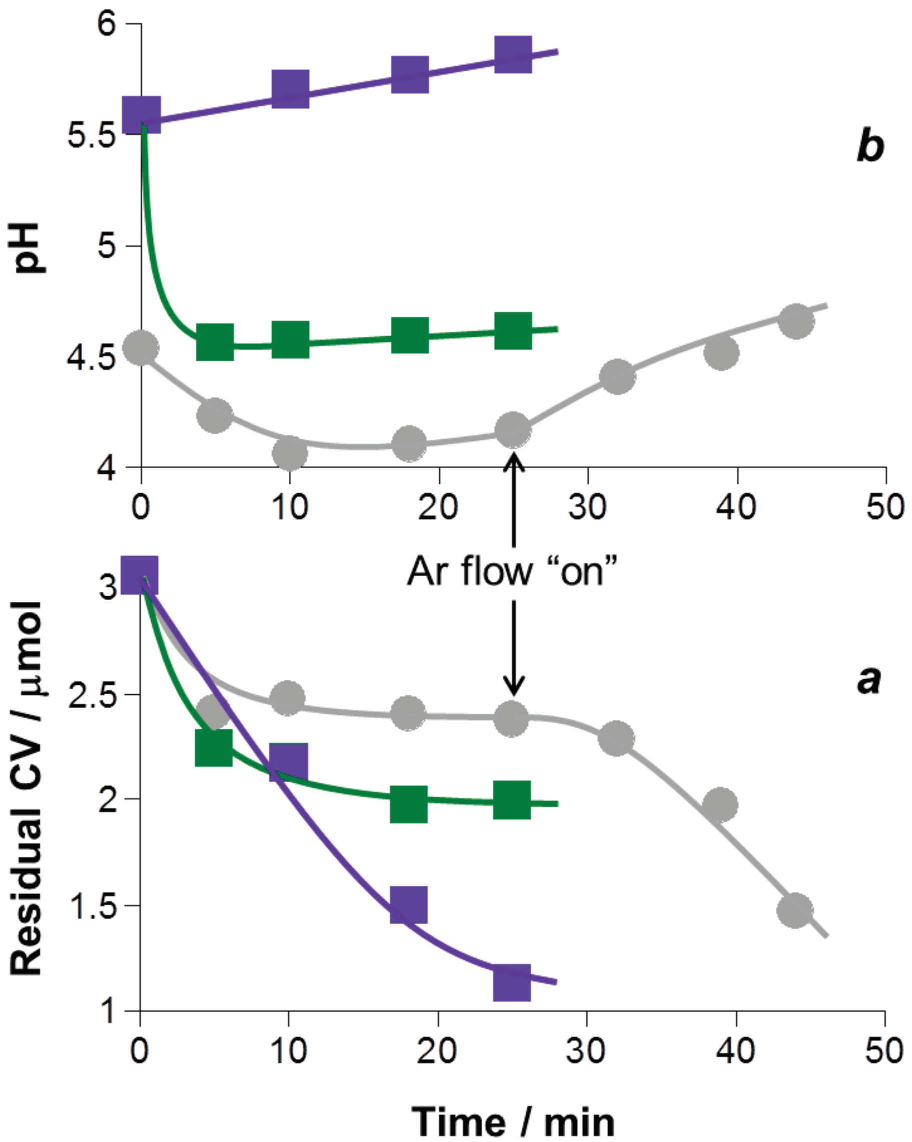

Fig. 3-4 Time-course curves of (a)amount of CV adsorbed from water on P25 under air flow (■), Ar flow (■) and CO_2-saturated water in air and then under Ar flow (●), and (b) pH of aqueous solution.

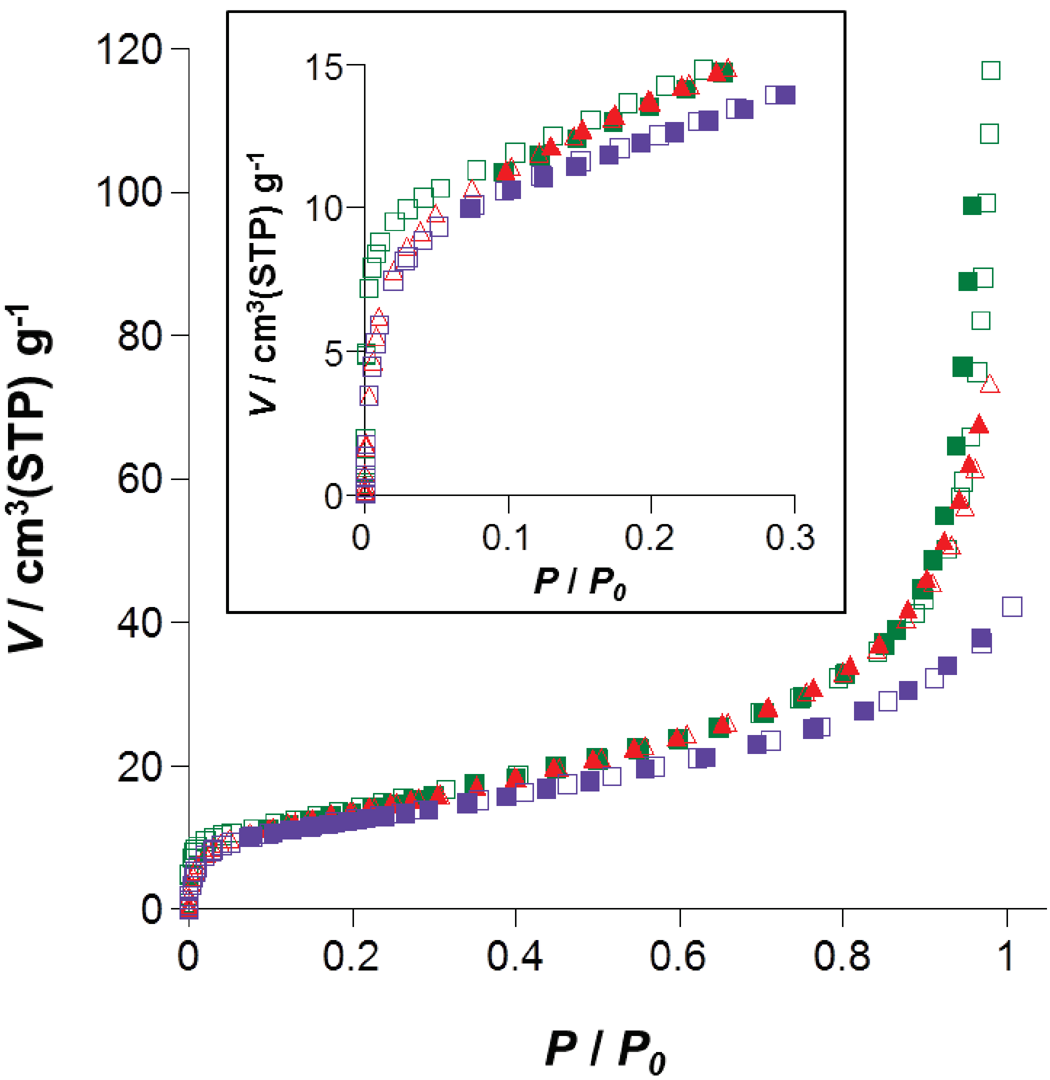

Fig. 3-5 Adsorption/desorption isotherms of (□/■) N_2, (△/▲) O_2, and (□/■) Ar on P25 at 77 K. Inset shows the expanded figure at lower partial pressure.

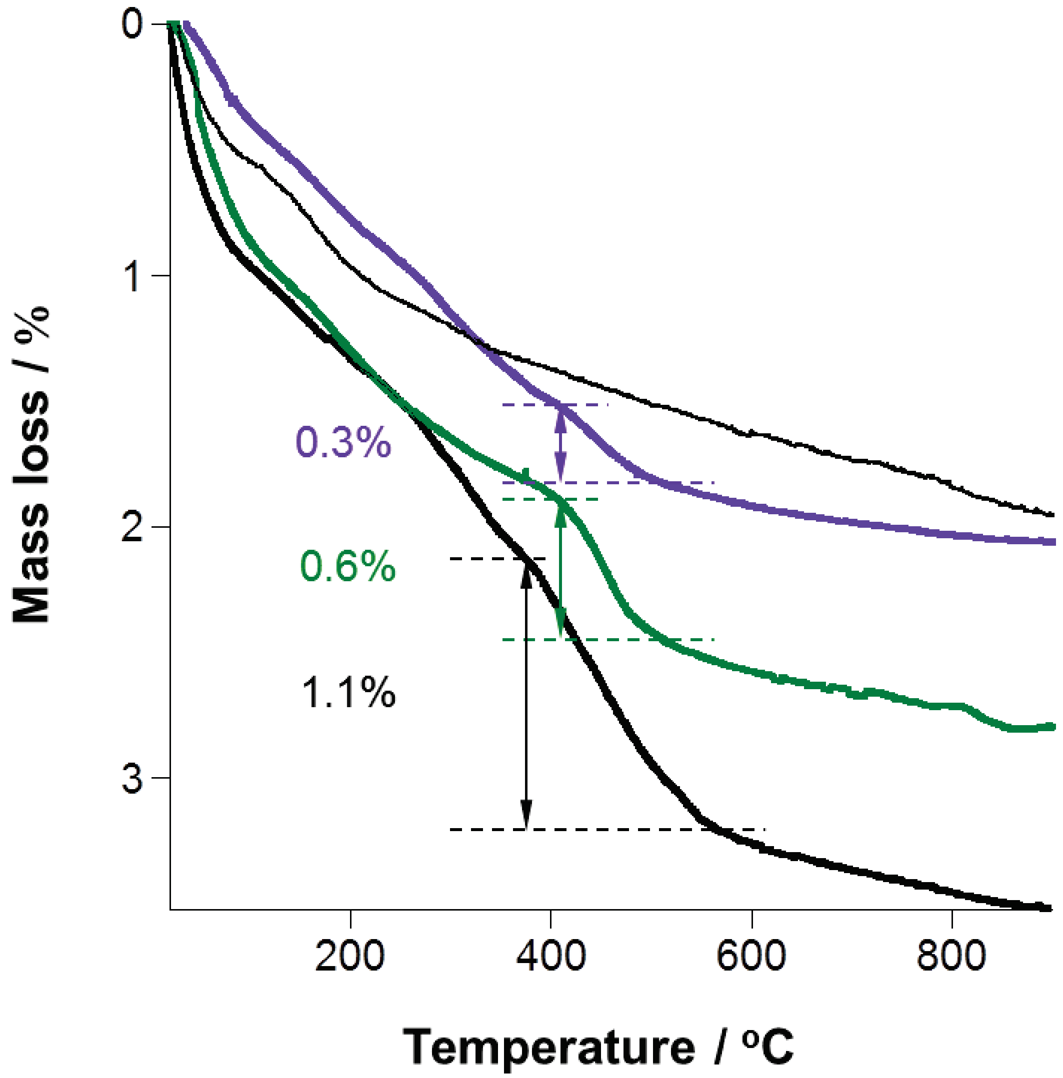

Fig. 3-6 Thermogravimetric curves recorded in air of (—) P25 and recovered P25 after photocatalytic CV decomposition (▬) in air for 240 min, (▬) under air flow for 120 min, and (▬) under Ar flow for 15 min.

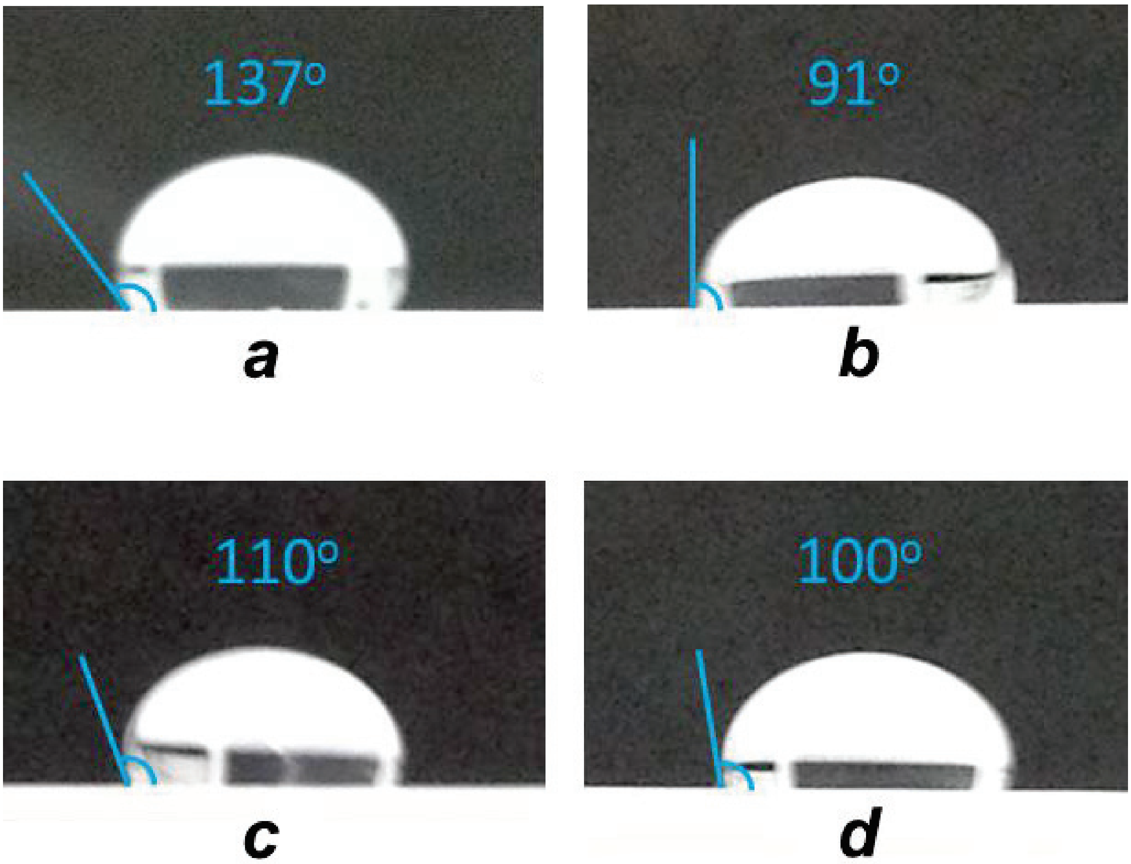

Fig. 3-7 (a) CO_2-, (b) N_2-, (c) O_2- and (d) Ar-saturated water contact angles on PTFE substrates.

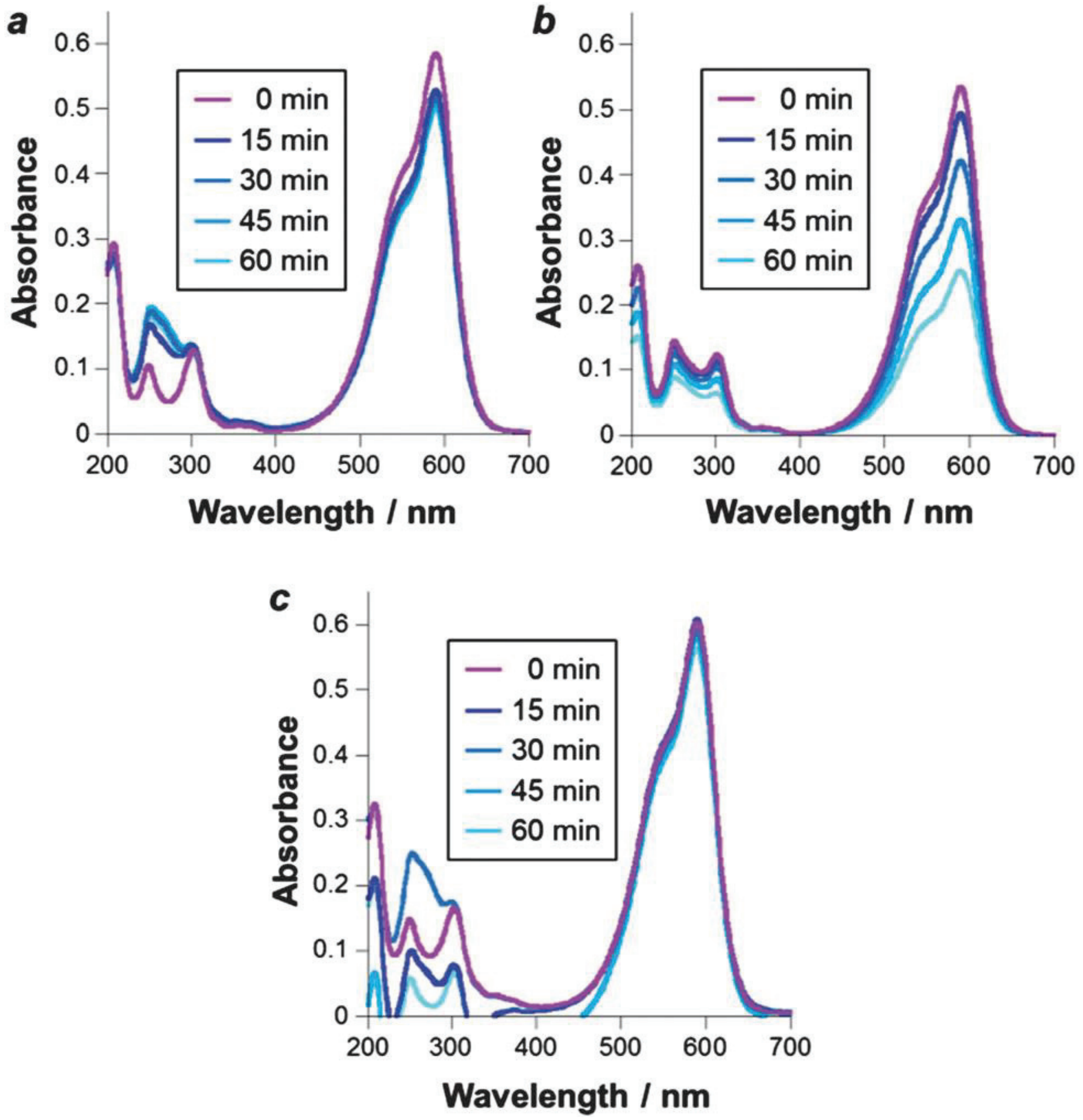

Fig. 3-8 Typical UV-vis absorption spectra of CV in water during the photocatalysis over P25 (a) in air, (b) under Ar flow and (c) under O_2 flow.

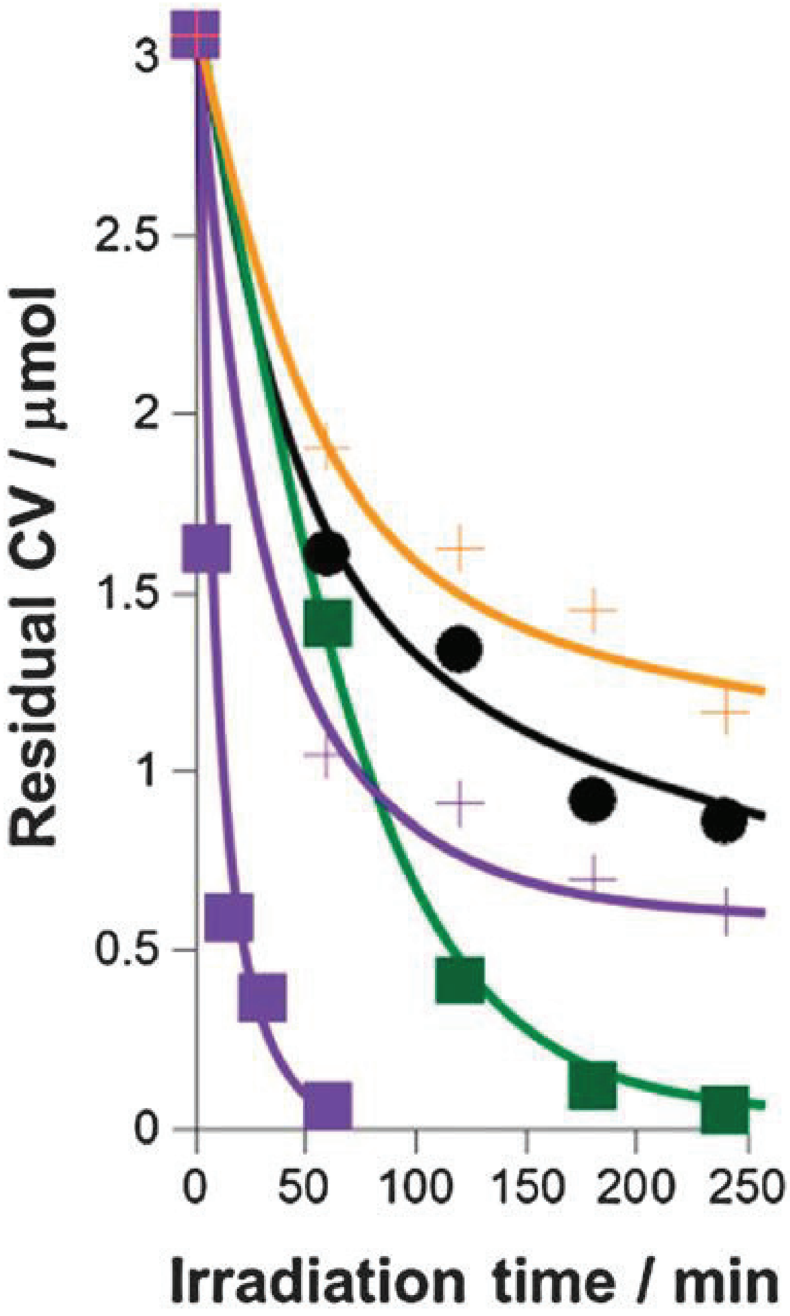

Fig. 3-9 Time-course curves of CV decomposition over P25 in air (●), under air flow (■) and Ar flow (■) and under an Ar atmosphere (+) and a N_2 atmosphere (+). Plots for (●), (■) and (■) were the same to those in Fig. 3-2a.

3-4. Conclusion

I have reported a conceptually new methodology to substantially improve the photocatalytic activity of TiO_2 under solar light irradiation, which is achieved by conducting the reaction under an Ar atmosphere. [21] Ar, a noble gas, is widely used as inert gas in industry but still scientifically investigated in a number of disciplines. I anticipate that many known photocatalytic processes are investigated under an Ar atmosphere to improve their photocatalytic activities and fully understand the reaction mechanisms.

3-5. References

[1] M. A. Fox and M. Dulay, Chem. Rev., 1993, 93, 341.

[2] R. Asahi, T. Morikawa, T. Ohwaki, K. Aoki and Y. Taga, *Science*, **2001**, *293*, 269.

[3] M. Anpo and M. Takeuchi, *J. Catal.*, **2003**, *216*, 505.

[4] A. Fujishima, X. Zhang and D. A. Tryk, *Surf. Sci. Rep.*, **2008**, *63*, 515.

[5] H. Tada, T. Kiyonaga and S. Naya, *Chem. Soc. Rev*., **2009**, *38*, 1849.

[6] N. Teshima, S. Yamamoto, Q. Zhang, Z. Yamada and T. Sasaki, *Bunseki Kagaku*, **2007**, *56*, 99.

[7] W.-L. Lee, S.-T. Huang, J.-L. Chang, J.-Y. Chen, M.-C. Cheng and C.-C. Chen, *J. Mol. Catal. A: Chem.*, **2012**, *361*, 80.

[8] A. B. Prevot, C. Baiocchi, M. C. Brussino, E. Pramaurp, P. Savarino, V. Augugliaro, G. Marci and L. Palmisano, *Environ. Sci. Technol.*, **2001**, *35*, 971.

[9] C. Chen and C. Lu, *J. Phys. Chem. C*, **2007**, *111*, 13922.

[10] B. Ohtani, O. O. Prieto-Mahaney, D. Li and R. Abe, *J. Photochem. Photobiol. A*, **2010**, *216*, 179.

[11] T. Ohno, K. Sarukawa, K. Tokieda and M. Matsumura, *J. Catal*., **2001**, *203*, 82.

[12] P. W. Schindler and H. Gamesjager, *Colloid Polym. Sci.*, **1972**, *250*, 759.

[13] B. Ohtani, Y. Okugawa, S. Nishimoto nad T. Kagiya, *J. Phys. Chem.*, **1987**, *91*, 3550.

[14] N. Iyi and H. Yamada, *Chem. Lett.*, **2010**, *39*, 591.

[15] H. Einaga, S. Futamura and T. Ibusuki, *Phys. Chem. Chem. Phys.*, **1999**, *1*, 4903.

[16] P. Boarini, V. Carassiti, A. Maldotti and R. Amadelli, *Langumuir*, **1998**, *14*, 2080.

[17] Y. Ide, M. Matsuoka and M. Ogawa, *ChemCatChem,* **2012**, *4*, 628.

[18] Y. Ide, N. Nakamura, H. Hattori, R. Ogino, M. Ogawa, M. Sadakane and T. Sano, *Chem. Commun*., **2011**, *47*, 11531.

[19] Y. Ide, H. Hattori, S. Ogo, M. Sadakane and T. Sano, *Green Chem*., **2012**, *14*, 1264.

[20] Y. Ide, R. Ogino, M. Sadakane and T. Sano, *ChemCatChem,* **2013**, *5*, 766.

[21] Y. Ide, H. Hattori and T. Sano, *Phys. Chem. Chem. Phys*., **2014**, *16*, 7913.

Chapter 4

Ternary modified TiO_2 as simple and efficient photocatalyst for green organic synthesis

4-1. Introduction

As described in chapter 2, designing novel photocatalysts for effective and selective synthesis of fine chemicals has been extensively investigated in recent years.[1-5] The co-doping with two kinds of heteroelements [6] and the co-modification with two kinds of nanoparticles [7] or organic dyes [8] of a semiconductor photocatalyst can provide better photocatalytic performance of the catalyst as a result of the improved charge separation efficiency and the broadening of light absorption spectra, and so on. The modification (grafting) of TiO_2 with Fe^{3+} or Ni^{2+} has been known to improve the UV-induced activity and impart the visible light response. [9, 10] Au nanoparticle modification (loading) has also been known to cause the same effects on TiO_2. [11-13] On the other hand, Au nanoparticle modification on TiO_2 has been reported to drastically decrease the amount of the surface titanol, [14] which promotes the desorption of partially oxidized products from the catalyst surface, thus preventing the successive oxidation. [15] These reports motivate me to design TiO_2-based photocatalysts by the appropriate surface modification.

In chapter 2, I found that partial oxidation of cyclohexane, which is industrially very important reaction, selectively proceeds under simulated sunlight irradiation when using TiO_2 modified with Fe [16]. Although the selectivity was almost 100%, however, the yield is low and further improvement of the catalytic activity for practical application is necessary. In this chapter, I report, for the first time, the usefulness of the ternary modification of TiO_2 for substantially improving the photocatalytic organic synthesis activity, which is revealed by the fact that TiO_2 ternary-modified with Fe^{3+}, Ni^{2+}, and Au nanoparticles shows an unprecedentedly high photocatalytic efficiency for selective cyclohexane oxidation under sunlight irradiation.

4-2. Experimental

Reagents and materials

P25 was supplied by Nippon Aerosil. Gold (III) chloride trihydrate ($HAuCl_4 \cdot 3H_2O$) was purchased from SIGMA-ALDRICH. Fe(III)acetylacetonate ($Fe(acac)_3$), Ni(II) acetylacetonate ($Ni(acac)_2$), ethanol, hexane, naphthalene and NaOH were purchased from Wako Pure Chemical Industries, Ltd. Cyclohexane (named as CHA) and acetonitrile were purchased from Nacalai tesque Ltd. All reagents and materials were used as received.

Synthesis of ternary-modified TiO_2 with Fe^{3+}, Ni^{2+}, and Au nanoparticles (named as Fe/Ni/Au@P25)

Fe@P25 or Ni@P25 was prepared according to the literature: [18, 10] 1.0 g of P25 was added to 6.5×10^{-4} mol L^{-1} of iron(III) acetylacetonate (or nickel(II) acetylacetonate) in a mixed solvent (100 mL, ethanol/hexane = 3:17 v/v) and the mixture was stirred at room temperature for 24 h. The product was separated by centrifugation (3000 rpm, 20 min), washed repeatedly with the same solvent, and calcined at 500 ºC for 1 h. Fe/Ni@P25 was prepared by reacting 1.0 g of Ni@P25 with 6.5×10^{-4} mol L^{-1} of the iron complex in the mixed solvent followed by washing and calcination. Au@P25 was prepared by a deposition-precipitation method. P25 was added to an aqueous solution of $HAuCl_4 \cdot 3H_2O$ (400 mL, Au/TiO_2 ratio is 2 wt%) in which pH was adjusted to be 10 by 0.2 mol L^{-1} of an aqueous NaOH solution, and the mixture was ultrasonicated for 1 h and then stirred at 70 ºC for 2 h. The product was separated by ultracentrifugation (18000 rpm, 20 min), washed with water, and dried at 100 ºC overnight. Finally, the powder was calcined at 500 ºC in air for 4 h. Fe/Ni/Au@ P25 was synthesized by modifying Au@P25 (1.0 g) with Ni and Fe sequentially using the nickel and iron complexes (6.5 x 10^{-4} mol L^{-1} for each compound), respectively.

Oxidation of cyclohexane

Photocatalytic conversions were carried out by photo-irradiation with solar simulator (San-Ei Electric Co., Ltd.) to a mixture of catalyst (30 mg) and O_2-saturated acetonitrile (18 mL) solution of cyclohexane (2 mL) in a stainless-made closed container equipped with Pyrex glass (75 mL) at 42 ºC, under shaking. The container was placed by ca. 30 cm away from the light source to irradiate 1 solar (1000 w m^{-2})-power light to the mixture. For action spectra measurement, the full arc from a 500 W-Xe lamp (Ushio) was monochromated using SM-25 (Bunkoukeiki) and then irradiated to the mixture. Spectra and light intensity of monochromated Xe lamp were determined using a spectroradiometer USR-45D (Ushio). CO_2 and organic compounds were quantitatively analyzed by GC. Naphthalene was used as internal standard.

Measurement of action spectrum

For action spectra measurement, the full arc from a 500W-Xe lamp (Ushio) was monochromated using SM-25 (Bunkokeiki) and then irradiated mixture of catalyst (60 mg), O_2-saturated acetonitrile (18 mL) solution of cyclohexane (2 mL) in a stainless-made closed container equipped with Pyrex glass (75 mL). After analyzing gas phase, the irradiation was started for 24 h. Organic compounds recovered by filtration, and the resulting supernatant was analyzed by GC-FID (Shimazu GC-2014). Naphthalene was used as internal standard for GC-FID.

Adsorption of CHA on photocatalyst

Adsorption test were similar way that conducted in photocatalytic conversions exept that catalyst and an acetonitrile solution (20mL) containing CHA (1mL) and CHA-one (0.001-0.01 mL), which was not bubbled with O_2, were shaken in dark. Naphthalene was used as internal standard for GC-FID.

Analysis equipment and evaluation condition

Apparatus using for characterization of synthesis catalysts and quantification of substrate and products of photocatalytic test were shown below. Diffused reflectance UV-vis spectra measured with ultraviolet-visible near-infrared spectrophotometer (Nihonbunko, JASCO V-570). Measurement wavelength range were 200 - 800 nm, and $BaSO_4$ used for baseline. The successful surface modification of TiO_2 was confirmed by the X-ray Photoelectron Spectroscopy (XPS, Shimadzu, Kratos ESCA-3400). Coupled Plasma Atomic Emission Spectroscopy (ICP-AES, Seiko Instruments Inc., SPS7700) was used for confirming the amounts of the grafted Fe^{3+} and Ni^{2+}. Transmission electron microscopic (TEM) images were obtained with a JEOL JEM-2011.

4-3. Result and discussion

4-3-1. Characterization of catalysts

The successful surface modification of TiO_2 was confirmed by the XPS and TEM-EDS analyses of Fe/Ni/Au@ P25. Fig. 4-1 shows XPS spectra of Fe/Ni/Au@ P25. Peaks attributed to $Fe^{3+,}$ Ni^{2+}, and Au^0, which are reported for Fe^{3+} [9], Ni^{2+-} (or NiO^-),[10] and Au nanoparticle-modified TiO_2,[19] respectively, were observed. Fig. 4-2 shows the TEM image of Fe/Ni/Au/@P25, in which Au nanoparticles with a size of 5–10 nm were deposited on the TiO_2 surface. In the EDS spectrum (Fig. 4-2 inset), Fe, Ni, and Au, as well as Ti and O, were detected (Cu was also detected since a carbon-coated Cu grid was used for observation). The ICP analysis of the dissolved product confirmed that the amounts of the grafted Fe^{3+} and Ni^{2+} were 0.20 and 0.17 wt% (equivalent to 0.44 and 0.36 groups nm^{-2}), respectively. In the HRTEM image of Fe/Ni/Au@P25 (Fig. 4-3), particles smaller than 1 nm were observed, suggesting the formation of clusters such as NiO[10] on TiO_2.

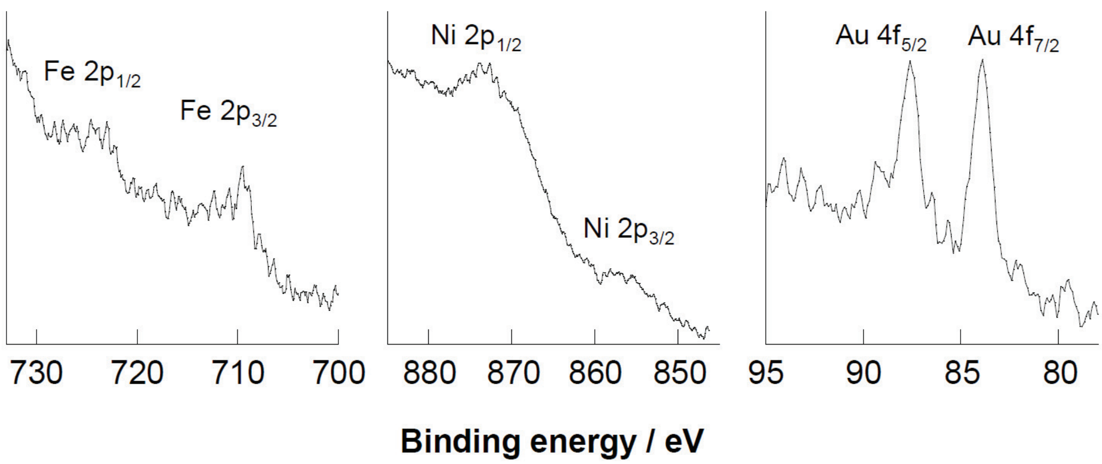

Fig. 4-1 Fe2p-, Ni2p- and Au4f-XPS spectra of Fe/Ni/Au@P25.

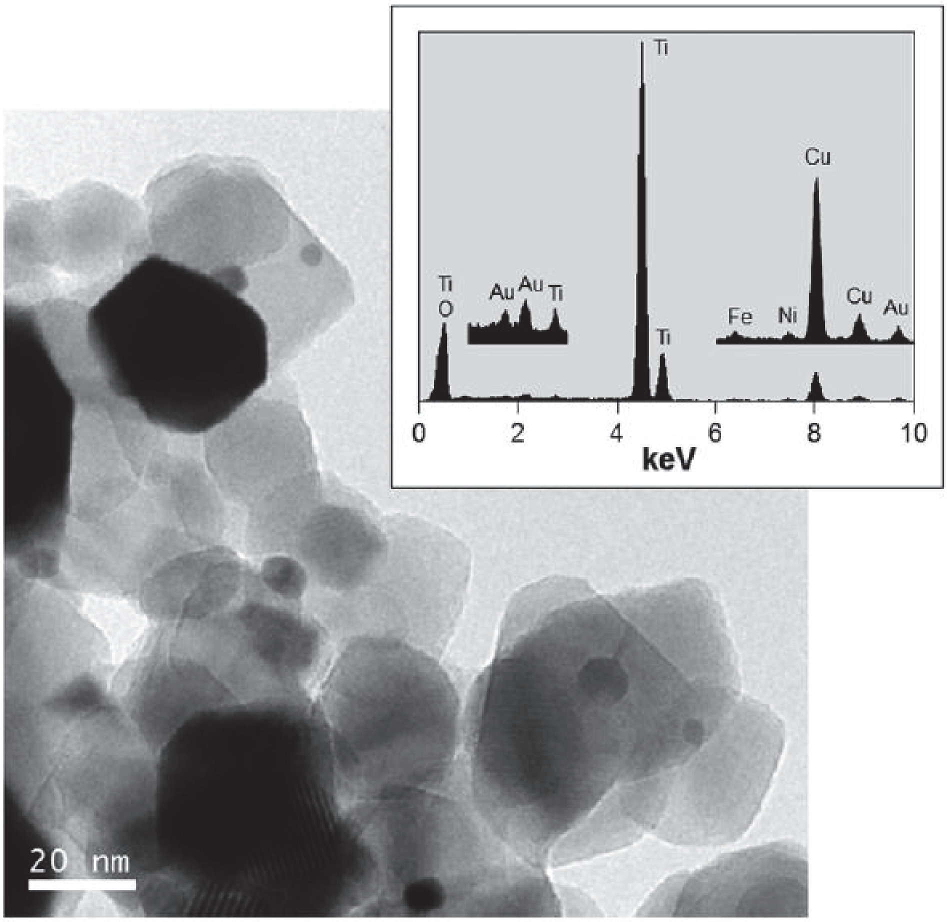

Fig. 4-2 TEM image and EDX spectrum of Fe/Ni/Au@P25.

Fig. 4-3 HRTEM image of Fe/Ni/Au@P25. Dashed circle indicates typical particles smaller than 1 nm.

4-3-2. Photocatalytic and adsorption test

Photocatalytic test

The photocatalytic cyclohexane (named as CHA) conversions were carried out under photoirradiation of Fe/Ni/Au@P25, Ni@P25, Au@P25, Fe/Ni@P25 and pristine P25 in an O_2-saturated acetonitrile solution containing cyclohexane by a simulated solar light. Table 4-1 summarizes the yields of cyclohexanone (named as CHA-one), cyclohexanol (named as CHA-ol), and CO_2 (only the three compounds were detected in gas chromatography), and the efficiency and selectivity for the partial oxidation. With P25, Ni@P25, Au@P25 or Fe/Ni@P25, the amount of CO_2 evolved was much larger than those of CHA-one and CHA-ol (Table 4-1, entries 1–4), indicating that the once-formed CHA-one and CHA-ol were successively decomposed to CO_2.[20] On the other hand, under the identical conditions, Fe/Ni/Au@P25 produced CHA-one and CHA-ol with 91% selectivity (entry 5). It should be noted here that Fe/Ni/Au@P25 gave a high selectivity (91%) even at a cyclohexane conversion (0.97%) higher than that (0.94%) attained on TiO_2 (entries 1 and 5). Such high activity observed on Fe/Ni/Au@P25 is worth mentioning, because (i) a >90% selectivity at cyclohexane conversion up to 1% has never been reported for heterogeneous photocatalytic systems and (ii) in the current commercial aerobic oxidation process CHA conversion is kept at 4% to give 70–85% partial oxidation selectivity.[21] Furthermore, Fe/Ni/Au@P25 was reusable for further reactions: typically, the catalyst recovered after reaction (entry 5), when used after simple washing with acetonitrile, showed almost the same cyclohexane conversion and partial oxidation selectivity as the virgin catalyst (entry 6). All the results obtained indicate high oxidation selectivity and efficiency of Fe/Ni/Au@P25.

The mechanism of the highly active Fe/Ni/Au@P25 was considered. Depicted in Fig. 4-4 is the UV-Vis diffused reflectance spectrum of Fe/Ni/Au@P25 together with those of Fe/Ni@P25, Ni@ P25, Au@P25, P25, and Fe@P25). After the modification with Fe^{3+} or Ni^{2+}, TiO_2 absorbed visible light at around 420 nm. Similar phenomena have been reported for Fe^{3+}- or Ni^{2+}-modified TiO_2 obtained by procedures that were used to prepare the present Fe@P25 and Ni@P25 and thus explained by the formation of the surface d sub-band of the grafted Fe or Ni species.[18, 10] Noticeably, the co-modification of TiO_2 with Fe^{3+} and Ni^{2+} further broadened the visible light absorption. The action spectrum of CHA-one and CHA-nol formation on Fe/Ni@P25 was in good agreement with the UV-Vis spectrum of Fe/Ni@P25 (Fig. 4-5). Therefore, Fe/Ni@P25 gave higher CHA conversion than Ni@P25 (Table 4-1, entries 2 and 3) due to the broadening of visible light absorption spectra. CHA conversion on Fe/Ni@P25 (and Ni@P25) was considerably lower than that on P25 (Table 4-1, entries 1–3), which is explained as follows. In the photocatalytic formation of CHA-one and CHA-ol on TiO_2, the cyclohexyl radical, formed by the reaction of cyclohexane with either the valence band hole or the hydroxyl radical derived from the reduction of OH^- with the valence band hole, is considered to be a key intermediate and is oxidized by oxidizing species such as the hydroxyl radical and the superoxide anion, which is generated by the reduction of O^2 with the conduction band electron, to give CHA-one and CHA-ol. [22] When Fe/Ni@P25 absorbs the visible light spectrum of sunlight, electrons in the surface d sub-bands of the grafted Fe and Ni are excited to the conduction band of TiO_2, leaving holes in the surface d sub-bands.[18] The absorption of the UV light spectrum of sunlight by Fe/Ni@P25 leads to electron excitation from the valence band of TiO_2 to the conduction band and the generated holes can transfer from the valence band to the surface d subbands.[18] The excited electrons effectively reduce O_2 to the superoxide anion. On the other hand, the hole oxidation power of the surface d sub-bands is considerably lower than that of TiO_2.[18, 16] Accordingly, when irradiated by sunlight (UV and visible light), Fe/Ni@P25 (and Ni@P25) forms a smaller amount of oxidizing species than P25, giving lower cyclohexane conversion. The co-modification of TiO_2 with Fe^{3+} and Ni^{2+}, therefore, caused both the broadening of light absorption and the modulation of the oxidation power.

Next, the role of Au nanoparticles in the photocatalysis of Fe/Ni/Au@P25 was considered. As can been seen in Fig. 4-6, the action spectrum of CHA-one and CHA-ol formation on Fe/Ni/Au@P25 was in agreement with the UV-Vis spectrum of Fe/Ni@P25 rather than Fe/Ni/Au@P25. Au nanoparticles also did not enhance the UV light-induced activity of TiO_2 for the present reaction, which was revealed by the fact that CHA conversion of P25 was higher than that of Au@P25 (Table 4-1, entries 1 and 4). Although modifying TiO_2 with Au nanoparticles has been known to enhance the UV light-induced activity and impart the visible light response activity,[11-13] in the present case, I should consider other reasons for more effective and selective CHA oxidation on Fe/Ni/Au@P25 than Fe/Ni@P25 (Table 4-1, entries 3 and 5). Fig. 4-7 depicts the time-dependent change in the yield of CHA-one, CHA-ol, and CO_2 during the photooxidation of cyclohexane over P25, Fe/Ni@P25, and Fe/Ni/Au@P25. During a relatively short irradiation period (>6 h), Fe/Ni@P25 and Fe/Ni/Au@P25 exhibited similar yields of CHA-one, CHA-ol, and CO_2. However, when irradiated for a longer time, Fe/Ni/Au@P25 showed the increase of CHA-one and CHA-ol yields with the suppression of CO_2 formation, which was due to the inhibition of the successive oxidation of the partially oxidized products. This factor is discussed in the next section.

Table 4-1 Oxidation of cyclohexane (CHA) to cyclohexanone (CHA-one) and cyclohexanol (CHA-ol) under simulated solar light[a].

Entry	Catalyst	Yield / μmol			CHA conversion / %[b]	[CHA-one + CHA-ol] selectivity / %[c]
		CHA-one	CHA-ol	CO_2		
1	TiO_2 (P25)	93.4	14.2	399.8	0.94	62
2	Ni@P25	7.1	9.6	102.7	0.18	49
3	Fe/Ni@P25	14.4	8.4	136.4	0.25	50
4	Au@P25	37.8	11.1	162.6	0.41	64
5	Fe/Ni/Au@P25	82.5	80.0	99.0	0.97	91
6	Fe/Ni/Au@P25 [d]	82.3	80.4	97.9	0.97	91

[a] Reaction conditions: substrate, cyclohexane (2 mL); solvent, acetonitrile (18 mL) saturated with O_2; catalyst, 30 mg; simulated solar light (λ > 320 nm) irradiation time, 24 h; temperature, 42 °C. [b] {[Formed CHA-one] + [formed CHA-ol] + 1/6[formed CO_2]}/[added CHA]×100. [c] {[Formed CHA-one] + [formed CHA-ol]}/{[formed CHA-one] + [formed CHA-ol] + 1/6[formed CO_2]}×100. [d] Reused after washing with acetonitrile.

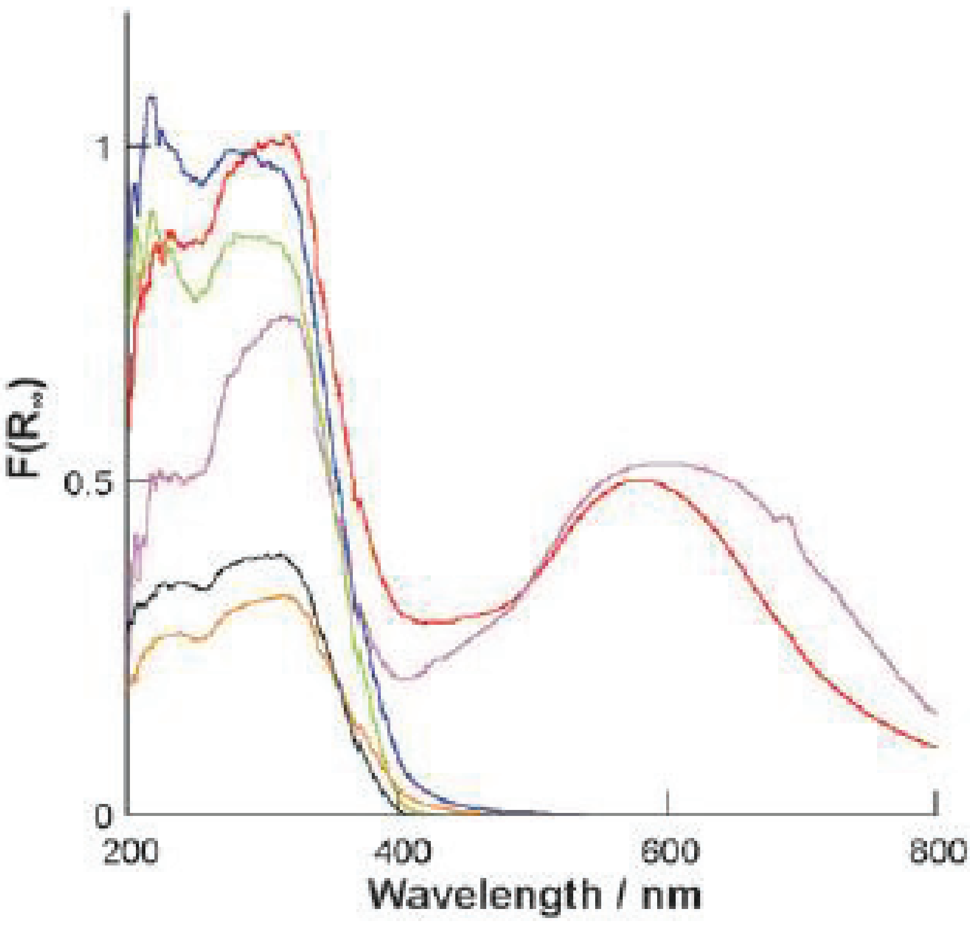

Fig. 4-4 UV-Vis diffused reflectance spectra of P25 (—) , Fe@P25 (—) , Ni@P25 (—) , Fe/Ni@P25 (—) , Au@P25 (—) and Fe/Ni/Au@P25 (—) .

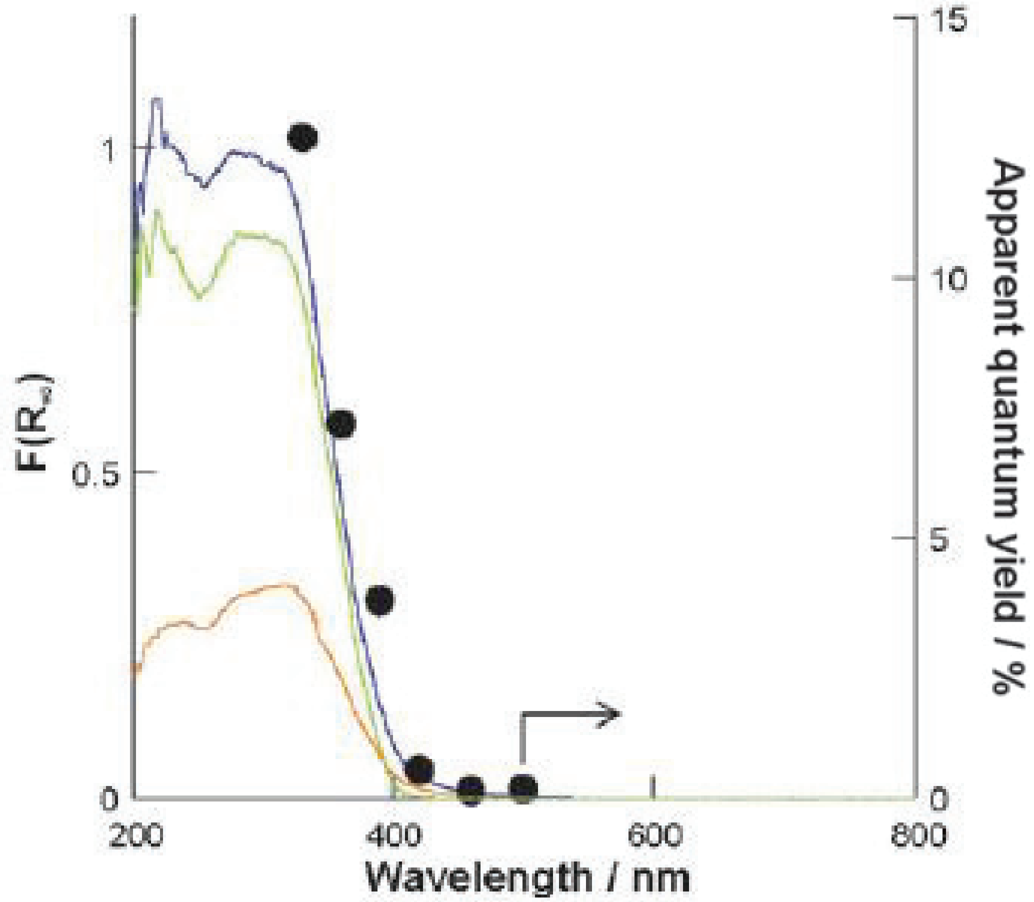

Fig. 4-5 UV-Vis spectra of Fe@P25 (—) , Ni@P25 (—) and Fe/Ni@P25(—) , and action spectra of cyclohexanone and cyclohexanol formation on Fe/Ni@P25.

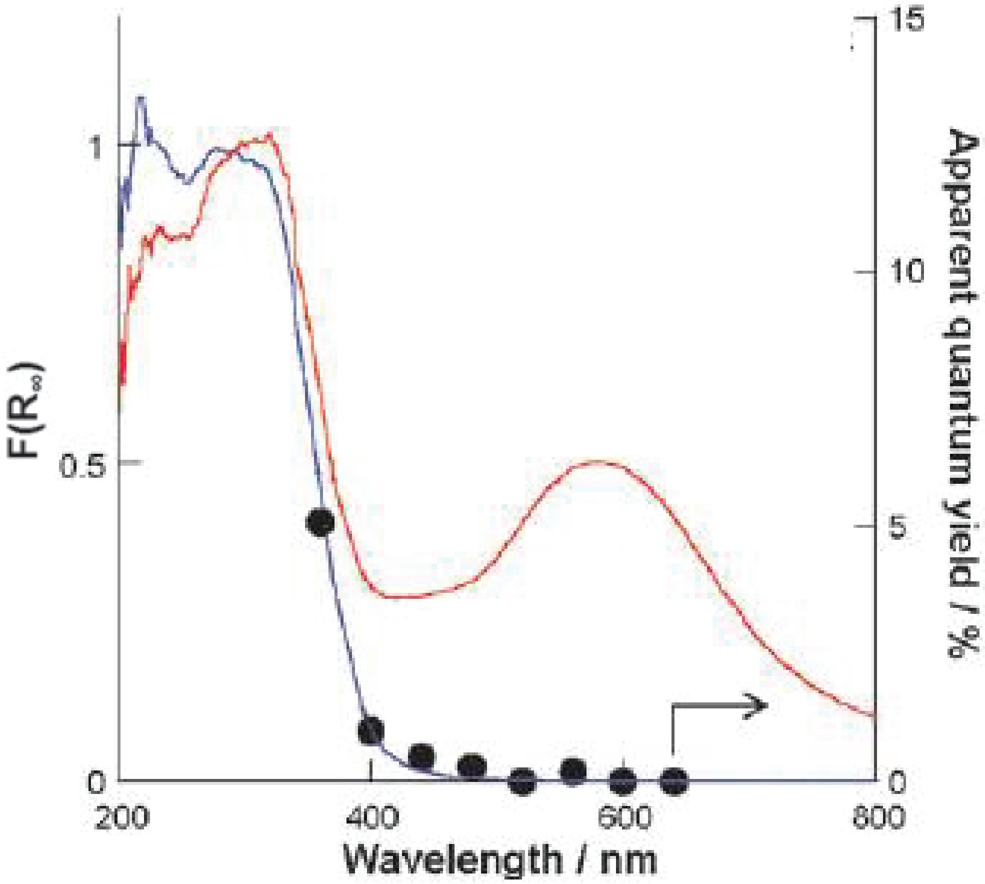

Fig. 4-6 UV-Vis spectra of Fe/Ni@P25 (—) and Fe/Ni/Au@P25 (—) , and action spectra of cyclohexanone and cyclohexanol formation on Fe/Ni@P25.

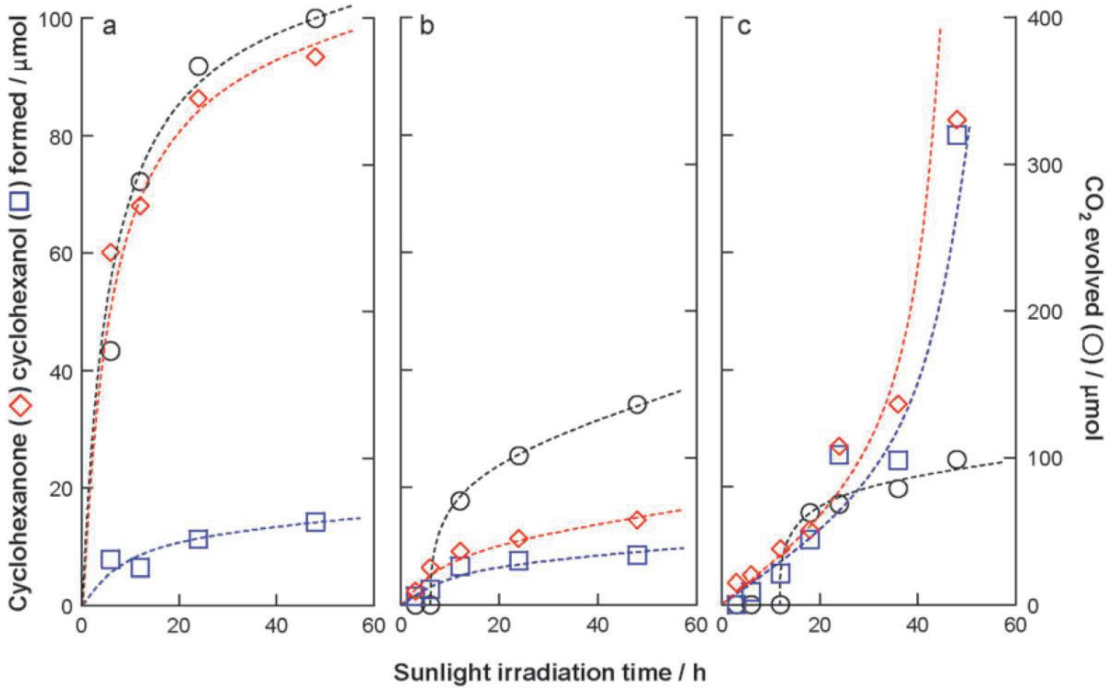

Fig. 4-7 Time-dependent formation of cyclohexanone (◇) , cyclohexanol (□) , and CO_2 (○) during photocatalytic cyclohexane oxidation on (a) P25, (b) Fe/Ni@P25 and (c) Fe/Ni/Au@P25.

Adsorption of CHA-one on photocatalysts

To confirm above hypothesis, suppression of the successive oxidation of the partially oxidized products, I examined the adsorption of a product CHA-one on Fe/Ni/Au@P25. Fig. 4-8 compares the adsorption isotherm of CHA-one from an acetonitrile solution containing CHA and CHA-one on Fe/Ni/Au@P25 with those on P25, Fe/Ni@P25, and Au@P25. It was apparent that when modified with Au nanoparticles, P25 adsorbed a smaller amount of CHA-one. Accordingly, Fe/Ni/Au@P25 desorbs the once-formed CHA-one (and CHA-ol) easily, as compared to Fe/Ni@P25, to prevent the successive oxidation, giving a larger amount of CHA-one and CHA-ol and a smaller amount of CO_2. It is difficult to clearly explain a reason for improved desorption of CHA-one from TiO_2 after the modification with Au nanoparticles at this point. However, it has been reported that the amount of surface titanol, which can interact with cyclohexanone, on TiO_2 is dramatically reduced during the deposition of Au nanoparticles on the surface.[14, 15] I cannot rule out the possibility that cluster-level Au particles (Fig. 4-3) effectively occupy the surface titanol group of TiO_2.

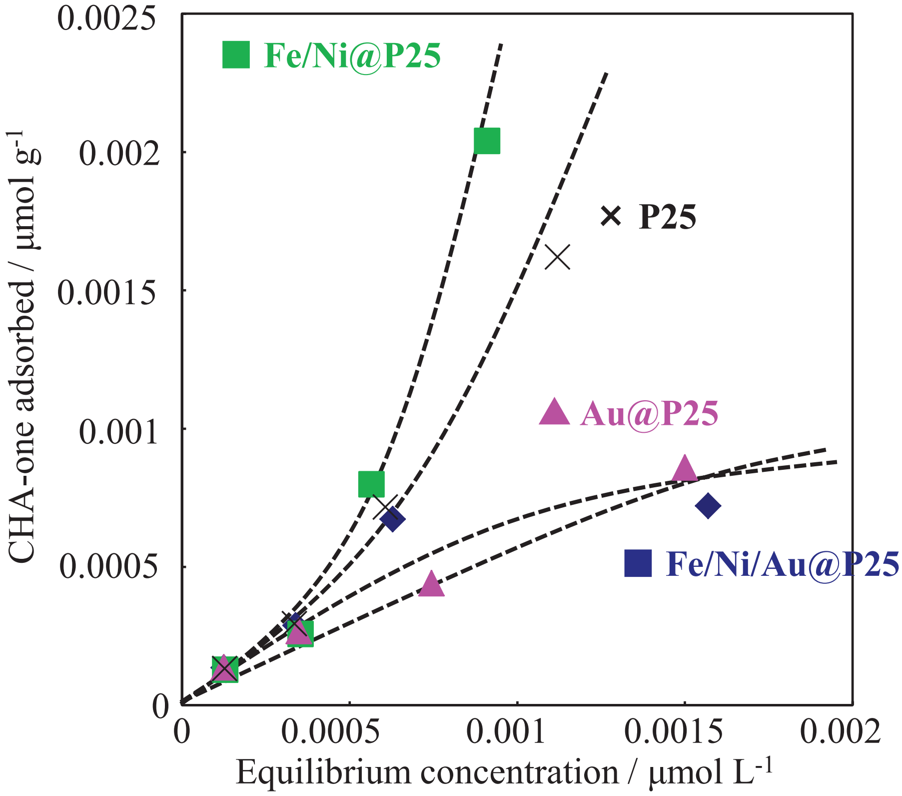

Fig. 4-8 Adsorption isotherms of cyclohexanone from an acetonitrile solution containing cyclohexane and cyclohexanone on P25 (×) , Fe/Ni@P25 (■) , Au@P25 (▲) and Fe/Ni/Au@P25 (■) .

4-4. Conclusion

The surface modification of TiO_2 with Fe^{3+}, Ni^{2+}, and Au nanoparticles has given rise to a noticeable photocatalytic activity for selective cyclohexane oxidation with O_2 under sunlight irradiation.[23] The surface modification of TiO_2 with three kinds of functional units can be a simple and useful way to attain green organic synthesis.

4-5. References

[1] M. A. Fox and M. Dulay, *Chem. Rev.*, **1993**, *93*, 341.

[2] A. Maldotti, A. Molinari and R. Amadelli, *Chem. Rev.*, **2002**, *102*, 3811.

[3] Y. Shiraishi and T. Hirai, *J. Photochem. Photobiol. C*, **2008**, *9*, 157.

[4] O. Tomita, R. Abe and B. Ohtani, *Chem. Lett.*, **2011**, 1405.

[5] S. Fukukawa, T. Shishido, K. Teramura and T. Tanaka, *ACS Catal.*, **2012**, *2*, 175.

[6] T. Ikeda, T. Nomoto, K. Eba, Y. Mizutani, H. Kato, A. Kudo and H. Onishi, *J. Phys. Chem. C*, **2008**, *112*, 1167.

[7] H. Tada, T. Mitsui, T. Kiyonaga, T. Akita and K. Tanaka, *Nat. Mater.,* **2006**, *5*, 782.

[8] D. Kuang, P. Walter, F. Nuuesch, S. Kim, J. Ko, P.Comte, S. M. Zakeeruddin, M. K. Nazeeryddin and M. Gratzel, *Langmuir*, **2007**, *23*, 10906.

[9] H. Yu, H. Irie, Y. Shimodaira, Y. Hosogi, Y. Kuroda, M. Miyauchi and K. Hashimoto, *J. Phys. Chem. C*, **2010**, *114*, 16481.

[10] Q. Jin, T. Ikeda, M. Fujishima and H. Tada, *Chem. Commun.*, **2011**, *21*, 20.

[11] H. Tada, T. Kiyonaga and S. Naya, *Chem. Soc. Rev.*, **2009**, *38*, 1849.

[12] Y. Tian and T. Tatsuma, *J. Am. Chem. Soc.*, **2005**, *127*, 7632.

[13] E. Kowalska, R. Abe and B. Ohtani, *Chem. Commun.*, **2009**, 241.

[14] J. T. Carneiro, C.-C. Yang, J. A. Moma, J. A. Moulijn and G. Mul, *Catal. Lett.*, **2009**, *129*, 12.

[15] Y. Ide, R. Ogino, M. Sadakane and T. Sano, *ChemCatChem,* **2013**, *5*, 766.

[16] Y. Ide, H. Hattori, S. Ogo, M. Sadakane and T. Sano, *Green Chem.*, **2012**, *14*, 1264.

[17] C. G. Silva, R. Juarez, T. Marino, R. Molinari and H. Garcia, *J. Am. Chem. Soc.*, **2011**, *133*, 595.

[18] H. Tada, Q. Jin, H. Nishijima, H. Yamamoto, M. Fujishima, S. Okuoka, T. Hattori, Y. Sumida and H. Kobayashi, *Angew. Chem. Int. Ed*., **2011**, *50*, 3501.

[19] D. Tsukamoto, Y. Shiraishi, Y. Sugano, S. Ichikawa, S. Tanaka and T. Hirai, *J. Am. Chem. Soc*., **2012**, *134*, 6309.

[20] D. Tsukamoto, A. Shiro, Y. Shiraishi and T. Hirai, *J. Phys. Chem. C*, **2011**, *115*, 19782.

[21] Y. Shiraishi, N. Saito and T. Hirai, *J. Am. Chem. Soc*., **2005**, *127*, 12820.

[22] C. B. Almquist and P. Biswas, *Appl. Catal. A*, **2001**, *214*, 259.

[23] Y. Ide, N. Kawamoto, Y. Bando, H. Hattori, M. Sadakane and T. Sano, *Chem. Commun.*, **2013**, *49*, 3652.

Chapter 5

Efficient and selective photocatalytic cyclohexane oxidation on a layered titanate modified with iron oxide under sunlight and CO_2 atmosphere

5-1. Introduction

Designing novel photocatalysts for effective and selective synthesis of fine chemicals has been extensively investigated in recent years. A great deal of endeavor has been spent on modifying TiO_2 by heteroelemental doping and hybridization with organic dyes and nanoparticles as well as designing novel catalysts, such as molecular-sieve-like TiO_2 and non-TiO_2 materials. [1-5] In particular, iron doping and iron or iron oxide modification of TiO_2 has merit in that iron is also harmless and abundant in nature; however, only a limited number of works have been reported to attain increased UV light-induced activity and visible light response of TiO_2,[6, 7] which are necessary for the application under sunlight. Moreover, there are few reports on photocatalytic synthetic reactions over such materials under sunlight.[8]

Utilization of nanostructured TiO_2 is a useful way for catalytic function design. Shiraishi et al. reported that the oxidation of benzene to phenol selectively progressed using mesoporous TiO_2[9]. It is concluded that selective oxidation was promoted because the benzene of the substrate was adsorbed to the catalyst, but phenol as the product was easily released from the catalyst and sequential oxidation was suppressed. Moreover, structural design using layered titanate has also been reported. Layered titanate incorporates substances into layers by intercalation. Specific structure and functional design are possible depending on the type and amount of the interlayer functional unit, so selective organic synthesis is also possible. [10-12] Ide et al. reported that the interlayer distance of potassium lithium titanate with hydration by changing the interlayer K^+ to Li^+ or Na^+ caused molecular recognition-like adsorption, so benzene is selectively adsorbed and disassembled from a mixed aqueous solution of benzene, phenol and 4-butylphenol.[13] Layered titanate responds only to ultraviolet light, but by incorporating a substance having visible light absorption, it can be applied as a photocatalyst having visible light activity. Ide et al. reported conversion of benzene to phenol was carried out by visible light irradiation with a catalyst in which gold was pillared between layers of layered titanate.[11] Choy et al. reported efficient decomposition of organic compounds in water under visible light irradiation by supporting a cluster of chromium oxide that absorbs visible light between layers of layered titanate.[14]

In this chapter, the interlayer of the layered titanate was modified with iron, and the obtained product was applied to perform the partial oxidation reaction of cyclohexane which is an industrially important reaction under simulated sunlight irradiation. Moreover, this photocatalytic reaction was carried out under a CO_2 atmosphere reported in Chapter 2 to further improve the catalytic activity.

5-2. Experimental

Reagents and materials

P25 was supplied by Nippon Aerosil. K_2CO_3, $LiCO_3$, acetone, Iron(Ⅲ) acetylacetonate ($Fe(acac)_3$), ethanol, toluene, hexane and hydrochloric acid were purchased from Wako Pure Chemical Industries, Ltd. Cyclohexane (named as CHA) and acetonitrile were purchased from Nacalai tesque Ltd. Dodecyl amine hydrochloride and cyclohexanone were purchased from Tokyo Kasei Ind. Co., Ltd. All reagents and materials were used as received.

Synthesis of photocatalyst[15, 16]

A layered titanate, $K_{0.7}Ti_{1.73}Li_{0.27}O_4$ (named KTLO), was reacted with an aqueous solution of dodecylammine hydrochloride (>97%, Tokyo Chemical Industry Co., Ltd.) according to the reported procedure to prepare the dodecylammonium-exchanged layered titanate (named $C_{12}N^+$-TLO). $C_{12}N^+$-TLO (0.6 g (2.9×10^{-3} mol)) was added to a solution of Fe(III) acetylacetonate complex (named $Fe(acac)_3$, Wako Pure Chemical Industries, Ltd.) in a mixed solvent (200 mL, ethanol/hexane = 3:17 v/v), and the mixture was stirred at room temperature for 3 days. The product was separated by centrifugation (3500 rpm, 20 min), washed repeatedly with the same solvent, and then washed with a mixed solution of ethanol and 0.1 mol L^{-1} of aqueous hydrogen chloride (1:1 v/v). The amount of the added $Fe(acac)_3$ was tuned (1.5×10^{-3} or 2.9×10^{-3} mol) to control the amount of the attached $Fe(acac)_3$ on the titanate. The iron oxide-modified layered titanate thus obtained was named FeO_x-TLO, where x denoted the number of the attached Fe (groups) per a unit cell of $K_{0.7}Ti_{1.73}Li_{0.27}O_4$. The layered titanate in which only the particle outer surface was modified with iron oxide (named

FeO@KTLO) and a commercially available TiO_2 (Aerosil P25) modified with iron oxide (named FeO@P25) were synthesized in a way similar to that in the synthesis of FeO_x-TLO, except that pristine KTLO and P25 were used, respectively, and the products after $Fe(acac)_3$ adsorption were washed with the ethanol/hexane mixed solvent and then calcined at 500 °C for 1 h.

Photocatalytic tests

A mixture of catalyst (30 mg) and O_2-saturated acetonitrile (18 mL) solution of cyclohexane (2 mL) in a stainless-made closed container equipped with Pyrex glass (75 mL) was irradiated with solar simulator (San-Ei Electric Co., Ltd.) at 42 °C, under shaking. The container was placed ~30 cm away from the light source to irradiate 1 solar (1000 W m^{-2})-power light to the mixture. After the reaction, the gas-phase product was analyzed by GC-TCD (Shimazu GC-8A). The solution was mixed with toluene (as internal standard) and then recovered by filtration, and the resulting supernatant was analyzed by GC-FID (Shimazu GC-2014). Only three products, cyclohexanone, cyclohexanol, and CO_2, were detected in the present study. The intermediates, such as cyclohexyl hydroperoxide, were not detected.Oxidation of cyclohexane.

Adsorption tests

Adsorption was done in a way similar to that conducted in the photocatalytic conversions except that 10 mg (~30 µmol) of the catalyst and a mixed solution (20 mL) of cyclohexane and cyclohexanone (~90 µmol for each compound) in acetonitrile, which was not bubbled with O_2, were shaken in the dark at room temperature for 6 h.
Apparent quantum yield measurement.

The full arc from a 500 W Xe lamp (Ushio) was monochromated using SM-25 (Bunkoukeiki) and then used to irradiate a mixture of catalyst (30 mg) and O_2-saturated acetonitrile (18 mL) solution of cyclohexane (2 mL) in the container. The light intensity of the monochromated Xe lamp was determined using a spectroradiometer, USR-45D (Ushio).

Materials characterization.

X-ray diffraction (XRD) patterns of solid products were collected using a powder Xray diffractometer (Bruker D8 Advance) with graphitemonochromatized Cu K α radiation at 40 kV and 30 mA. UV−vis spectra were recorded with a Jasco V-579 UV/vis/NIR spectrophotometer. X-ray photoelectron spectra (XPS) were taken with a Kratos ESCA-3400 electron spectrometer, where the binding energies were calibrated by the O 1s peak. Thermogravimetric-differential thermal analysis (TG-DTA) curves were collected using a SSC/5200 apparatus (Seiko Instruments). The sample was heated from room temperature to 800 °C in an air flow (50 mL min^{-1}) at a rate of 10 °C min^{-1}. The crystalmorphology of products was observed by scanning electron microscopy (SEM, Hitachi S-4800), and the elemental mapping was conducted by SEM and energydispersive X-ray analysis. Inductively coupled plasma optical emission spectroscopy was performed on a Seiko SPS7000. The solid products were decomposed for the measurements with an aqueous H_2SO_4 solution. Nitrogen adsorption isotherms at −196 °C were obtained using a conventional volumetric apparatus (BELSORP-mini, Bel Japan). Prior to the adsorption measurements, the samples were evacuated at 120 °C for 12 h.

5-3. Result and discussion

5-3-1. Characterization of catalysts

The interlayer modification of KTLO with molecular-level iron oxide was performed by adsorption with $Fe(acac)_3$. A direct reaction between KTLO and $Fe(acac)_3$ did not lead the intercalation of the complex into the interlayer space; therefore, the interlayer K^+ was first exchanged with dodecylammonium cation to expand the interlayer space, and the resulting $C_{12}N^+$-TLO was reacted with $Fe(acac)_3$, followed by removal of the dodecylammonium with washing. Similar procedures have often been employed to introduce bulky silane coupling reagents into the interlayer space of layered silicates and titanates.[17, 18]

The XRD patterns of KTLO, $C_{12}N^+$-TLO, and $FeO_{0.13}$-TLO before and after the washing are depicted in Fig. 5-1. The basal spacing (2.7 nm) of $C_{12}N^+$-TLO increased to 3.1 nm and then decreased to 1.3 nm after the reaction with $Fe(acac)_3$ and the subsequent washing, respectively. The elemental mapping of $FeO_{0.13}$-TLO revealed that Fe was not concentrated on the particle outer surface but distributed entirely within the particle (Fig. 5-2). The XPS spectrum of the $FeO_{0.13}$-TLO confirmed the presence of Fe^{3+} on the surface[6, 7] (data not shown). Since $Fe(acac)_3$ has been reported to irreversibly react with the surface Ti−OH group to form a Ti−O−Fe covalent bond via a ligand exchange reaction,[6] the data provided above indicate that $Fe(acac)_3$ is immobilized on the interlayer space of KTLO, and dodecylammonium is removed. In the XRD pattern of the $FeO_{0.13}$-TLO, the peak attributed to the (200) lattice plane of the KTLO was observed at 49°, confirming that the structural regularity on the layered titanate is retained after the modification with $Fe(acac)_3$.

The composition of the attached iron oxide species in $FeO_{0.13}$-TLO was estimated to be $Fe(C_5H_7O_2)_{0.8}$, which was on the basis of the amounts of Fe and acetylacetonate ligand determined by the ICP of the dissolved product (Table 5-1) and the TG-DTA curves of the product (Fig. 5-3), respectively. The amount of the attached $Fe(C_5H_7O_2)_{0.8}$ was 0.13 groups per $Ti_{1.73}Li_{0.27}O_4$ unit cell, which was equivalent to the distance between the adjacent iron oxides of 0.9 nm (Table 5-1). When the amount of the added $Fe(acac)_3$ was smaller, the iron oxidemodified layered titanate with smaller basal spacing (1.1 nm), a different kind of the attached iron oxide species (Fe- $(C_5H_7O_2)_{1.8}$), and a smaller amount of the attached $Fe(acac)_3$ (0.09 groups per a $Ti_{1.73}Li_{0.27}O_4$ unit cell) was synthesized. The results are summarized in Table 5-1.

Fig. 5-4 shows the N_2 adsorption isotherms of FeO_x-TLO and pristine KTLO. The N_2 adsorption capacity of KTLO was enhanced after the modification with iron oxide. The N_2 adsorption capacity of $FeO_{0.13}$-TLO was larger than that of $FeO_{0.09}$-TLO. Smaller gallery height and a larger amount of the remaining acetylacetonate ligand of $FeO_{0.09}$-TLO possibly made the access of N_2 into the interlayer space more difficult (Table 5-1). Judging from the distance between the adjacent iron oxides and the gallery height, $FeO_{0.09}$-TLO and $FeO_{0.13}$-TLO have the interlayer pores to concentrate cyclohexane ($0.5 \times 0.5 \times 0.4$ nm^3). The composition of iron oxide species (Fe- $(C_5H_7O_2)_{0.8}$, that is, only one-third of the acetylacetonate ligands remain) of $FeO_{0.13}$-TLO suggests that $Fe(acac)_3$ is immobilized on the titanate sheets to pillar the adjacent sheets, as schematically shown in the inset of Figure 1d. The attachment by bridging three or four Ti−OH's on the titanate sheet seems impossible taking the flat surface of the titanate sheet and the spherical geometry of free $Fe(acac)_3$ into account.

On the other hand, $Fe(acac)_3$ is possibly immobilized on the titanate sheet in a dipodal fashion to leave two acetylacetonate ligands in $FeO_{0.09}$-TLO.

The UV−vis diffused reflectance spectra of FeO_x-TLO are depicted in Fig. 5-5, together with that of KTLO and FeO@KTLO. FeO_x-TLO showed shoulders around 420 nm and absorption bands centered at 490 nm. In the absorption spectrum of $Fe(acac)_3$, an absorption band due to d−d transition in the acetylacetonate ligands was observed at 430 nm (Fig. 5-5, e). On the other hand, it is difficult to assign the latter absorption bands for FeO_x-TLO. Fe(III)-grafted TiO_2, prepared by the impregnation with $FeCl_3$, showed a weak absorption band centered around 500 nm ascribable to electron transfer from the valence band of TiO_2 to Fe^{3+}. [7] Moreover, similar absorption bands were observed for $Fe(acac)_3$-modified TiO_2 (P25) after calcination,[6] FeO@P25,[8] and FeO@KTLO (Fig. 5-5, d). Therefore, the absorption around 490 nm for FeO_x-TLO implies the presence of molecular level iron oxides.

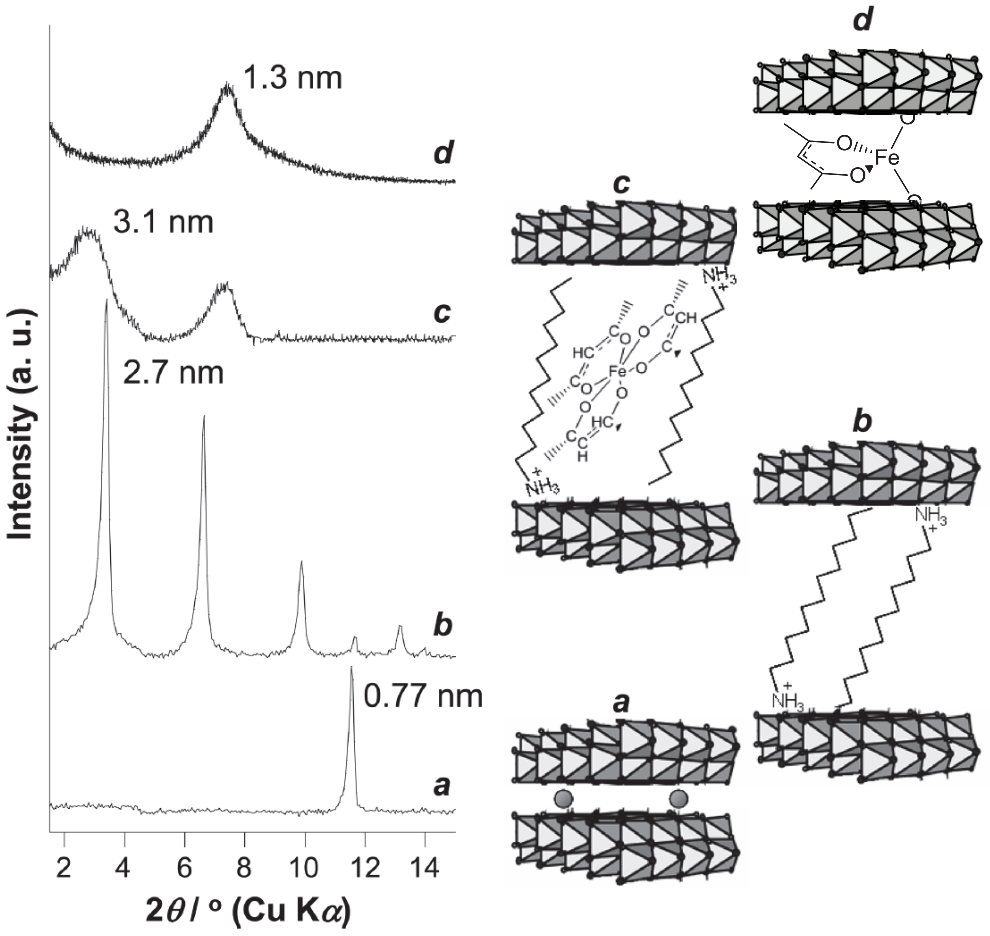

Fig. 5-1 XRD patterns of (a) KTLO, (b) $C_{12}N^{+}$-TLO and $FeO_{0.13}$-TLO (c) before and (d) after washing. Insets show the schematic structures of the corresponding products.

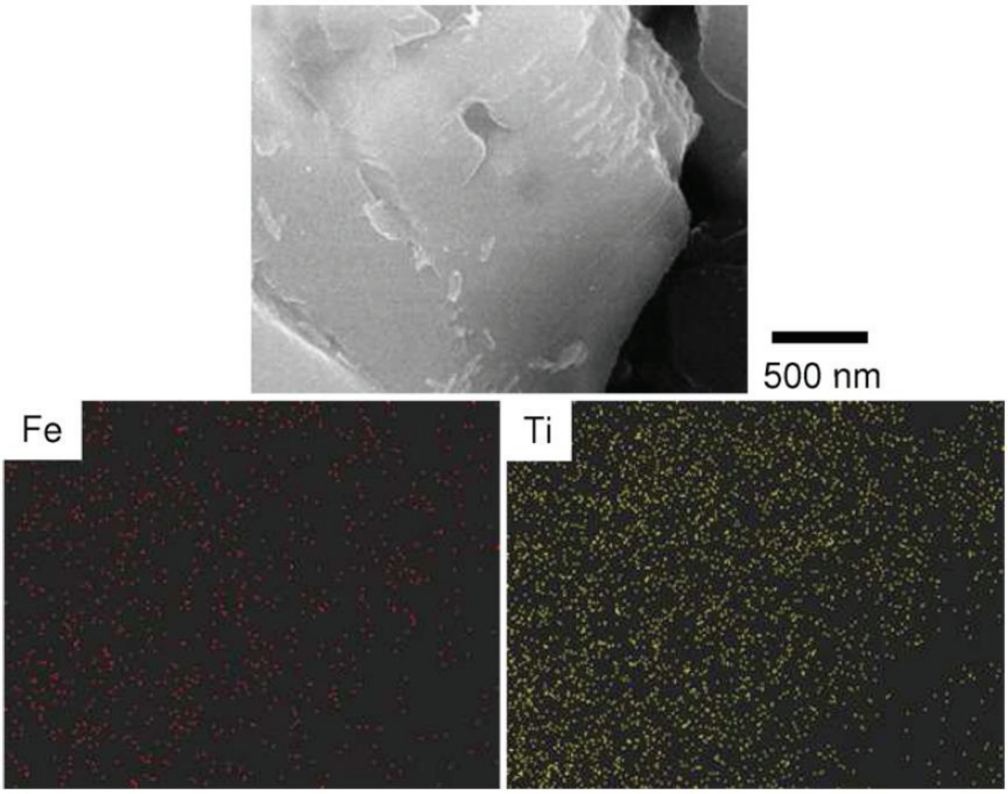

Fig. 5-2 SEM image of $FeO_{0.13}$-TLO and the corresponding elemental mapping.

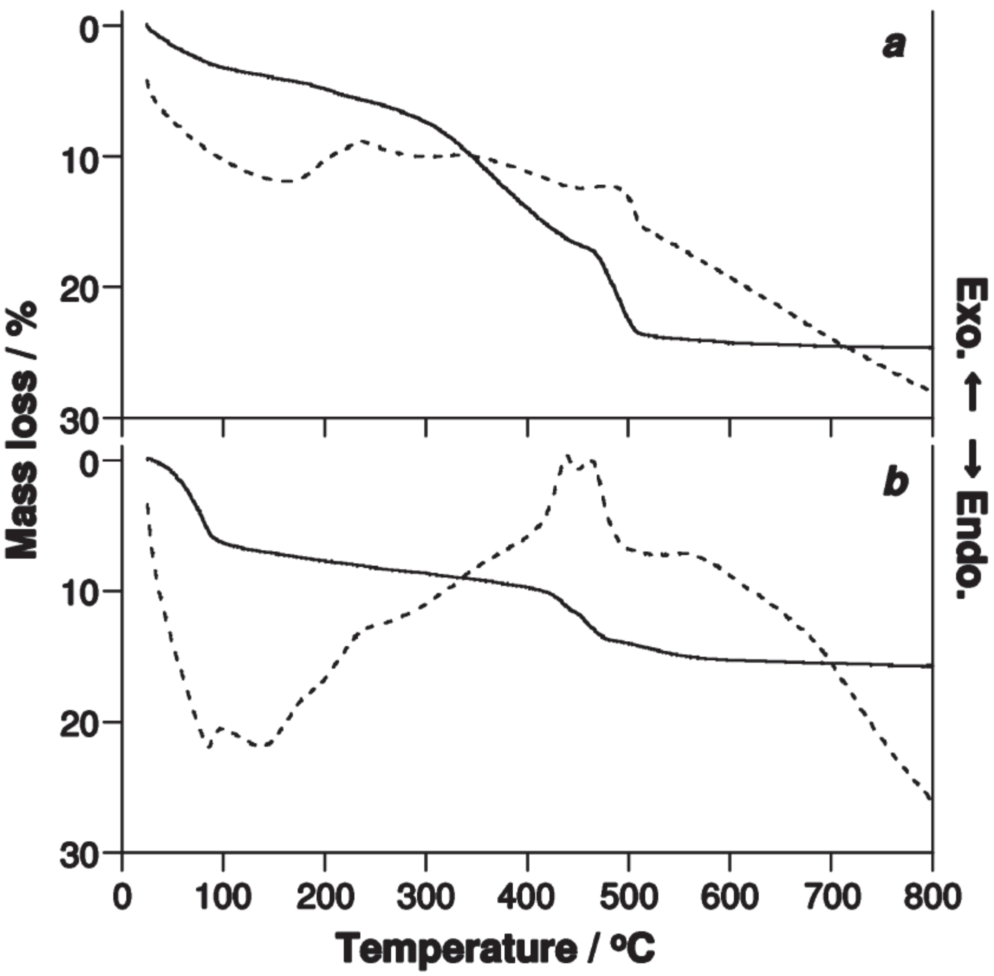

Fig. 5-3 TG (solid)-DTA (dashed) curves of (a) $FeO_{0.09}$-TLO, and (b) $FeO_{0.13}$-TLO recorded in air.

Table 5-1 Characteristics of FeO_x-TLO.

Catalyst	Fe / wt%	Aattached Fe [a]	Gallery height [b] / nm	Fe-Fe [c] distance / nm
$FeO_{0.09}$-TLO	2.7	$Fe(C_5H_7O_2)_{1.8}$	0.6	1.1
$FeO_{0.13}$-TLO	4.0	$Fe(C_5H_7O_2)_{0.8}$	0.8	0.9

[a] On the assumption that all mass loss from 300 to 500 °C in the TG curves of FeO_x-TLO (Fig. 5-3) is due to the oxidative decomposition of acetylacetonate ligands. [b] The single layer thickness of KTLO (0.5 nm)[30] was subtracted from the observed basal spacing. [c] Calculated as $(2\ ab/x)^{1/2}$, ab and x denote basal area of KTLO ($0.38 \times 0.30\ nm^2$) and Fe/TLO molar ratio, respectively[31].

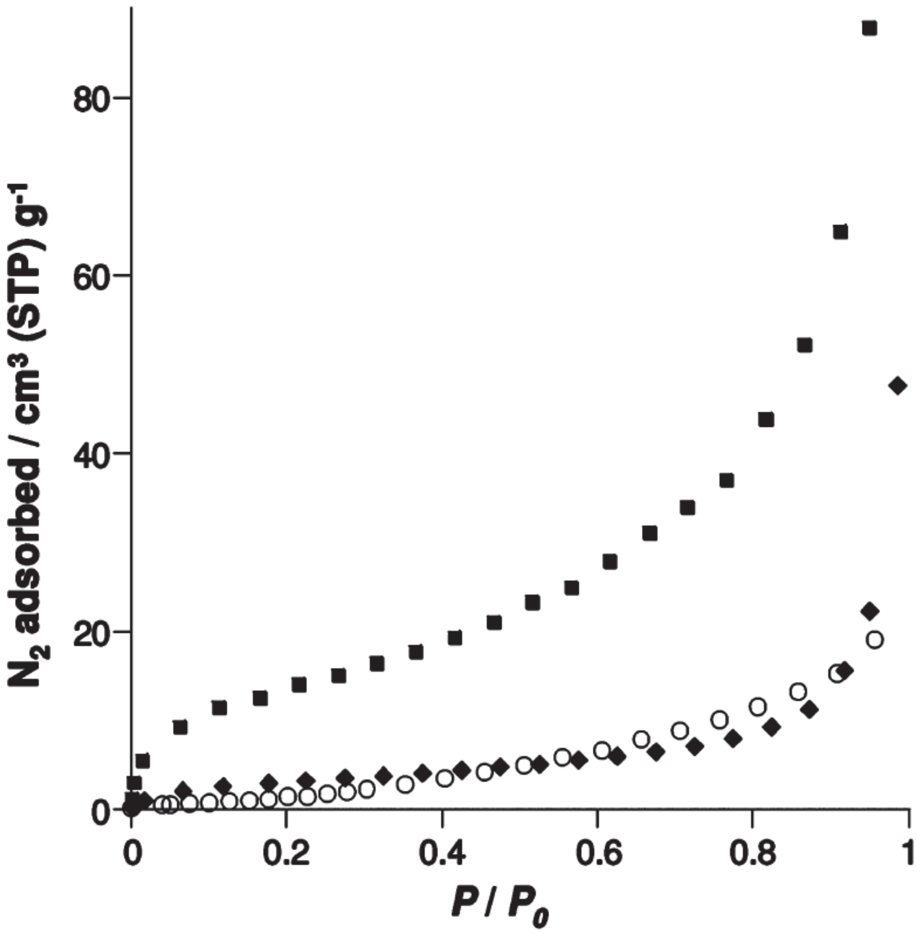

Fig. 5-4 N_2 adsorption isotherms of (○) KTLO, (◆) $FeO_{0.09}$-TLO, and (■) $FeO_{0.13}$-TLO.

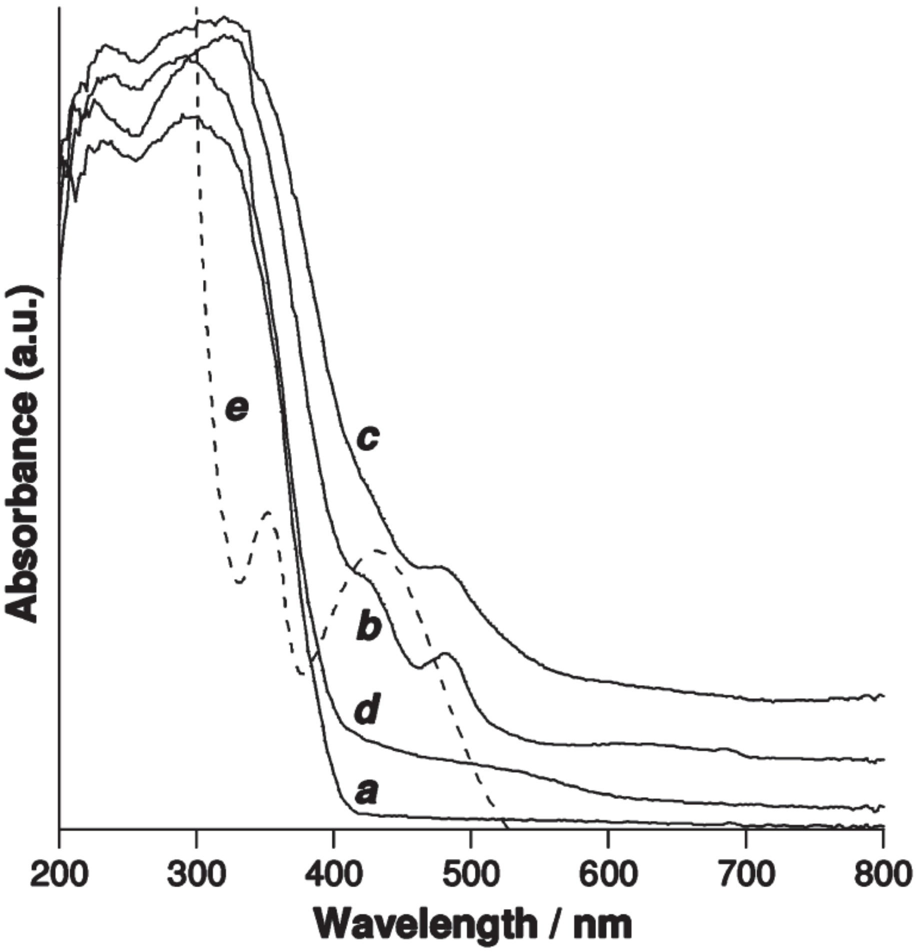

Fig. 5-5 Diffused reflectance UV−vis spectra of (a) KTLO, (b) $FeO_{0.09}$-TLO, (c) $FeO_{0.13}$-TLO and (d) FeO@KTLO. Dashed line (e) denotes UV−vis absorption spectrum of $Fe(acac)_3$ in an ethanol/ hexane mixture.

5-3-2. Photocatalytic and adsorption tests

Cyclohexane oxidation

To assess a high level of photocatalytic activity of FeO_x-TLO toward selective cyclohexane (named as CHA) oxidation under sunlight, the activity of FeO_x-TLO was compared with those of a commercially available TiO_2 (P25), FeO@P25[8] and FeO@KTLO under the same irradiation conditions and with the same amount of photocatalysts (Table 5-2). FeO_x-TLO showed selectivity up to 100% (Table 5-2, entries 1, 2, 5, and 8), which was considerably higher than that obtained on P25 (Table 5-2, entry 9). The extremely high selectivity resulted from the suppression of CO_2 evolution. $FeO_{0.13}$-TLO gave the best result, with the conversion comparable to that obtained on P25 (Table 5-2, entries 5, 8, and 9).

To the best of our knowledge, the activity obtained on $FeO_{0.13}$-TLO at 6 h of sunlight irradiation (0.14% conversion, ~100% selectivity, and 28% apparent quantum yield at 380 nm) was superior or comparable to those that had been reported for photocatalytic cyclohexanone (named as CHA-one) and cyclohexanol (named as CHA-ol) production under visible light,[19, 20] although the present material is cheap and abundant. For example, 0.09% conversion and >99% selectivity were obtained on Cr/Ti/Si ternary mixed oxide[20]. The activity of FeO@P25[8] was lower than that of FeO_x-TLO under identical conditions (Table 5-2, entries 2, 5, 8, 10, and 11), showing a merit of the presently proposed material design. Further improvement of the photocatalytic activity of FeO_x-TLO seems possible by controlling reaction environments, since I have reported the positive effects of a reaction environment (as described in chapters 2 and3), such as the presence of a target product in the starting mixture[11] and CO_2 atmosphere,[21, 8] on photocatalytic selective oxidations. Indeed, CHA conversion of

FeO_x-TLO was substantially improved, with 100% selectivity maintained by conducting the reaction under a CO_2 atmosphere (Table 5-2, entries 1, 4, 5, and 7). The XRD patterns and the UV−vis spectra of FeO_x-TLO did not change after the photocatalytic reaction, and Fe was not detected by the UV−vis absorption spectra of the supernatant after the reaction. Therefore, FeO_x-TLO was stable during the present photocatalysis. As a result, it could be reused without loss of the original activity (Table 5-2, entries 5 and 6), which was a merit for the practical application.

When sunlight only with wavelength longer than 420 nm was used to irradiate $FeO_{0.09}$-TLO, CHA-one, CHA-ol and CO_2 hardly formed (Table 5-2, entry 3). Therefore, the attached $Fe(acac)_3$ did not work as a visible light harvester. It should be noted here that the presently designed FeO_x-TLO effectively photocatalyzes CHA using only the UV spectrum of sunlight. It has been suggested that in TiO_2 modified with molecular level iron oxide, the iron oxide accepts electrons generated by the band gap excitation of TiO_2 to improve the charge separation efficiency.[6,8]

Table 5-2 Oxidation of cyclohexane (CHA) to cyclohexanone (CHA-one) and cyclohexanol (CHA-ol) under simulated solar light.

Entry	Catalyst	Irradiation time / h	Yield / μmol			Selectivity / % [b]	Conversion of CHA / % [c]
			CHA-one	CHA-ol	CO_2 [a]		
1	$FeO_{0.09}$-TLO	6	0.90	0.29	trace	> 99	0.006
2	$FeO_{0.09}$-TLO	12	6.4	5.0	trace	> 99	0.062
3	$FeO_{0.09}$-TLO [d]	6	n.d.	trace	trace		
4	$FeO_{0.09}$-TLO [e]	6	2.7	1.2	trace	> 99	0.020
5	$FeO_{0.13}$-TLO	6	15.4	10.5	n.d.	> 99.9	0.14
6	$FeO_{0.13}$-TLO [f]	6	15.3	10.2	n.d.	> 99.9	0.14
7	$FeO_{0.13}$-TLO [g]	6	18.8	21.2	trace	> 99	0.22
8	$FeO_{0.13}$-TLO	12	22.5	16.2	57.9	> 80.0	0.26
9	P25	12	34.0	3.2	144.5	55.5	0.33
10	FeO@P25	6	3.6	trace	trace	> 99	0.020
11	FeO@P25	12	4.6	trace	19.6	58.2	0.043
12	FeO@KTLO	6	n.d.	n.d.	67.3		

[a] Measurement error of within 1%. [b] {[formed CHA-one] + [formed CHA-ol]}/{[formed CHA-one] + [formed CHA-ol] + 1/6[formed CO_2]} × 100.

[c] {[formed CHA-one] + [formed CHA-ol] + 1/6[formed CO_2]}/[added CHA] × 100.

[d] Sunlight with a wavelength shorter than 420 nm was the cutoff.

[e] Under CO_2 atmosphere (40 kPa). [f] Reused after washing with acetonitrile.

[g] Under CO_2 atmosphere (20 kPa).

Adsorption test of CHA and CHA-one

The roles of the immobilized iron oxide species of FeO_x- TLO in the present photocatalytic CHA oxidation were discussed. When FeO_x-TLO was mixed with a mixture of CHA and CHA-one in the dark, CHA was selectively adsorbed depending on the amount of Fe (Table 5-3). The surface Ti−OH (which can interact with CHA-one and CHA-ol) on FeO_x-TLO is occupied with iron oxide species so effectively that interactions between the catalysts and the partially oxidized products are relatively weak. Accordingly, the photocatalytically formed CHA-one and CHA-ol promptly desorb from the active center (interlayer spaces) of FeO_x-TLO, giving the effective and selective formation of the products. As shown in Table 5-2 (entry 12), only trace amounts of CHA-one and CHA-ol formed on FeO@KTLO that did not adsorb CHA effectively. This result supports the above idea. $FeO_{0.13}$-TLO adsorbs CHA more effectively than $FeO_{0.09}$-TLO due to the larger surface area, giving higher CHA conversion. Studies on the catalytic or photocatalytic conversion of organic substrates using zeolites[22] and mesoporous materials[23,11,24] have demonstrated that the separation of target products from the catalysts plays an important role in the efficient formation of the products. Further studies on the nanostructural design of FeO_x-TLO by changing the amount of the attached $Fe(acac)_3$ and coimmobilizing other functional units[25, 26] are worth conducting to optimize the molecular recognition ability and then the photocatalytic performance.

Table 5-3 Adsorption of cyclohexane (CHA) and cyclohexanone (CHA-one) on Fe_x-TLO from acetonitrile solution containing two components.[a]

Catalyst	Amount adsorbed / μmol		CHA/CHA-one separation
	CHA	CHA-one	
$FeO_{0.09}$-TLO	43.7	30.0	1.5
$FeO_{0.13}$-TLO	47.1	25.9	1.8

[a] The catalyst (~30 μmol) was mixed with a mixed solution of CHA and CHA-one (~90 μmol for each compound) in the dark.

5-3-3. Catalytic reaction mechanism

Fig. 5-6 shows the time-dependent change in the yields of CHA-one, CHA-ol, and CO_2 during the photocatalytic CHA oxidation over $FeO_{0.09}$-TLO. Almost equivalent amounts of CHA-one and CHA-ol formed, and a much smaller amount of CO_2 evolved. From all the results obtained, a possible mechanism for the present reaction was proposed as follows: First, the intercalated CHA is reacted with either a hole or $OH^{\bullet}$ (or $OH_2^{\bullet}$), which are photogenerated on the titanate valence band of FeO_x-TLO, to form cyclohexyl radical. The formed radical is then reacted with $OH^{\bullet}$ (or $OH_2^{\bullet}$) and $O_2^{\bullet -}$, which is derived from the reduction of O_2 by the excited electron on the titanate conduction band, to generate CHA-ol and CHA-one, respectively.[27,28] The generated products are promptly desorbed from the interlayer space to prevent successive oxidation.

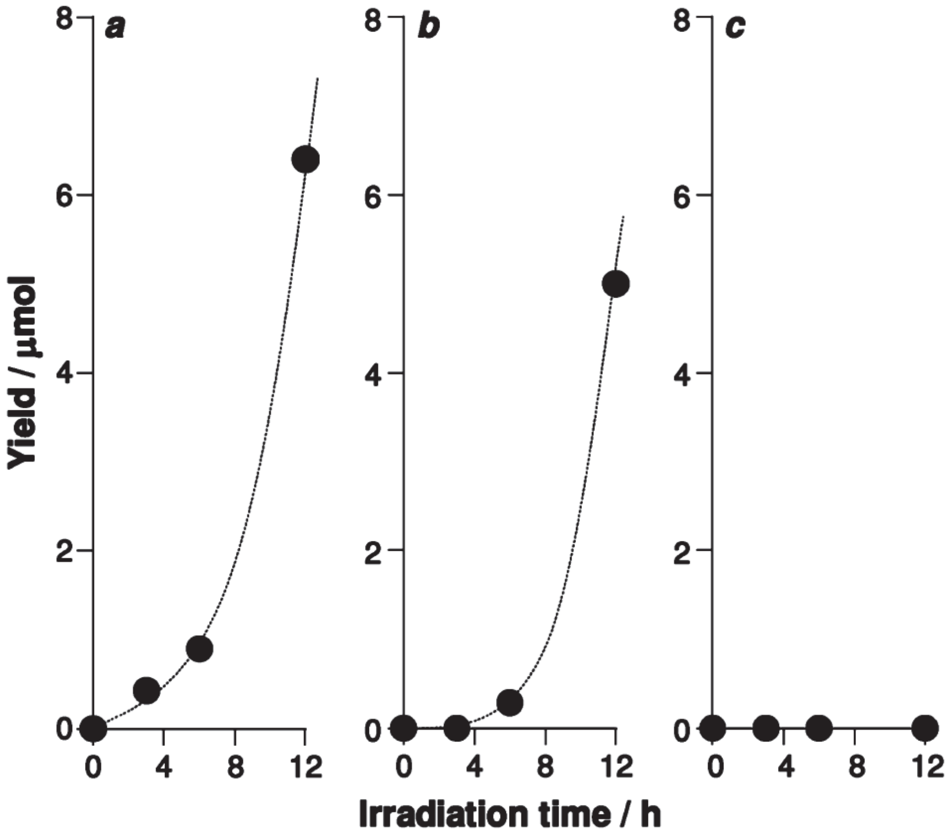

Fig. 5-6 Time-dependent changes in the amounts of (a) cyclohexanone, (b) cyclohexanol, and (c) CO_2 during photooxidation of cyclohexane on $Fe_{0.09}$-TLO.

5-4. Conclusion

A layered titanate containing immobilized molecular level iron oxide in the interlayer space was successfully synthesized by the reaction between a layered titanate and iron(III) acetylacetonate complex. The obtained material was found to effectively and selectively catalyze the oxidation of cyclohexane to cyclohexanone and cyclohexanol with molecular O_2 under sunlight irradiation.[29] The photocatalytic activity was substantially modified by conducting the reaction under a CO_2 atmosphere, as previously reported photocatalysyts.[8, 21] Because of the potential for further nanostructure design of the hybrid photocatalyst, the present result opens up new opportunities for the production of various commodity chemicals in an economically and environmentally favorable fashion.

5-5. References

[1] M. A. Fox and M. Dulay, *Chem. Rev*., **1993**, *93*, 341.

[2] A. Maldotti, A. Molinari and R. Amadelli, *Chem. Rev*., **2002**, *102*, 3811.

[3] Y. Shiraishi and T. Hirai, *J. Photochem. Photobiol. C*, **2008**, *9*, 157.

[4] H. Tada, T. Kiyonaga and S. Naya, *Chem. Soc. Rev*., **2009**, *38*, 1849.

[5] S. Fukukawa, T. Shishido, K. Teramura and T. Tanaka, *ACS Catal*., **2012**, *2*, 175.

[6] H. Tada, Q. Jin, H. Nishijima, H. Yamamoto, M. Fujishima, S. Okuoka, T. Hattori, Y. Sumida and H. Kobayashi, *Angew. Chem. Int. Ed*., **2011**, *50*, 3501.

[7] H. Yu, H. Irie, Y. Shimodaira, Y. Hosogi, Y. Kuroda, M. Miyauchi and K. Hashimoto, *J. Phys. Chem. C*, **2010**, *114*, 16481.

[8] Y. Ide, H. Hattori, M. Sadakane and T. Sano, *Green Chem*., **2012**, *14*, 1264.

[9] Y. Shiraishi, Y. Teshima and T. Hirai, *Chem. Commun*., **2005**, 4569.

[10] T. W. Kim, S. G. Hur, S.-J. Hwang, H. Park, W. Choi and J.-H. Choy, *Adv. Funct. Mater*., **2007**, *17*, 304.

[11] Y. Ide, M. Matsuoka and M. Ogawa, *J. Am. Soc. Chem*., **2010**, *132*, 16762.

[12] T. Okada, Y. Ide and M. Ogawa, *Chem. Asian J*., **2012**, *7*, 1980.

[13] Y. Ide, Y. Nakasato and M. Ogawa, *J. Am. Chem. Soc.,* **2010**, *132*, 3601.

[14] T. Kim, S. G. Hur, S.-J. Hwang, H. Park, W. Choi and J.-H. Choy, *Adv. Funct. Mater.,* **2007**, *17*, 307.

[15] T. Sasaki, F. Kooli, M. Iida, Y. Miyauchi, Y. Yajima, F. Izumi, B. C. Chakoumakos and M. Watanabe, *Chem. Mater*., **1998**, *10*, 4123.

[16] Y. Fuse, Y. Ide and M. Ogawa, *Bull. Chem. Soc. Jpn*., **2008**, *81*, 767.

[17] Y. Ide and M. Ogawa, *Chem. Commun.*, **2003**, 1262.

[18] T. Sasaki, Y. Ebina, Y. Kitami, M. Watanabe and T. Oikawa, *J.Phys. Chem. B*, **2001**, *105*, 6116.

[19] Y. Shiraishi, H. Ohara and T. Hirai, *New. J. Chem*., **2010**, *34*, 2841.

[20] D. Tsukamoto, A. Shiro, Y. Shiraishi and T. Hirai, *J. Phys. Chem. C.,* **2011**, *115*, 19782.

[21] Y. Ide, N. Nakamura, H. Hattori, R. Ogino, M. Ogawa, M. Sadakane and T. Sano, *Chem. Commun*., **2011**, *47*, 11531.

[22] E. Suzuki, K. Nakamura and Y. Ono, *Chem. Lett*., **1988**, 953.

[23] Y. Shiraishi, N. Saito and T. Hirai, *J. Am. Chem. Soc*., **2005**, *127*, 12820.

[24] T. W. Kim, S.-J. Hwang, S. H. Jhung, J.-S. Chang, H. Park, W. Choi and J.-H. Choy, *Adv. Mater*., **2008**, *20*, 539.

[25] Y. Ide and M. Ogawa, *Angew. Chem., Int. Ed.,* **2007**, *46*, 8449.

[26] Y. Ide, S. Iwasaki and M. Ogawa, *Langmuir*, **2012**, *27*, 2522.

[27] Y. Shiraishi and T. Hirai, *J. Photochem. Photobiol. C*, **2008**, *9*, 157.

[28] E. Sahle-Demessie, M. Gonzalez, Z.-M. Wang and P. Biswas, *Ind. Eng. Che. Res*., **1999**, *38*, 3276.

[29] H. Hattori, Y. Ide, S. Ogo, K. Inumaru, M. Sadakane and T. Sano, *ACS Catal*., **2012**, *2*, 1910.

[30] T. Sasaki, Y. Ebina, Y. Kitani, M. Watanabe M. Oikawa, *J. Phys. Chem. B*, **2001**, *105*, 6116.

[31] Y. Ide and M. Ogawa, *Angew, Chem. Int. Ed*., **2007**, *46*, 8449.

Chapter 6

Enhanced photocatalytic activity of a layered titanate by simply mixing with TiO_2-based photocatalysts as additives

6-1. Introduction

Owing to its high photocatalytic activity, low cost, and non-toxicity, TiO_2 is a promising photocatalyst with environmental and energy applications.[1-4] Since the photocatalytic activity of TiO_2 largely depends on charge separation efficiency, commercial and synthesized TiO_2 are often used after hybridization with co-catalysts, such as precious metals, to considerably improve their photocatalytic activity.[5] One of the most important challenges of the near future will be the development of cheap and active TiO_2-based photocatalytic systems, with[6] or without[7-11] the addition of small amounts of co-catalysts.

Layered titanates, composed of titania nanosheets, have been widely investigated as photocatalysts because, upon intercalation of functional units including co-catalyst metal or metal oxide nanoparticles, they show remarkable enhancements in photocatalytic performance. This is possibly due to prompt charge migration to the surface due to the ultrathin thickness of the nanosheets.[12-15] However, despite the time-consuming intercalation processes, the photocatalytic activity of these intercalated compounds is often lower than that of conventional or state-of-the-art TiO_2-based materials. Recently, Ide et al. have reported that a layered titanate ($H_{1.07}Ti_{1.73}\square_{0.27}O$, named HTO), which scarcely shows any photocatalytic activity as is, shows greatly enhanced activity upon simply mixing with a lower amount (~10 wt.%) of P25 in water (reaction media).[11] The activity of the mixture was up to 5 times higher than that of

P25, a benchmark TiO_2 photocatalyst. More importantly, when P25 was replaced with Pt-loaded P25 (0.5 wt.% of Pt), also a benchmark photocatalyst, the mixture showed activity comparable to that of pure Pt-loaded P25, using an equal amount of each powder. Accordingly, I successfully obtained similar photocatalytic activity using a considerably reduced amount of Pt (from 0.5 wt.% to < 0.06 wt.%).

In the previous report,[11] it was proposed that electron transfer from excited HTO to P25 (or Pt-loaded P25) enhanced charge separation and photocatalytic efficiency. However, the following points are ambiguous: i) Do these particles really form particle interfaces for electron transfer? ii) Are there more effective additives than Pt-loaded P25? iii) Does electron transfer occur in the opposite-direction, from P25 to HTO? In other words, if visible-light-induced photocatalysts based on P25 are used as additives of HTO, is the visible-light-induced activity improved? In this chapter, I tested various P25-based photocatalysts, including visible light-responsive ones, and investigated the mixing states and photocatalytic activities of the resulting mixtures.

6-2. Experiment

Reagents and materials

P25 was supplied by Nippon Aerosil. Fe(Ⅲ)acetylacetonate ($Fe(acac)_3$), Platinum(IV) Chloride hexahydrate ($H_2PtCl_6•6H_2O$), ethanol, dehydrated ethanol, $NaBH_4$, ammonium fluoride (NH_4F), Formic acid and hexane were purchased from Wako Pure Chemical Industries, Ltd. Gold (III) Chloride Trihydrate ($HAuCl_4•3H_2O$) was purchased from SIGMA-ALDRICH. K_2CO_3 and $LiCO_3$ were purchased from Kanto Chem. Ind. Ltd. Tetrapropylammonium hydroxide (named as TPAOH) was purchased from Tokyo Kasei Ind. Co., Ltd. All reagents and materials were used as received.

Synthesis of layered titanate ($H_{1.07}Ti_{1.73}\square_{0.27}O$)

$K_{0.8}Ti_{1.73}Li_{0.27}O_4$ was prepared according to the literature.[16] K_2CO_3, Li_2CO_3, and P25 were mixed using a planetary ball mill (Planet M2-3, Gokin Planetaring) and the mixture was calcined in air at 600 °C for 30 min. After cooling to room temperature, the sample was mixed again and heated at 600 °C for 20 h in air. The protonation of $K_{0.8}Ti_{1.73}Li_{0.27}O_4$ was conducted according to a previous report using dilute HCl treatment.[17]

Synthesis of Pt-loaded and Au-loaded TiO_2

Pt-loaded P25 (named Pt@P25)[6] and Au-loaded P25 (named Au@P25)[18] were also prepared according to the method described in the literature. The nominal metal loadings were 0.5 and 2.0 wt.%, respectively.

Synthesis of Fe-grafted TiO_2

Fe-grafted P25 (named Fe@P25) was prepared as follows:[19,20] P25 and iron(III) acetylacetonate in a binary solvent (ethanol/hexane = 3:17 v/v) were mixed at room temperature for 24 h. Next, the solid product was separated and washed repeatedly with the same solvent system, and then calcined at 500 °C for 1 h. The nominal metal loading of Fe was 1.0 wt.%.

Synthesis of hydrothermal TiO_2

Hydrothermal treatment of P25 was conducted in the presence of TPAOH and NH_4F at 170 °C for 7 days.[8] After the reaction, the solid was washed repeatedly with water. The resulting product was named Hyd-P25.

Oxidation of formic acid

Oxidative decomposition of formic acid in water was performed in a stainless steel container (75 mL) equipped with a Pyrex window as follows: one or two kinds of the sample were added to an O_2-saturated aqueous solution (5 mL) containing 5 vol.% formic acid, and the mixture was ultrasonicated for 1 min and then stirred for 5 min in the dark. The resulting suspension was irradiated by a solar simulator (San-Ei Electric, $\lambda > 300$ nm, 1000 Wm^{-2}) under stirring. The headspace gas in the reactor was sampled with a gas-tight syringe and quantified using a BID gas chromatograph (ShimadzuBID-2010 plus) equipped with a Micropacked ST column. Helium was used as carrier gas.

Analysis equipment and evaluation condition

Apparatus using for characterization of synthesis catalysts and quantification of substrate and products of photocatalytic test were shown below. The crystal morphology was observed using a field-emission scanning electron microscope (FE-SEM) (JEOL JEM-6500F). Transmission electron microscopy (TEM) images were obtained with a JEOL JEM-2100F. Particle size distributions of the samples in water were determined by dynamic light scattering (DLS) using a Nanotrac Wave instrument (MicrotracBel). Zeta potentials were measured with an ELSZ-1PL (Ostuka Electronics） and calculated using the Smoluchowski equation with the mobility determined by the LASER Doppler method. Mixtures of HTO and each additive were prepared by mixing them in water by ultrasonication for 1 min and subsequent stirring for 5 min. These mixtures were used as is for DLS and zeta potential analyses, while the samples were dried by evaporation prior to use in TEM imaging. The mixing ratio of each powder for these characterizations was identical to that for the photocatalytic reactions. After the photocatalytic reaction, headspace analyzed by gas chromatograph.

6-3. Result and discussion

6-3-1. Characterization of addtives and mixtures

Fig. 6-1 shows SEM images of HTO and P25 (images a and b respectively). HTO was composed of plate-like particles with a size of 100–200 nm. P25 was composed of smaller-sized plate-like particles (20–50 nm). No significant difference was observed in the shape and size of the primary particles of P25 and the modified P25 (Pt@P25, Au-loaded P25 named as Au@P25, Fe-grafted P25 named as Fe@P25) and the hydrothermally treated P25 (Hyd-P25). Fig. 6-1 c shows the TEM image of the mixture of HTO and P25. It was found that some of HTO and P25 particles contacted each other. Similar results were observed when HTO was mixed with Au@P25, Pt@P25, Fe@P25 or Hyd-P25 (TEM image of HTO/Au@P25 mixture shown in Fig. 6-1 d as a representative example).

In order to evaluate the mixing states of the mixtures in water, we performed by dynamic light scattering (DLS) analysis (Fig. 6-2). HTO and P25 showed peaks corresponding to a size of ~1.3 μm and ~0.3 μm, respectively. They were assigned to aggregate particles, since the primary particle sizes of HTO and P25 were 100–200 nm and 20–50 nm, respectively, as mentioned above. While Pt@P25, Au@P25 and Fe@P25 had an almost identical particle size compared to P25 (data not shown), Hyd-P25 showed a peak corresponding to a size of ~0.6 μm, due to the high interconnection of primary particles upon the special hydrothermal treatment.[10] All the mixtures had peaks with a size comparable to, or larger than, that of HTO and did not show peaks due to the pure additives. These results suggest that HTO and each additive contacted each other even in water.

I further performed zeta potential analyses of HTO and the additives in water to confirm possible electrostatic interactions between them. The isoelectric points of HTO and P25 are ~2.0[21] and 6.4,[22] respectively. Given that the pH of the aqueous HTO/P25 mixture dispersion was 4.0, HTO and P25 must be oppositely charged in water to interact electrostatically with each other. Table 6-1 shows the zeta potentials of HTO and P25. As expected, the zeta potential of HTO was negative, while that of P25 and the modified P25 were positive. From the results described above, we can conclude that when HTO particles are simply mixed with P25 or modified P25 particles in water, they can form composites by electrostatic interactions.

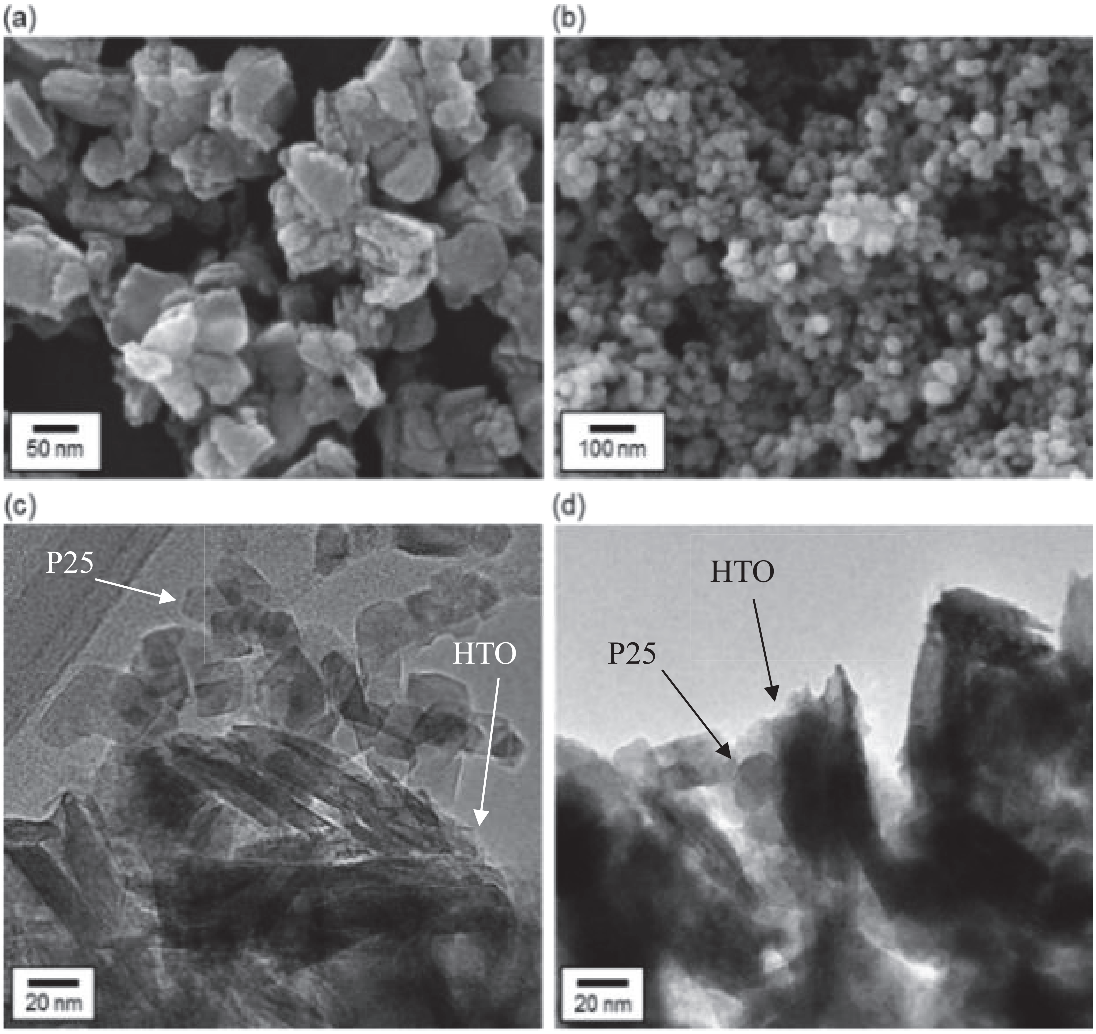

Fig. 6-1 SEM images of (a) HTO and (b) P25, and TEM images of (c) HTO/P25 mixture and (d) HTO/Au@P25 mixture

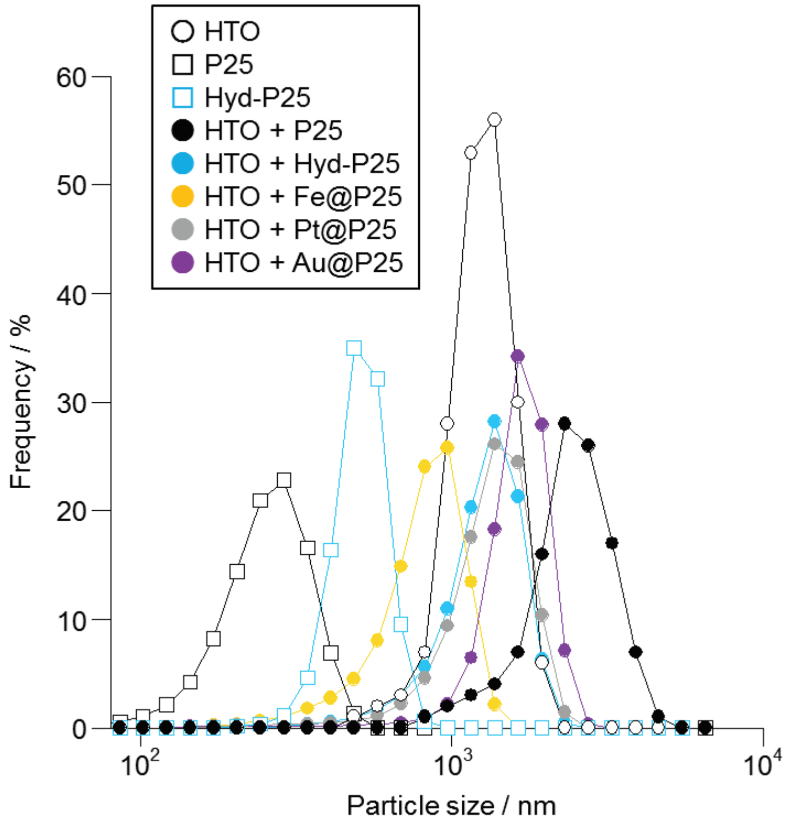

Fig. 6-2 Particle size distributions determined by DLS of different materials.

Table 6-1 Zeta potential of different materials.

	HTO	P25	Hyd-P25	Fe@P25	Pt@P25	Au@P25
Zeta potencial /mV	-20.5	19.0	25.7	16.8	34.7	23.2

6-3-2. Photocatalytic test

The photocatalytic performance of these mixtures was evaluated through the oxidation of formic acid to CO_2 in water under solar light irradiation ($\lambda > 300$ nm). In a previous study, we optimized the mixing ratio of HTO and P25 particles (HTO/P25 = 13 mg/2 mg).[11] Thus, we used the same mixing ratio in this study. Fig. 6-3 summarizes the results of the photocatalytic experiments. HTO showed no activity for this reaction. However, it showed a greatly enhanced activity upon mixing with any additives and the activity of the mixtures roughly depended on that of the additives (Fig. 6-4). The HTO/Au@P25 mixture showed the best activity, which was 8- and 1.5-times higher than that of P25 and the HTO/Pt@P25 mixture, respectively. The activity of HTO/Au@P25 was comparable to that of pure Au@P25, using the same amount of powder (15 mg), while the amount of Au contained in the HTO/Au@P25 mixed system was only 0.27 wt.%, which was considerably smaller than that contained in the pure Au@P25 system (2.0 wt.%).

Considering the electronic band structures of HTO and P25 (Fig. 6-5),[23,24] we proposed that the enhanced photocatalytic activity of the HTO/P25 mixture (or the HTO/Pt@P25 mixture) resulted from the transfer of photoexcited electrons from HTO to P25 (or Pt@P25) and retardation of charge recombination.[11] To confirm this, I investigated the possibility of opposite-direction charge transfer in the HTO/Au@P25 system. As shown in Fig. 6-3 (below dashed line), under the irradiation of > 450 nm solar light, at which only Au@P25 was excited, the HTO/Au@P25 mixture and Au@P25 showed almost identical activity when using the same amount of Au@P25 (2 mg). This indicates that the electron transfer from the excited Au@P25 to HTO did not occur to enhance the activity of Au@P25.[25] Therefore, as proposed in the previous study, the enhancedphotocatalytic activity of the mixture of HTO with P25, or the modified P25, results from enhanced charge separation via electron transfer from HTO to the additive. On the other hand, considering electric band structures of HTO and P25 (Fig. 6-5), transfer of photogenerated holes from Au@P25 to HTO upon UV excitation is thermodynamically unfavorable.

It should be also noted that the HTO/Hyd-P25 mixture exhibited activity comparable to that of HTO/Pt@P25 (Fig. 6-3). Hyd-P25 is composed of anatase and rutile nanoparticles, which are much more interconnected than in P25, and thus exhibits remarkably enhanced charge separation and photocatalytic efficiency.[10] Owing to its high charge separation efficiency, Hyd-P25 was likely to be a good additive comparable to Pt@P25, where the Pt co-catalyst effectively accumulates electrons. The modification of Hyd-P25 with Pt or Au and the use of modified Hyd-P25 as additive to HTO are worth investigating in the search for more effective photocatalytic systems.

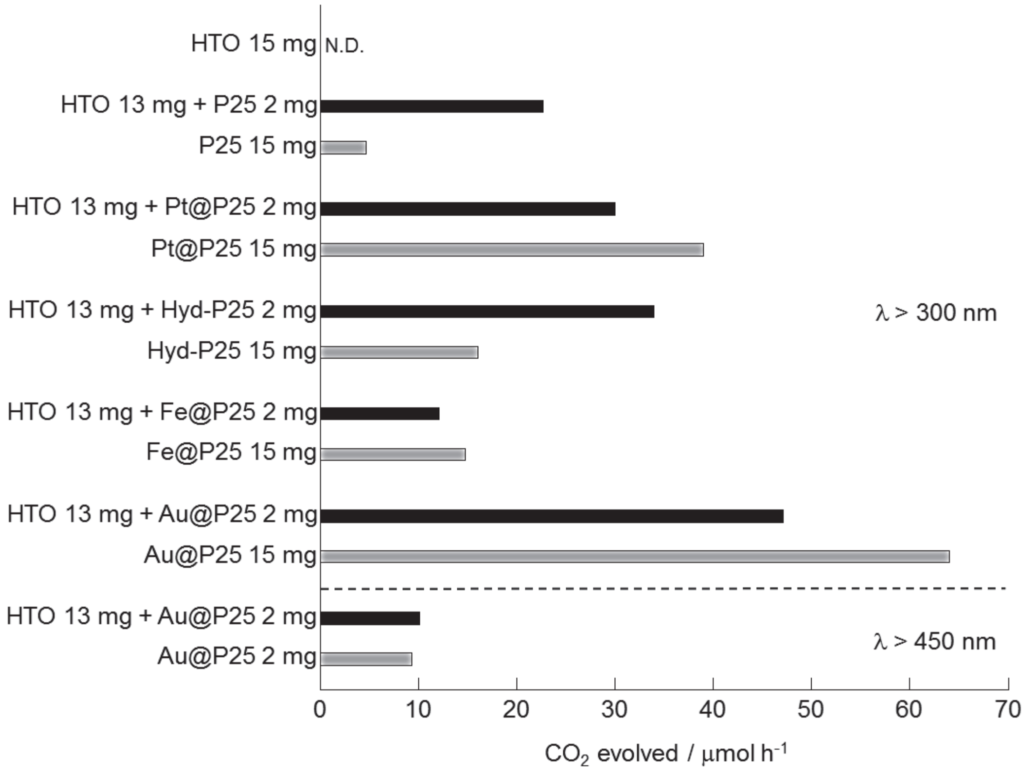

Fig. 6-3 Photocatalytic activity of different materials.

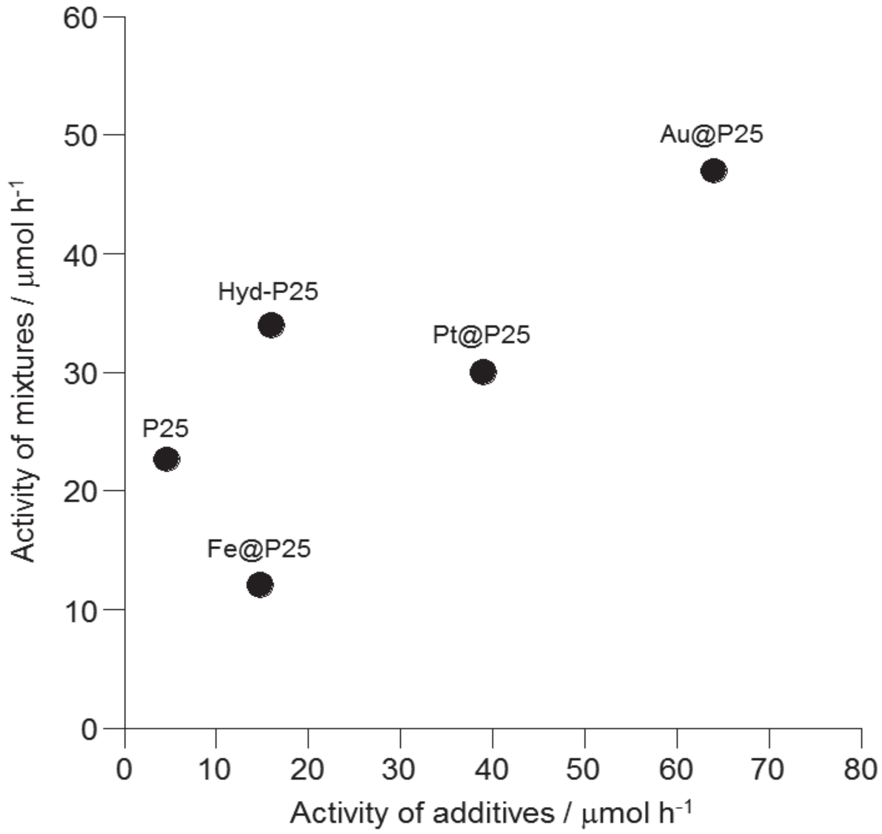

Fig. 6-4 Photocatalytic activity of HTO mixtures and pure additives.

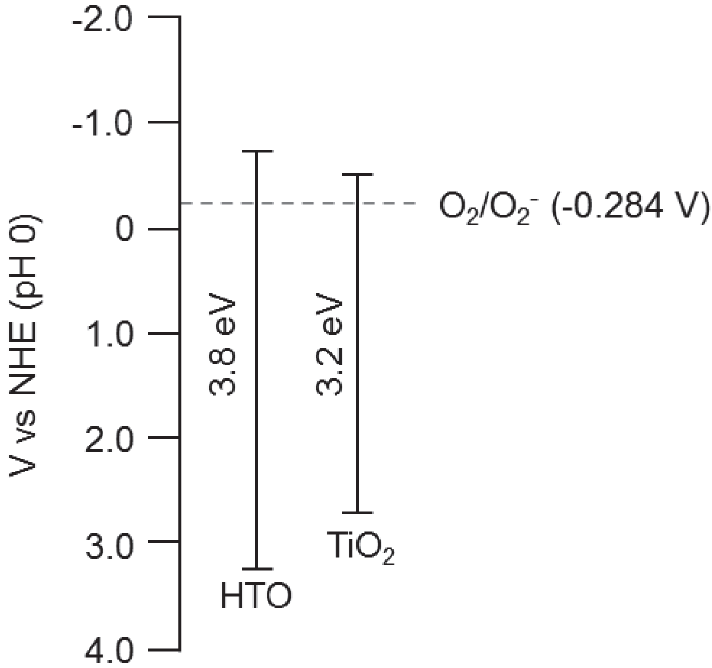

Fig. 6-5 Electric band structures of HTO and P25.

6-4. Conclusion

I found the positive effects of particle-level mixing of a layered titanate (HTO) and a much smaller amount (~10 wt.%) of various additives, including Pt or Au-loaded TiO_2 (P25), on the photocatalytic activity of the mixtures for the oxidation of formic acid in water under solar light irradiation. Pure HTO scarcely showed any activity, but the mixtures showed remarkably enhanced activity, roughly depending on the activity of the individual additives. I could conclude that this enhancement resulted from electron transfer from the excited HTO to the additive via their particle interfaces, enhancing charge separation and UV-induced photocatalytic efficiency of HTO. The mixture of HTO with Au-loaded P25 showed the best activity, which was 8 times higher than that of P25, a benchmark photocatalyst, and comparable to that of pure Au-loaded P25 (Au loading of 2.0 wt.%), using the same amount of powder. I thus attained largely enhanced activity despite the use of an unusually small amount (0.27 wt.%) of the noble metal. Since a wide variety of advanced TiO_2 materials, including those with precious metal co-catalysts, are available, their use as additives in conventional photocatalytic systems is underway in our laboratory.

6-5. References

[1] M. Anpo, *Bull. Chem. Soc. Jpn.,* **2004**, *77*, 1427.

[2] A. Fujishima, X. Zhang and D. A. Tryk, *Surf. Sci. Rep.,* **2008**, *63*, 515.

[3] A. Kudo and Y. Miseki, *Chem. Soc. Rev.,* **2009**, *38*, 253.

[4] J. L. Vivero-Escoto, Y.-D. Chiang, K. C.-W. Wu and Y. Yamauchi, *Sci. Technol. Adv. Mater.,* **2012**, *13*, 13003.

[5] H. Tada, T. Kiyonaga and S. Naya, *Chem. Soc. Rev.*, **2009**, *38*, 1849.

[6] T. Tatsuma, *Bull. Chem. Soc. Jpn.,* **2013**, *86*, 1.

[7] H. Kominami, T. Matsuura, K. Iwai, B. Ohtani, S. Nishimoto and Y. Kera, *Chem. Lett.,* **1995**, 693.

[8] F. Amano, O. O. Prieto-Mahaney, Y. Terada, T. Yasumoto, T. Shibayama and B. Ohtani, *Chem. Mater.,* **2009**, *21*, 2601.

[9] Z. Bian, T. Tachikawa and T. Majima, *J. Phys. Chem. Lett.*, **2012**, *3*, 1422.

[10] Y. Ide, N. Inami, H. Hattori, K. Saito, M. Sohmiya, N. Tsunoji, K. Komaguchi, T. Sano, Y. Bando, D. Golberg and Y. Sugahara, *Angew. Chem. Int. Ed.*, **2016**, *55*, 3600.

[11] K. Saito, M. Kozeni, M. Sohmiya, K. Komaguchi, M. Ogawa, Y. Sugahara and Y. Ide, *Phys. Chem. Chem. Phys.*, **2016**, *18*, 30920.

[12] Y. I. Kim, S. Salim, M. J. Huq and T. E. Mallouk, *J. Am. Chem. Soc.*, **1991**, *113*, 9561.

[13] J. L. Gunjakar, I. Y. Kim, J. M. Lee, Y. K. Jo and S. Hwang, *J. Phys. Chem. C*, **2014**, *118*, 3847.

[14] Y. Ide, M. Sadakane, T. Sano and M. Ogawa, *J. Nanosci. Nanotechnol.*, **2014**, *14*, 2135.

[15] T. Okada, Y. Ide and M. Ogawa, *Asian J. Chem.*, **2012**, *7*, 1980.

[16] M. Ogawa, M. Morita, S. Igarashi and S. Sato, *J. Solid State Chem.*, **2013**, *206*, 9.

[17] T. Sasaki, F. Kooli, M. Iida, Y. Michiue, S. Takenouchi, Y. Yajima, F. Izumi, B. C. Chakoumakos and M. Watanabe, *Chem. Mater.*, **1998**, *10*, 4123.

[18] D. Tsukamoto, Y. Shiraishi,Y. Sugano, S. Ichikawa, S. Tanaka and T. Hirai, *J. Am. Chem. Soc.*, **2012**, *134*, 6309.

[19] H. Tada, Q. Jin, H. Nishijima, H. Yamamoto, M. Fujishima, S. Okuoka, T. Hattori, Y. Sumida and H. Kobayashi, *Angew. Chem. Int. Ed.*, **2011**, *50*, 3501.

[20] Y. Ide, H. Hattori, S. Ogo, M. Sadakane and T. Sano, *Green Chem.*, **2012**, *14*, 1264.2

[21] S. Tsukahara, N. Soh and K. Kamada, *J. Phys. Chem. C*, **2012**, *116*, 19285.

[22] B. Ohtani, Y. Okugawa, S. Nishimoto and T. Kagiya, *J. Phys. Chem.,* **1987**, *91*, 3550.

[23] N. Sakai, Y. Ebina, K. Takada and T. Sasaki, *J. Am. Chem. Soc.*, **2004**, *126*, 5851.

[24] D. E. Scaife, *Sol. Energy*, **1980**, *25*, 41.

[25] Y. Ide, K. Nagao, K. Saito, K. Komaguchi, R. Fuji, A. Kogure, Y. Sugahara, Y. Bando and D. Golberg, *Phys. Chem. Chem. Phys.*, **2016**, *18*, 79.

Chapter 7

Microporous titanate nanofibers for highly efficient UV-protective transparent coating

7-1. Introduction

UV caused DNA damage, immune suppression and skin photoaging for people, and is also responsible for the decomposition and degradation of organic compounds including plastics, polymers, dyes, pigments, wood and paper that compose most of modern commonly used articles and devices. Therefore, the protection against UV irradiation damage is of a great interest for ordinary people, scientists and industries. Organic UV absorbers, embedded in polymer coatings, have been extensively used to protect organic materials against UV irradiation by transforming the absorbed radiation energy into the less damaging thermal energy through photophysical processes. [1, 2] However, its application has been limited because the polymer may be decomposed at the excited state on absorbers under UV light irradiation. [3]

Due to its abundance, non-toxicity, high stabilities and UV absorbing property, titania (and titanate) has been expected as the alternative to organic UV absorbers. However, titania presents major drawbacks to be used as UV absorbers: i) it exhibits a high UV-induced photocatalytic activity that can induce the photodegradation of organic media in which they are embedded; ii) it possesses a considerably higher refractive index than those of commodity polymer matrices, thus lowering the diffusion of visible light to whiten the medium (that limits its usage in color sensible applications, such as artwork protection and optical device). To overcome the drawbacks, development of new titania-based UV-absorbers has been actively investigated under size control of titania,[4] and its heteroelement doping[5] and hybridization with other inorganic semiconductors (e.g. cerium dioxide).[6] New non-titania inorganic UV absorbers have also been developed.[7, 8]

In this chapter, I report the synthesis of a new titanate material, a microporous titanate nanofiber, by a new route inspired by a zeolite synthesis method. Zeolite, which is an aluminosilicate of a microporous structure widely used industrially, has been conventionally synthesized by trial and error, but in recent years a relatively rational method has been developed. This method called interzeolite conversion which synthesizes target zeolites by hydrothermal treatment of starting zeolite [9-11]. In the interzeolite conversion, a zeolite as a raw material is decomposed into aluminosilicate species (nano parts) having locally ordered structure, and these nano parts are reconstructed to obtain another zeolite having the framework similar to source material. By changing the starting material zeolite and hydrothermal synthesis conditions, expensive, high quality, or novel zeolite is being designed. Therefore, not only in the case of aluminosilicate but also in other inorganic nanostructures, the same conversion strategy can be applied to synthesis of porous structures with different composition and physical properties.

In this study, therefore, I tried to synthesize a new microporous titanate by hydrothermal treatment of potassium dititanate [12], one of layered titanates, as a source material. By optimizing synthesis conditions, I succeeded in synthesis of titanium oxide nanofibers having a plurality of one-dimensional pores. The newly developed material effectively absorbs UV, hardly shows photocatalytic activity and exhibits an extremely low refractive index, and then can be applied to a highly efficient UV protective transparent coating.

7-2. Experiment

Reagents and materials

TiO_2 (anatase), K_2CO_3 (99.9%), NH_4F (97.0%), $CaCl_2$ (>95%) and 2-propanol (99.5%) were purchased from Wako Pure Chemical Industry. Tetrapropylammonium (TPA) hydroxide (as a 40 wt% aqueous solution), crystal violet (CV, >95.0%) and dodecylamine hydrochloride (>97.0%) were purchased from Tokyo Chemical Industry. Cyclohexane (99.7%) and acetonitrile (99.8%) were purchased from Nacalai Tesque. Rhodamine 101 and polycaprolactone (PCL) were obtained from Sigma-Aldrich. P25, rutile (JRC-TIO-06) and synthetic saponite were supplied by Nippon Aerosil, Catalysis Society of Japan and The Clay Science Society of Japan, respectively. TPA hydroxide was used after the evaporation of the solvent to tune a molar ratio of TPA and H_2O for hydrothermal reactions. All the other reagents and materials were used as received.

Hydrothermal reactions

$K_2Ti_2O_5$, prepared by a solid state reaction between K_2CO_3 and anatase according tothe literature[12],was mixed with TPA hydroxide, water and NH_4F at a molar ratio of $K_2Ti_2O_5$: TPA : H_2O : NH_4F = 1 : 0.8 : 5 : 0.2 in an Teflon-lined stainless steel autoclave, and the mixture was heated at 170 °C for a week. After the hydrothermal treatment, the dried gel-like solidwaswashedwithwater and dried at 70 °C to give the product and eluate. Control experiments were conducted without TPA hydroxide and/or NH_4F. P25 and $K_{0.66}Ti_{1.73}Li_{0.27}O_4$, which was prepared according to the literature[13], were also hydrothermally treated under identical conditions.

Characterization

The crystal morphology was observed by scanning electron microscopy (SEM, Hitachi S-4800) and elemental mapping of products was conducted by SEM and energy-dispersive X-ray (EDX) analysis. High resolution transmission electron microscopy (HRTEM) was performed with a JEOL JEM-3000F highresolution transmission electron microscope equipped with an EDX analyser. X-ray diffraction (XRD) patterns of the solid products were collected using a powder X-ray diffractometer (Bruker D8 Advance) with graphite monochromatized Cu Ka radiation at 40 kV and 30 mA. N_2 and Ar adsorption/desorption isotherms were obtained using a Belsorp-max apparatus (Bel Japan). Prior to the adsorption measurements, the samples were evacuated at 120 °C for 12 h. Infrared spectra were recorded using a FT-IR spectrometer (Nicolet 6700) with a resolution of 4 cm^{-1}. The sample was pressed into a self-supporting thin wafer, and then placed into a quartz cell equipped with CaF_2 windows. Prior to the measurements, the sample was evacuatedat 200 °C for 3 h. Thermogravimetric-differential thermal analysis (TG-DTA) curves were collected using a SSC/5200 apparatus (Seiko Instruments). The sample was heated from room temperature to 800 °C in an air fow (50 mL min^{-1}) at a rate of 10 °C min^{-1}. Inductively coupled plasma atomic emission spectroscopy (ICP-AES) was performed on a SPS 7700 plasma spectrometer (Seiko Instruments). Ultraviolet-visible (UV-vis) spectra were recorded with a JASCO V-579 UV/Vis/NIR spectrophotometer. X-ray photoelectron spectroscopy (XPS) was performed with a Kratos ESCA-3400 electron spectrometer, where the binding energies were calibrated using the O 1s peak. The electrospray ionization (ESI) mass spectrum was recorded on a LCMS-8040 liquid chromatograph mass spectrometer (Shimadzu) in the negative ion mode at a desolvation temperature of 200 °C.

Ion exchange

50 and 5 mg of MPTNF powders were mixed with an aqueous solution containing $CaCl_2$ (40 mL, 0.06-60 mmol L^{-1}) and CV (200 mL, 0.000875-0.0875 mmol L^{-1}), respectively, and the mixtures were stirred at room temperature for 3 days. The products were separated from the mixtures by centrifugation (3500 rpm, 15 min). The amounts of the adsorbed/desorbed Ca/K ions and the adsorbed CV ions were determined on the basis of ICP-AES and UV-vis spectroscopy, respectively, of the supernatants. For dodecylammonium adsorption, MPTNF (200 mg) was mixed with an aqueous solution containing dodecylammonium hydrochloride (100 mL, 19.4 mmol L^{-1}), and the mixture was stirred at room temperature for 6 h. The product was separated from the mixtures by centrifugation, and the amounts of the adsorbed dodecylammonium ions and the desorbed K ions were determined on the basis of TG curve of the recovered solid and ICP-AES of the supernatant, respectively.

Photocatalysis

Photocatalytic conversions were carried out by photoirradiation with solar simulator (San-Ei Electric Co., Ltd) to a mixture of catalyst (60 mg), O_2-saturated acetonitrile (18 mL) solution of CH (2 mL) in a stainless-made closed container equipped with Pyrex glass (75 mL) under controlled atmosphere at 42 °C, with shaking (3-24 h). After analyzing gas phase, the irradiation was started. The container was placed by ca. 30 cm away from the light source to irradiate 1 solar (1000 W m^{-2})-power light to the mixture.

After the reaction, the gas-phase product was analyzed by GC-TCD (Shimazu GC-8A). The solution was mixed with naphthalene (as internal standard) and then recovered by filtration, and the resulting supernatant was analyzed by GC-FID (Shimazu GC-2014). The oxidation of 2-propanol in water was conducted in a way similar to that conducted for cyclohexane oxidation.

Preparation and evaluation of UV protective coatings.

Rhodamine 101 film was prepared by casting a portion (2 mL) of a mixture of the dye (10.2 mol L-1) and synthetic saponite (5.0 g L-1) in an aqueous ethanol (30 mL, 1/1 in v/v) onto a glass substrate (28 mm-width and 48 mm-length) followed by evaporation of the solvent. A solution of PCL (200 mg) in chloroform (10 mL) was mixed with MPTNF or P25 (20 mg for each sample) and a portion (1.0 mL) of the mixture was casted onto the Rhodamine 101 film. After the evaporation of the solvent, the coated film was irradiated by 1000 W m^{-2} power solar simulator ($\lambda > 300$ nm) at room temperature. Uncoated Rhodamine 101 film was also irradiated for comparison. The cast film of only MPTNF, P25 or $K_2Ti_2O_5$ embedded in PCL was also prepared on a quartz glass substrate to evaluate the transparency of the coating itself.

7-3. Results and discussion

7-3-1. Characterization of products

Potassium dititanate (named as $K_2Ti_2O_5$) has a plate-like morphology with a lateral size of a few μm and a thickness up to several hundreds of nm (Fig. 7-1 a and b) and is composed of corrugated layers that are comprised of a distorted TiO_5 trigonal bipyramid and the interlayer K ions,[14] giving a basal spacing (multilayer repeat distance) of 0.64 nm (Fig. 7-2 a). When the layered titanate was hydrothermally treated under an alkali condition in the presence of TPA hydroxide and NH_4F, which are often used in interzeolite conversion as a mineralizer and/or a structure-directing agent and a mineralizer, respectively, a product whose morphology and structure were different from those of $K_2Ti_2O_5$ was obtained. The product had a fibrous morphology with a diameter up to 10 nm and a length up to several hundreds of nm (so called "nanofiber") as can be seen in the SEM image and HRTEM image (Fig. 7-1 c and d), showed a XRD pattern almost completely different from that of the starting $K_2Ti_2O_5$ (Fig. 7-2 a) and exhibited abrupt N_2 uptake at lower partial pressure, which is indicative of the presence of micropores (a pore diameter < 2 nm) or microchannels, in the N_2 adsorption/desorption isotherms (Fig. 7-2 b). Careful HRTEM observations revealed that neither nanotube-like particles nor small platy particles like $K_2Ti_2O_5$ fragments observed in Fig. 7-1 a and b were not contained in the product at all, suggesting again that the product is microporous nanofibers derived from $K_2Ti_2O_5$.

EDX spectroscopy revealed the presence of O, K and Ti, and the absence of F in MPTNF (Fig. 7-1 e), indicating that F was not incorporated in the product, or NH_4F acted as a mineralizer in the formation of MPTNF (this point will be described in detail below). I could not rule out the possibility of the occurrence of the only trace amount of

F in MPTNF only from the EDX analysis; on the other hand, it is known that titania and titanate require substantial amounts of the incorporated F to slightly decrease the refractive indices[15] and then the amount of the incorporated F is negligible judging from the extremely low refractive index of MPTNF described below. The ICP-AES of the dissolved MPTNF determined the Ti and K contents (Ti, 42.1 wt%; K, 12.1 wt%). The TG-DTA curves of MPTNF did not show the weight loss due to the oxidative decomposition of TPA, confirming that TPA was not incorporated in the product; therefore, TPA hydroxide acted as a mineralizer rather than a structure directing agent (this point will be also described below). The TG-DTA curves also showed the weight loss (ca. 2.3 wt%) ascribable to the dehydration and condensation of the surface OH groups in a temperature range from 200 to 800 ºC. The infrared spectrum of MPTNF shown in Fig. 7-2 c confirmed the presence of isolated Ti-OH groups and hydrogen-bonded Ti-OH groups (peaks at 3721 and 3652 cm^{-1}, respectively). On the basis of Ti, K and OH contents, the chemical formula of MPTNF was calculated to be $H_{0.65}K_{0.75}Ti_{2.15}O_5$ (H exists as OH or partially H_2O; which will be described below).

I investigated the structure of MPTNF in more detail. When treated with an aqueous solution containing Ca ions, MPTNF adsorbed Ca ions accompanied by the desorption of K ions. As shown in Fig. 7-2 d, the adsorption isotherm revealed the H-type adsorption according to the Giles classification,[16] which indicates strong interactions between MPTNF and Ca, and Ca adsorption capacity of ~ 2.3 mmol g^{-1}, which was comparable to the cation exchange capacity (1.75 mmol g^{-1}) of MPTNF for divalent cations predicted on the basis of the K content. These results indicate that K ions are located on the surfaces of the micropores or microchannels as exchangeable cations. A part of protons of the surface Ti-OH groups is also cationexchangeable, judging from the fact that MPTNF could adsorb Ca ions more than the predicted cation exchange capacity. On the other hand, the adsorption of a cationic organic dye, crystal violet (CV; Fig. 7-2 d inset) with a molecular size of $1.4 \times 1.4 \times 0.4$ nm^3, from water on MPTNF was also the H-Type; however CV adsorbed considerably less effectively on MPTNF than Ca (Fig. 7-2 d), implying that CV could not penetrate effectively along a nanofiber axial direction due to diffusion limitation. It should be noted here that the XRD pattern of MPTNF did not change significantly (e.g. the diffraction peak corresponding to the d value of 0.83 nm did not shift to a lower 2θ region) after the cation exchange reactions (similar phenomenon was observed when K ions were almost quantitatively exchanged with dodecylammonium ions), supporting that MPTNF does not have a layered structure.[17] Horwarth-Kawazoe analysis,[18] which had successfully evaluated the microchannels (so called "tunnels" with a cross-section dimension of about 1.1×0.4 nm^2) of sepiolite that is a microfibrous silicate,[19] was applied to the treatment of the adsorption isotherms of Ar on MPTNF and the CV-exchanged MPTNF. From the analysis (Fig. 7-2 b inset), MPTNF possessed a pore size distribution showing an effective pore diameter of ca. 0.5 nm and adsorbed a significantly smaller amount of Ar atoms after cation exchange with CV ions, which was explained by the fact that CV molecules inside (mainly in the vicinity of the particle outer surface of) MPTNF prevented the entrance of Ar atoms.[19] Such significant decrease of Ar uptake must not be observed if MPTNF has randomly oriented micropores or microchannels perpendicular to or across a nanofiber axial direction and similar phenomena have been observed for sepiolite[19] and zeolites with threedimensional interconnecting microchannels.[20,21] Furthermore, as confirmed by the appearance of broad absorption at 3600- 3000 cm^{-1} in the infrared spectrum measured after evacuation at 200 ºC (Fig.

7-2 c), significant amount of H_2O molecules adsorbed inside MPTNF, not but on the particle outer surface (thus a part of the surface OH groups are H_2O) and such phenomena have also been reported for sepiolite and zeolites. From the all results and facts described above, I deduce that MPTNF has one-dimensional microchannels rather than micropores. From the high micro pore volume up to 0.08 cm^3 g^{-1} (see below), that is comparable to that of sepiolite,[19] MPTNF presumably has a number of microchannels in a particle like sepiolite or TON-type zeolites. The expanded HRTEM image presented in Fig. 7-1 d inset may show the edge of a MPTNF particle.

Besides its unique microstructure, MPTNF possessed i) a chemical stability toward water (acidic and basic solutions) and organic solvents, ii) an extraordinarily high cation exchange capacity (4.6 meq g^{-1} = 2 × 2.3 mmol g^{-1} for divalent cations) like a layered titanate, $H_2Ti_2O_5$, which is one of the most highcapacity (5.0 meq g^{-1}) cation exchangers among known materials but unstable in water[22] and iii) a fibrous morphology; therefore, it can be used as molecular sieve-like adsorbents, especially in chromatographic separations,[23] as well as UV absorbers.

I discussed the formation mechanism of MPTNF. After the hydrothermal reaction between $K_2Ti_2O_5$, TPA hydroxide, NH_4F and water, only dried gel-like product was recovered, and the product was washed with water to obtain MPTNF with a 76 % of yield on the basis of Ti content. On the other hand, the transparent eluate with water, which must contain 24 % of the added Ti, was also obtained. I thus thought that the eluate contained remnants of titania species (possibly “titania nanoparts”) which assembled into MPTNF. In the UV-vis spectrum of the eluate, a sharp absorption peak centered at 270 nm, which was not appeared in the UV-vis spectrum of MPTNF, was observed (Fig. 7-2 e). Zeolites or mesoporous silicas having isolated tetrahedral Ti species (highly dispersed titania species) show absorption at 220 nm in the UV-vis spectra.[24] While, in the UV-vis spectra for colloidal suspensions of titanate nanosheets derived from the exfoliation (delamination) of layered titanates, a well-developed absorption peak centered around 270 nm is often observed, which is explained by the presence of nanosheets with molecular-level thickness.[25,26] In the SEM image of the dried eluate, neither nanosheet-like particles derived from $K_2Ti_2O_5$ nor their ensembles were observed at all (only KOH particles with a size up to a few hundreds of nm were observed, although the corresponding SEM-EDX spectrum confirmed the presence of Ti, K and O). Also, in the XRD pattern of MPTNF, the (020) peak due to the diffraction within the titanate layers of $K_2Ti_2O_5$ was still observed (Fig. 7-2 a). XPS revealed that MPTNF had unique fivecoordinated Ti atoms like the starting $K_2Ti_2O_5$[8] although most titania and titanate, such as anatase and rutile (main components of a commercially available TiO_2, P25), had sixcoordinated ones (Fig. 7-2 f). Furthermore, the ESI-MS spectrometry, which had been applied to investigate speciation in silica and silicate solutions,[27,28] of the eluate showed the presence of a multitude of species up to approximately 400 Da (data not shown). Therefore, I thought that Ti species in the eluate were not Ti atoms derived from the complete dissolution of $K_2Ti_2O_5$, but “titania nanoparts” composed of TiO_5 trigonal bipyramid units (Fig. 7-2 a, inset), whose molecular weight is much smaller than that of the exfoliated $K_2Ti_2O_5$ single-layer nanosheet.

To understand the role of TPA and NH_4F in the formation of MPTNF, control hydrothermal reactions with or without the two compounds were conducted (Fig. 7-3). When neither TPA hydroxide nor NH_4F were added, split plate-like particles and bundled nanofibrous particles were predominantly obtained (Fig. 7-3 a) and they possessed a poor crystallinity (Fig. 7-3 b) and low mesopore (inter-particle pore) and micropore (intra-particle pore) volumes (Fig. 7-3 c). By adding either TPA or NH_4F, well defined nanofibrous products were obtained and they had a higher crystallinity than the product obtained in the absence of TPA and NH_4F; while, NH_4F gave a higher micropore volume product than did TPA. The addition of both TPA and NH_4F gave the best product (MPTNF) in terms of crystallinity and micropore volume, although the mesopore volume of MPTNF was similar to those for products obtained in the presence of TPA or NH_4F. From these results, both TPA and NH_4F promoted the decomposition of $K_2Ti_2O_5$ into titnia nanoparts and NH_4F acted as a mineralizer to promote the assembling of the obtained titania nanoparts into MPTNF more effectively than TPA did.

It is well-known that TiO_2 (anatase, rutile, brookite or amorphous phase) can transform into titania nanotube under alkaline hydrothermal conditions (without any organic ammoniums and fluorides), and it is generally agreed that titania nanotubes form through the dissolution and subsequent recrystallization of TiO_2 particulate precursor into single- or multi-walled nanosheets, which then scroll or wrap into nanotubes.[29] Under the similar hydrothermal conditions at higher temperature, non-porous titania nanofibers (or nanorods) have also been obtained.[29] Furthermore, it has been reported that $K_2Ti_2O_5$ transforms into anatase (or TiO_2 (B)) with a microfibrous morphology when treated with acid (cationexchanged with proton) and then heated.[30-32] The XRD pattern of the present MPTNF was not in agreement with those of such conventional titania and titanate materials. These facts support my hypothesis that MPTNF forms through a new route involving the formation and assembling of titania nanoparts.

To further demonstrate our hypothesis, other inorganics were hydrothermally treated under the identical condition. After the hydrothermal treatment of P25 (composed of anatase, rutile and amorphous titania[33]), the intensity of the XRD diffraction peaks due to anatase and rutile increased (Fig. 7-4 a) and smaller particles deposited on the original P25 particles (Fig. 7-4 b), which were explained by the fact that amorphous titania converted into anatase and rutile. On the other hand, after the hydrothermal treatment of a layered titanate with lepidocrocite structure, $K_{0.66}Ti_{1.73}Li_{0.27}O_4$ (Fig. 7-4 a inset),[34] anatase with a particle size less than 100 nm deposited on platy particles of the original titanate (Fig. 7-4 a and b). This resulted from that amorphous phase or lower crystallinity-$K_{0.66}Ti_{1.73}Li_{0.27}O_4$ converted into anatase. Furthermore, a layered niobate, $K_4Nb_6O_{17}{\cdot}3H_2O$,[35] converted into a product whose structure and morphology were different from those of the starting niobates, nanotubular niobate (data not shown). Therefore, as reported for interzeolite conversion,[36] the local structures of starting materials is a key for the present hydrothermal conversion; it is difficult for anatase, rutile and $K_{0.66}Ti_{1.73}Li_{0.27}O_4$, in which TiO_6 octahedra are strongly connected each other by both point and edge shearing (Fig. 7-4 a inset), to decompose into nanoparts under the present hydrothermal condition, on the other hand, $K_2Ti_2O_5$, amorphous titania (or lower crystallinity-$K_{0.66}Ti_{1.73}Li_{0.27}O_4$) and $K_4Nb_6O_{17}{\cdot}3H_2O$ possesses weakly connected TiO_5 trigonal bipyramids, TiO_6 and NbO_6 octahedra, respectively, each other only by point shearing and thereby can easily decompose into nanoparts. A wide variety of crystalline inorganics with different local structures is available and various hydrothermal conditions (higher temperature, stronger bases, structure directing agents, and so on) can be used; therefore, the presently proposed interzeolite conversion-inspired method seems versatile to design metal oxides nanostructured materials.

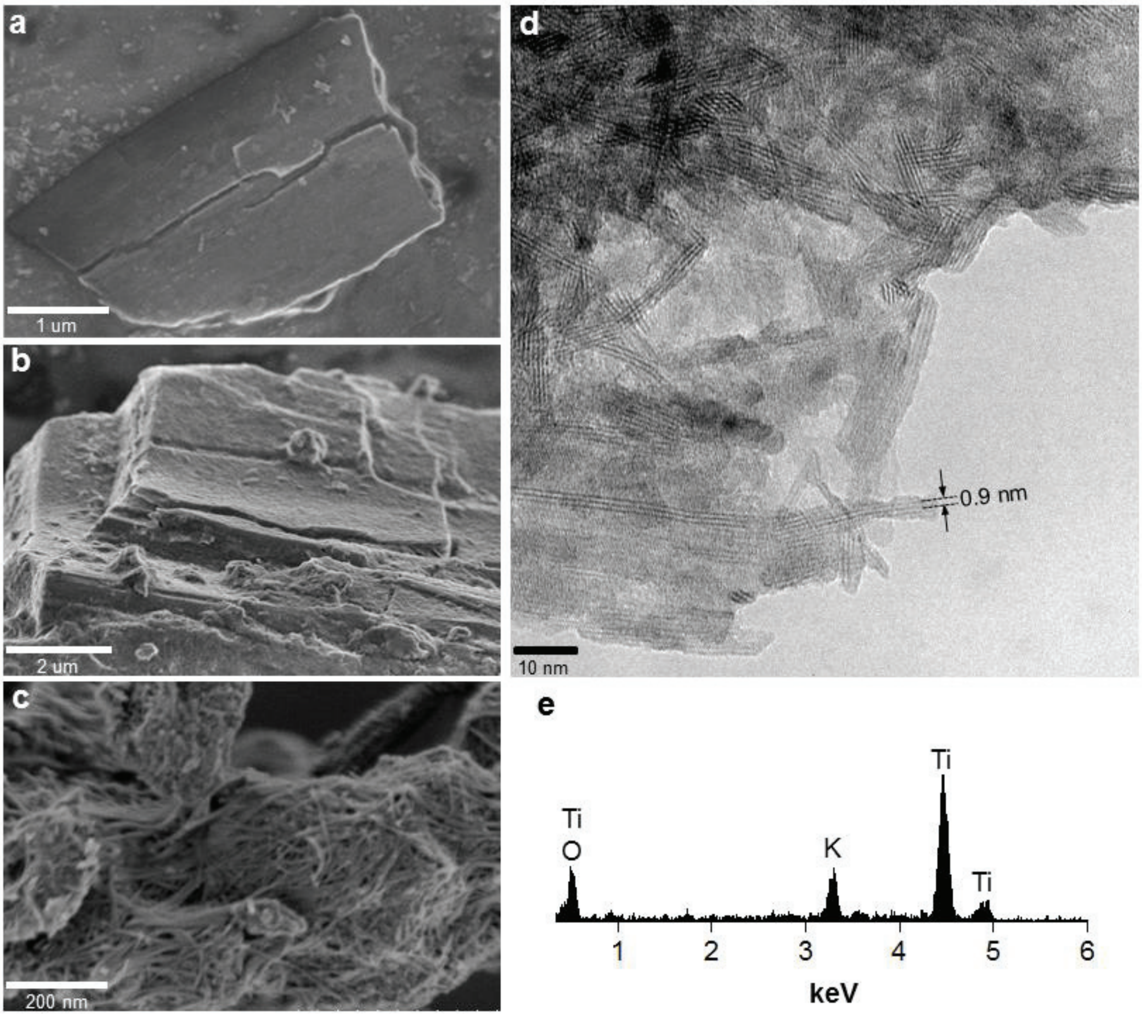

Fig. 7-1 (a) and (b) SEM images of $K_2Ti_2O_5$. (c) SEM image of MPTNF.

(d) and (e) HRTEM image and EDX spectrum of MPTNF, respectively.

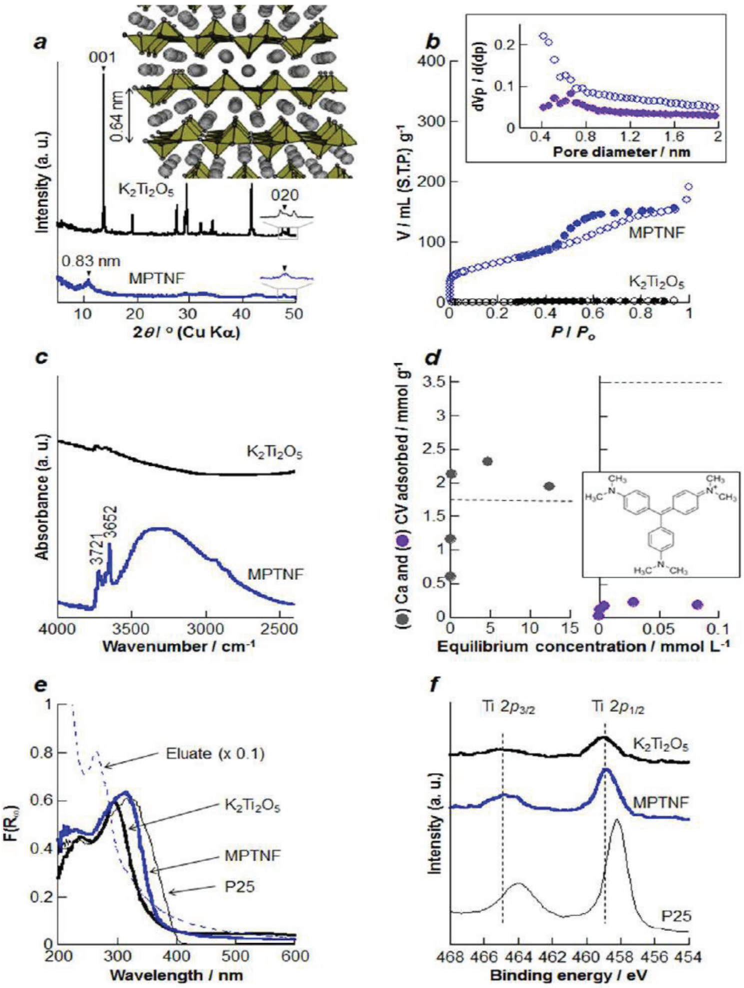

Fig. 7-2 (a) XRD patterns of $K_2Ti_2O_5$ and MPTNF. Inset shows the crystal structure of $K_2Ti_2O_5$. (b) N_2 adsorption (open circles)/desorption (filled circles) isotherms of $K_2Ti_2O_5$ and MPTNF. Inset shows the pore size distribution of MPTNF (top) and the CV-exchanged MPTNF (bottom) determined by adsorption isotherms of Ar. (c) IR spectra of $K_2Ti_2O_5$ and MPTNF. (d) Adsorption isotherms of Ca (left) and CV (right) from water on MPTNF. Horizontal dashed lines denote the cation exchange capacity of MPTNF based on the K content for divalent and monovalent cations, respectively. Inset shows the structure of CV. (e) Diffused reflectance UV-vis spectrum of $K_2Ti_2O_5$, MPTNF and P25. UV-vis absorption spectrum of an eluate obtained during MPTNF synthesis is also shown. (f) Ti 2p XPS results of $K_2Ti_2O_5$, MPTNF and P25.

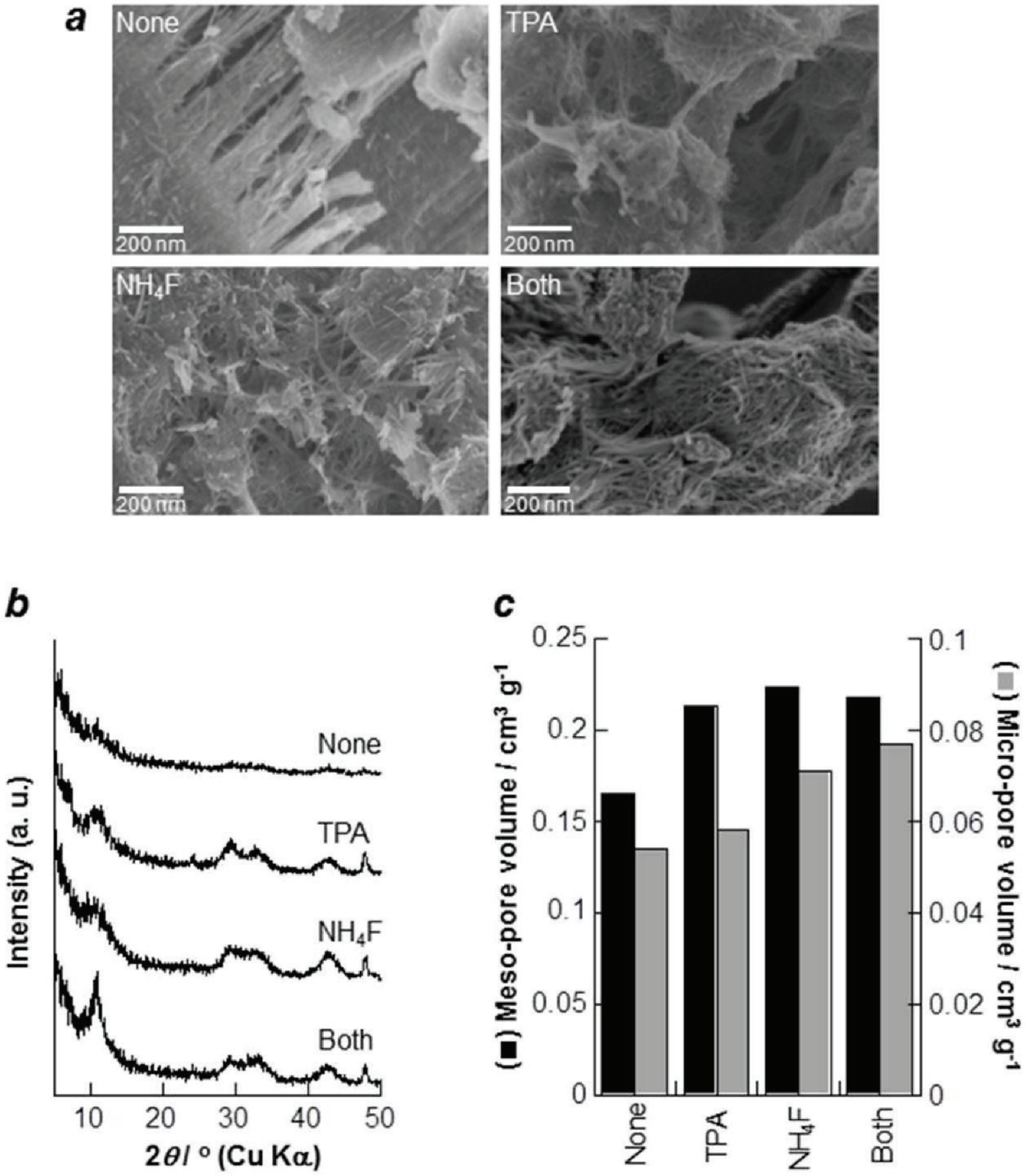

Fig. 7-3 (a) SEM images, (b) XRD patterns and (c) mesopore and micropore volumes, respectively, of hydrothermal products synthesized with and without TPA hydroxide and/or NH_4F. Mesopore and micropore volumes are determined by BJH method and from N_2 uptake at lower partial pressure, respectively.

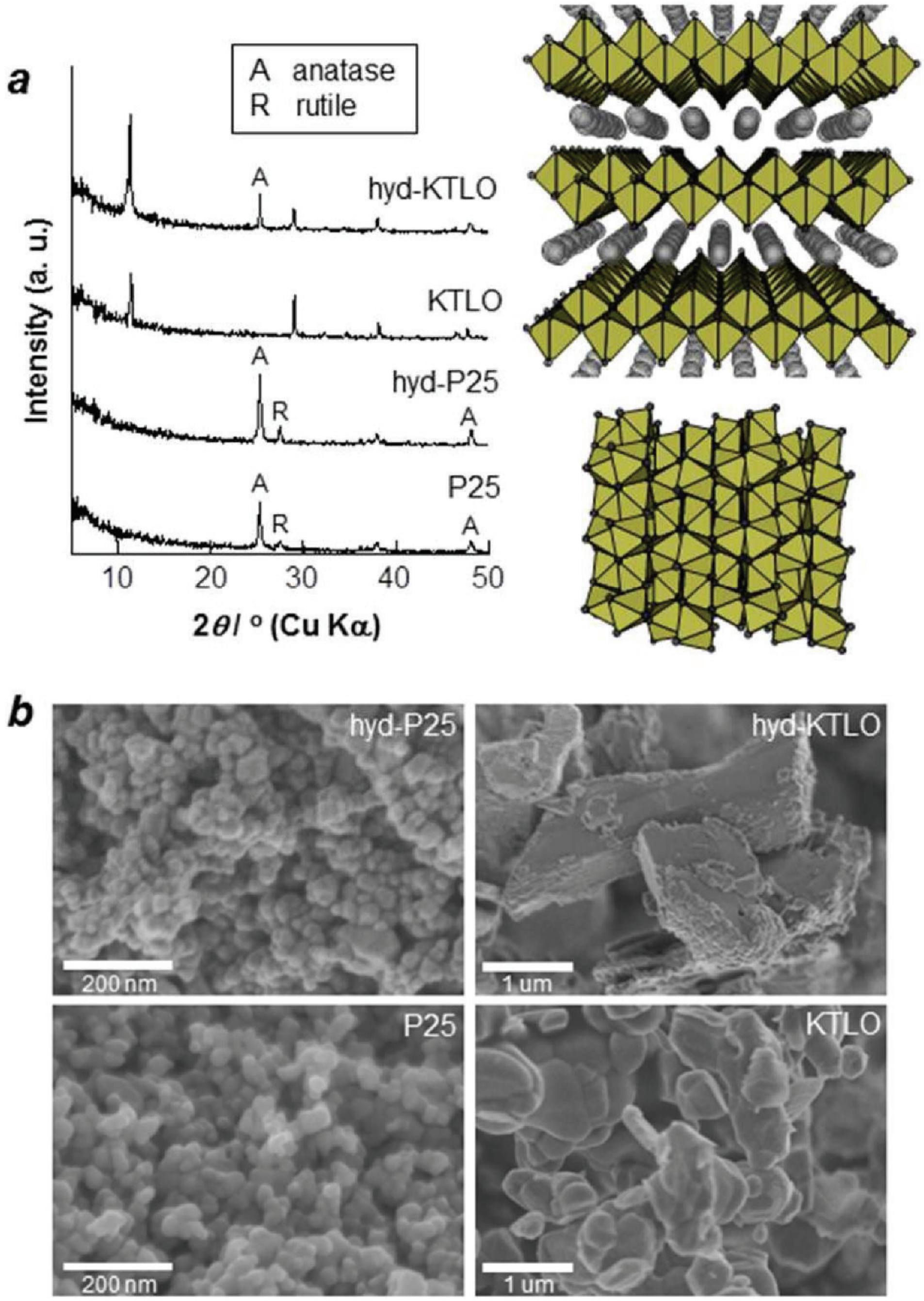

Fig. 7-4 (a) XRD patterns of P25 and $K_{0.66}Ti_{1.73}Li_{0.27}O_4$ (KTLO) and their hydrothermally treated products (hyd-P25 and hyd-KTLO, respectively). Inset show the crystal structures of rutile (bottom) and KTLO (top; grey spheres denote the interlayer K ions). (b) SEM images of P25, hyd-P25, KTLO and hyd-KTLO.

7-3-2. Evaluation of optical properties of MPTNF

I investigated the photoproperties of MPTNF. Fig. 7-2 e shows the UV-vis spectrum of MPTNF recorded in a diffused reflectance mode together with those of the starting $K_2Ti_2O_5$ and P25. The absorption onset (380 nm) of MPTNF was shifted to a longer wavelength region from that (345 nm) of $K_2Ti_2O_5$ (which is a merit of MPTNF as a UV absorber, because the most damaging natural UV radiation is between 290 nm and 350 nm[37]). It was noteworthy that MPTNF effectively absorbed UV like P25; therefore, we thought that analogous to P25 MPTNF showed a high photocatalytic activity when irradiated by UV. Fig. 7-5 a shows the time-course change in the yield of products during the irradiation of simulated solar light (λ > 320 nm) to cyclohexane (named as CH) in the presence of dissolved O_2 over P25 or MPTNF. With P25, cyclohexanone (named as CH-one) and cyclohexanol (named as CH-nol), and a considerably larger amount of CO_2 formed. This resulted from that cyclohexyl radical, formed by the reduction of CH with either the valence band hole of P25 or hydroxyl radical derived from the reduction of OH^- with the valence band hole, was oxidized by oxidizing species such as the hydroxy radical and the superoxide anion, which was generated by the reduction of O_2 with the conduction band electron, to give CH-one and CH-nol that were easily overoxidized into CO_2.[38] On the contrary, MPTNF hardly gave even CO_2 and the products yield on MPTNF was considerably smaller even than rutile (JRC-TIO-06), one of the most inactive titanias for photocatalytic oxidations[39-41] (Fig. 7-5 b). A similar tendency was observed for the photocatalytic oxidation of 2-propanol in water into acetone and CO_2 (Table 7-1). These results are worth mentioning as a merit of the present titanate, because the state-of-the-art titania nanostructures have exhibited higher photocatalytic activities than conventional titania (e.g. P25 with a surface area of ca. 50 m^2 g^{-1}) due to some factors such as enhanced surface area. For example, titania nanotubes after calcination, with a surface area of ~150 m^2 g^{-1}, are effective UV-induced photocatalysts for the oxidation of various organic compounds (even as-synthesized titania nanotubes show significant photocatalytic activities).[42] The surface area (BET specific surface area) of MPTNF is up to 240 m^2 g^{-1} (vs < 1 m^2 g^{-1} for $K_2Ti_2O_5$), which is superior or comparable if compared to those of the state-of-the-art titania nanostructures. One possible reason for the low photocatalytic activity of MPTNF is the low crystallinity (Fig. 7-2 a), since it is generally considered that titania with higher crystallinity (or lesser surface and bulk defects) shows higher photocatalytic activity for various reactions due to diminished electron-hole recombination rate.[43] Another possible reason is an inherent nature of $K_2Ti_2O_5$ nanoparts judging from the fact that the starting $K_2Ti_2O_5$ is almost inactive for the present photocatalytic reactions (Fig. 7-5 b).

Due to its well-restrained photocatalytic activity for the complete oxidation of organic compounds into CO_2, MPTNF can be used as photocatalysts for partial oxidations of organic substrates,[44,45] after appropriate modifications such as calcination and metals deposition[46] and as fillers for organic resins,[47] as well as UV absorbers.

Another noticeable photoproperty of MPTNF is the extremely low refractive index. I used immersion method to determine the refractive index of MPTNF; the titanate powder (or P25 powder for reference) was dispersed in organic solvents with different refractive indices and the refractive index of the titanate was estimated by the transparencies of the dispersions observed with the naked eyes (Fig. 7-6). P25 was opaque in the all solvents, which was explained by the fact that the refractive indices of anatase and rutile (2.53 and 2.71, respectively[47]) were much higher than those of organic solvents (as another possible reason, P25, whose primary particle size of 20-50 nm, aggregates in the solvents into larger-size particles to scatter visible light). However, MPTNF was almost transparent in diiodomethane having a refractive index of 1.74 (by "refractive index matching"), giving the estimated refractive index of 1.7. This value was considerably lower than those (2.4 ~ 2.7)[48] of conventional TiO_2. It has been established that the refractive indices (n) and density (d) of crystalline compounds obey the relationship, $(n-1)/d$ = constant,[49] and this formula has been found to work well for TiO_2.[44] Therefore, one plausible reason for such low refractive index of MPTNF is the low density due to the highly porous structure. MPTNF may also aggregate in organic solvents; however, the presence of mesopores between each nanofibrous particle may play a role in the lowering of the refractive index of the aggregate.

Thanks to the unique photoproperties described above, MPTNF was successfully used as a UV absorber embedded in a commodity organic polymer, polycaprolactone (named as PCL). In order to evaluate the UV protection ability of MPTNF, a highly UVsensitive organic dye (Rhodamine 101) film and the same coated with PCL (having a refractive index of 1.53) in which MPTNF or P25 was embedded were irradiated by intense UV light ($\lambda > 300$ nm). The photodegradation of uncoated and coated Rhodamine 101 films was measured by monitoring their absorbance at 540 nm as a function of the irradiation time. As can be seen in Fig. 7-6 a, MPTNF was successfully embedded in PCL to form a highly transparent film as a result of a small difference between refractive indices of MPTNF and PCL. When irradiated by UV light, Rhodamine 101 sample coated with the MPTNF film showed a substantial reduction of the photodegradation of the organic dye, being approximately 30 times slower than the uncoated sample (estimated by the initial slopes of Fig. 7-6 b inset). On the contrary, P25, which has a much higher refractive index than that of PCL and a high photocatalytic activity, whitened the PCL matrix (Fig. 7-6 a) and degraded the matrix and/or the organic dye immediately after the irradiation (Fig. 7-6 b). $K_2Ti_2O_5$ could not be embedded homogeneously in PCL to form the whitened film (Fig. 7-6 a), because the layered titanate did not swell or exfoliate (disperse at a nanometer level) in PCL and presumably had much higher refractive index[50] than PCL. All above results indicate that the presently developed MPTNF has the high potential for versatile and reliable UV-protecting materials. So far, titania has been widely applied in sunscreen products (mainly as UV blocking materials, not but UV absorbing ones). However, for such applications, titania is often required to restrain the high photocatalytic activity by the appropriate surface modification. Also, due to its high refractive index, titania loses transparency in the visible region, limiting the usage in applications requiring high transparency, such as optical devices, seriously.

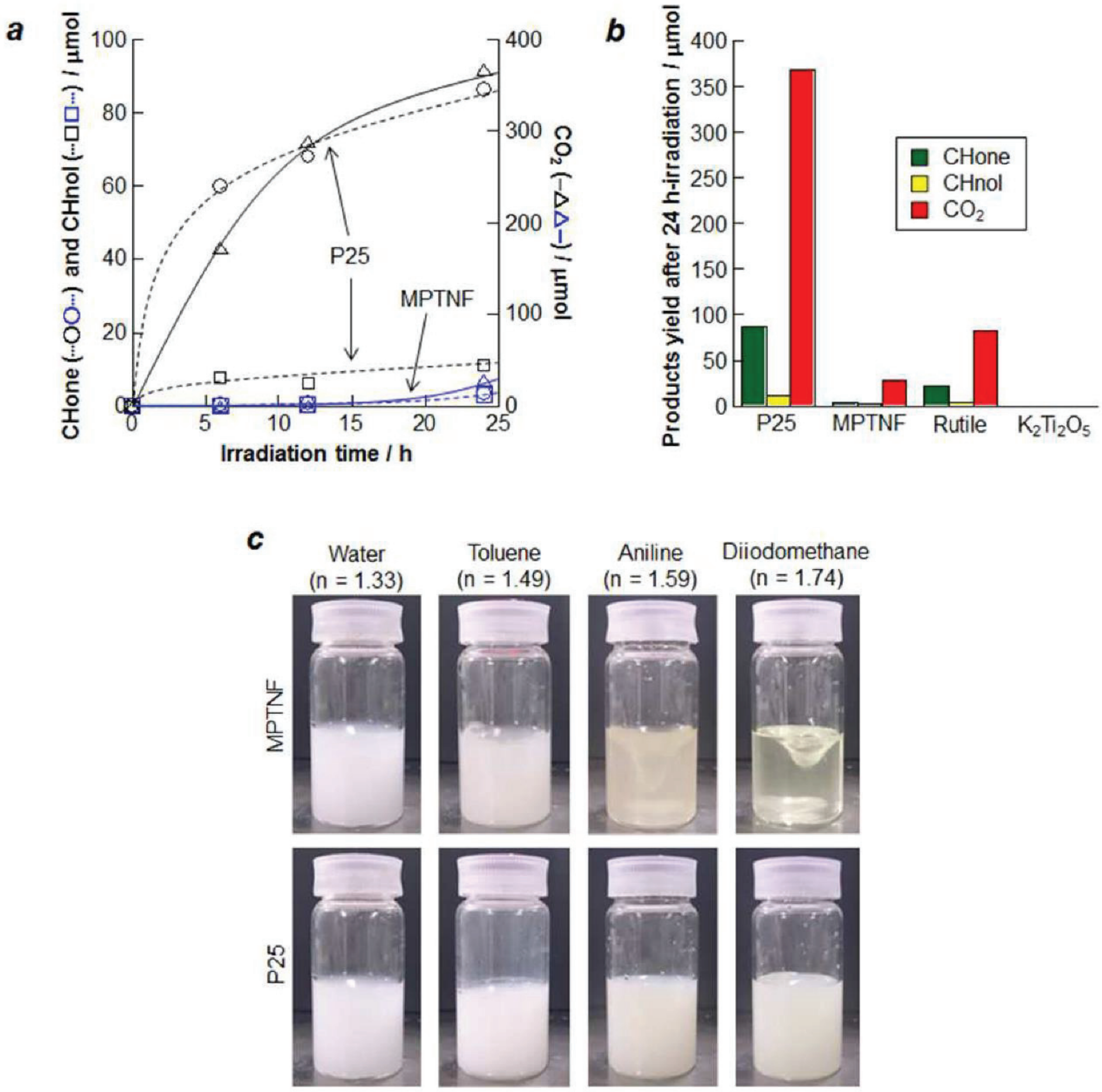

Fig. 7-5 (a) Time-course curves of photocatalytic oxidations of cyclohexane (CH) to cyclohexanone (CHone), cyclohexanol (CHnol) and CO_2 over P25 and MPTNF under simulated solar light irradiation ($\lambda > 320$ nm). (b) Yields of CHone, CHnol and CO_2 over P25, MPTNF, rutile and $K_2Ti_2O_5$ after the irradiation for 24 h. (c) Immersion tests to estimate the refractive index of MPTNF. 10 mg of powder samples are dispersed in 10 mL of organic solvents.

Table 7-1 2-Propanol oxidation on KTO MCNF and P25 under solar simulator irradiation for 24 h.

Catalyst	Yield / μmol		Select.[a] / %
	Acetone	CO_2	
P25	602.2	147.6	92.4
KTO MCNF	38.5	26.7	81.2

[a] Select. = [formed acetone] / {[formed acetone] + [(formed CO_2) / 3]} ×100.

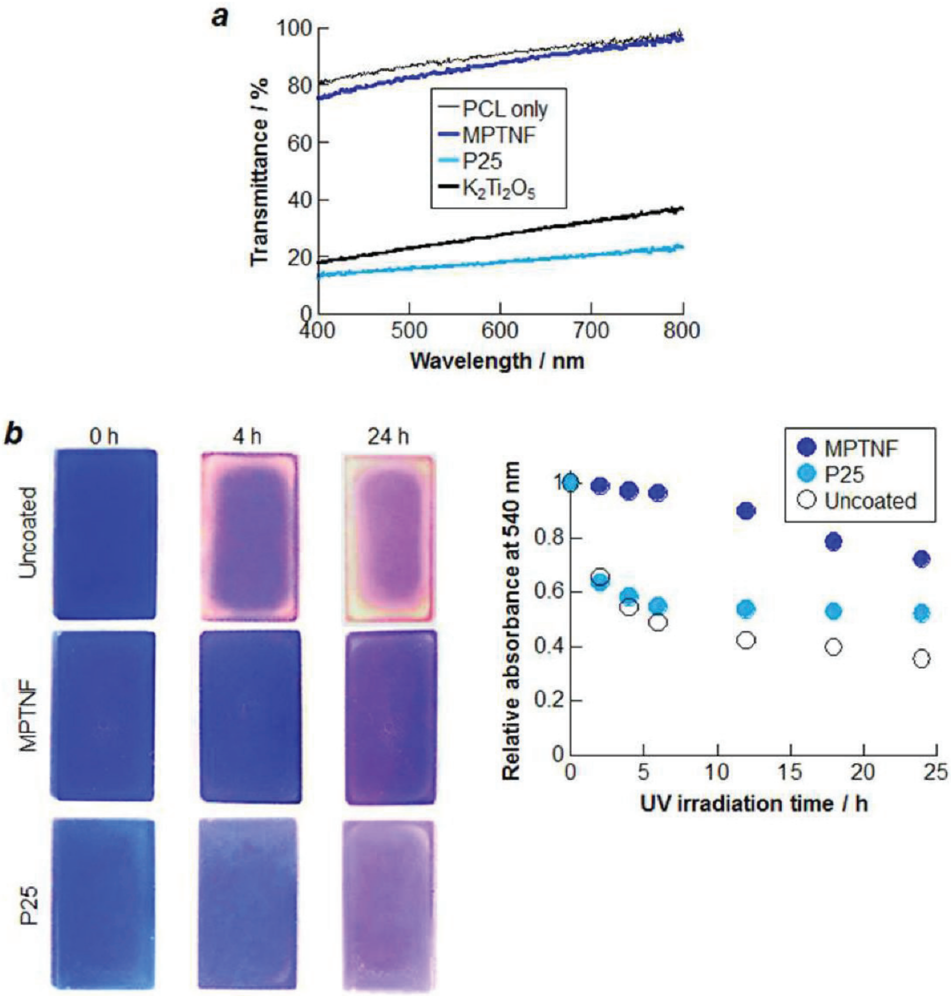

Fig. 7-6(a) UV-vis transmittance spectra of films of PCL and those containing MPTNF, P25 or $K_2Ti_2O_5$. (b) Pictures showing Rhodamine 101 films uncoated and coated with MPTNF and P25 embedded in PCL before and after UV irradiation ($\lambda >$ 300 nm). Inset shows time-course curves of the UV-induced photodegradation of the uncoated and coated Rhodamine 101 films.

7-4. Conclusion

I have reported that a layered titanate $K_2Ti_2O_5$ successfully converts into a new titanate nanostructured material, a microporous titanate nanofiber having possible onedimensional multi-microchannels, via interzeolite conversion method. [51] The new material exhibited a well-restrained photocatalytic activity and extremely low refractive index, which allowed us to create a highly efficient UV protective transparent coating on a UV-sensitive substrate. A wide variety of precursors (e.g. layered and microporous titanates[52]) with different compositions and local structures are available; therefore, the present synthetic strategy will make titania nanostructured materials’ design much more attractive and versatile.

7-5. References

[1] J. Keck, M. Roessler, C. Schroeder, G. J. Stueber, F. Waiblinger, M. Stein, D. LeGourriérec, H. E. Kramer, H. Hoier, S. Henkel, P. Fischer, H. Port, T. Hirsch, G. Rytz and P. Hayoz, *J. Phys. Chem. B*, **1998**, *102*, 6975.

[2] M. Zayat, P. Garcia-Parejo and D. Levy, *Chem. Soc. Rev.*, **2007**, *36*, 1270.

[3] P. Garcia-Parejo, M. Zayat and D. Levy, *J. Mater. Chem.*, **2006**, *16*, 2165.

[4] X. Chen and S. S. Mao, *Chem. Rev.*, **2007**, *107*, 2891.

[5] A. Demourgues, N. Penin, E. Durand, F. Weill, D. Dambournet, N. Viadere and A. Tressaud, *Chem. Mater.*, **2009**, *21*, 1275.

[6] H. Cui, M. Zayat, P. Garcia and D. Levy, *Adv. Mater.*, **2008**, *20*, 65.

[7] B. Subotić, D. Škrtić and I. Šmit, *J. Cryst. Growth*, **1980**, *50*, 498.

[8] H. Jon, N. Ikawa, Y. Oumi and T. Sano, *Chem. Mater.*, **2008**, *20*, 4135.

[9] K. Honda, M. Itakura, Y. Matsuura, A. Onda, Y. Ide, M. Sadakane and T. Sano, *J. Nanosci. Nanotechnol.*, **2013**, *13*, 3020.

[10] S. Andersson and A. D. Wadsley, *Nature*, **1960**, *187*, 499.

[11] T. Okada, Y. Ide and M. Ogawa, *Chem. Asian J.*, **2012**, *7*, 1980.

[12] F. Fan, Z. Feng and C. Li, *Acc. Chem. Res.*, **2010**, *43*, 378.

[13] T. Sasaki and M. Watanabe, *J. Phys. Chem. B*, **1997**, *101*, 10159.

[14] S. Andersson and A. D. Wadsley, *Nature*, **1960**, *187*, 499.

[15] X. Rocquefelte, F. Goubin, Y. Montardi, N. Viadere, A. Demourgues, A. Tressaud, M.-H. Whangbo and S. Jobic, *Inorg. Chem.*, **2005**, *44*, 3589.

[16] C. H. Giles, T. H. Macewan, S. N. Nakhwa and D. Smith, *J. Chem. Soc.*, **1960**, 3973.

[17] T. Okada, Y. Ide and M. Ogawa, *Chem. Asian J.*, **2012**, *7*, 1980.

[18] G. Horvath and K. Kawazoe, *J. Chem. Eng. Jpn.*, **1983**, *16*, 470.

[19] E. Ruiz-Hitzky, *J. Mater. Chem.*, **2001**, *11*, 86.

[20] T. Takaishi, Y. Yatsurugi, A. Yusa and T. Kuratomi, *J. Chem. Soc. Faraday Trans. 1*, **1975**, *71*, 97.

[21] M. Niwa, S. Kato, T. Hattori and Y. Murakami, *J. Chem. Soc. Faraday Trans. 1*, **1984**, *80*, 3135.

[22] Y. Fujiki, Y. Komatsu, T. Sasaki and N. Ohta, *Nippon Kagaku Kaishi*, **1981**, *10*, 1656.

[23] T. Sasaki, Y. Komatsu and Y. Fujiki, *J. Radioanal. Nucl. Chem. Lett.*, **1986**, *107*, 111.

[24] F. Fan, Z. Feng and C. Li, *Acc. Chem. Res.*, **2010**, *43*, 378.

[25] T. Sasaki and M. Watanabe, *J. Phys. Chem. B*, **1997**, *101*, 10159.

[26] Y. Ide and M. Ogawa, *Chem. Commun.*, **2003**, 1262.

[27] S. A. Pelster, F. Schüth and W. Schrader, *Anal. Chem.*, **2007**, *79*, 6005.

[28] B. B. Schaack, W. Schrader and F. Schüth, *Angew. Chem. Int. Ed.*, **2008**, *47*, 9092.

[29] D. V. Bavykin, J. M. Friedrich and F. C. Walsh, *Adv. Mater.*, **2006**, *18*, 2907.

[30] M. He, X.-H. Lu, X. Feng, L. Yu and Z.-H. Yang, *Chem. Commun.*, **2004**, 2202.

[31] W. Li, C. Liu, Y. Zhou, Y. Bai, X. Feng, Z. Yang, L. Lu, X. Lu and K.-Y. Chan, *J. Phys. Chem. C*, **2008**, *112*, 20539.

[32] W. Li, Y. Bai, W. Liu, C. Liu, Z. Yang, X. Feng, X. Lu and K.-Y. Chan, *J. Mater. Chem.*, **2011**, *21*, 6718.

[33] T. Ohno, K. Sarukawa, K. Tokieda and M. Matsumura, *J. Catal.*, **2011**, *203*, 82.

[34] Y. Fuse, Y. Ide and M. Ogawa, *Bull. Chem. Soc. Jpn.*, **2008**, *81*, 767.

[35] M. Gasperin and M.-T. le Bihan, *J. Solid State Chem.*, **1980**, *33*, 83.

[36] K. Honda, M. Itakura, Y. Matsuura, A. Onda, Y. Ide, M. Sadakane and T. Sano, *J. Nanosci. Nanotechnol.*, **2013**, *13*, 3020.

[37] J. Pospíšil and S. Nešpurek, *Prog. Polym. Sci.*, **2000**, *25*, 1261.

[38] C. B. Almquist and P. Biswas, *Appl. Catal. A*, **2001**, *214*, 259.

[39] B. Ohtani, O. O. Prieto-Mahaney, D. Li and R. Abe, *J. Photochem. Photobiol. A*, **2010**, *216*, 179.

[40] D. Tsukamoto, Y. Shiraishi, Y. Sugano, S. Ichikawa, S. Tanaka and T. Hirai, *J. Am. Chem. Soc.*, **2012**, *134*, 6309.

[41] Y. Ide, H. Hattori and T. Sano, *Phys. Chem. Chem. Phys.*, **2014**, *16*, 7913.

[42] J. Suetake, A. Y. Nosaka, K. Hodouchi, H. Matsubara and Y. Nosaka, *J. Phys. Chem. C*, **2008**, *112*, 18474.

[43] H. Kominami, S. Murakami, J. Kato, Y. Kera and B. Ohtani, *J. Phys. Chem. B,* **2002**, *106*, 10501.

[44] Y. Shiraishi, N. Saito and T. Hirai, *J. Am. Chem. Soc.*, **2005**, *127*, 12820.

[45] Y. Ide, M. Torii and T. Sano, *J. Am. Chem. Soc.*, **2013**, *135*, 11784.

[46] Y. Ide, N. Kawamoto, Y. Bando, H. Hattori, M. Sadakane and T. Sano, *Chem. Commun.*, **2013**, *49*, 3652.

[47] Y. Fuse, Y. Ide and M. Ogawa, *Polym. Chem.*, **2010**, *1*, 849.

[48] X. Rocquefelte, F. Goubin, H.-J. Koo, M.-H. Whangbo and S. Jobic, *Inorg. Chem.*, **2004**, *43*, 2246.

[49] H. W. Jaffe, *Am. Mineral.*, **1956**, *41*, 757.

[50] T. Sasaki, Y. Ebina, T. Tanaka, M. Harada, M. Watanabe and G. Decher, *Chem. Mater.*, **2001**, *13*, 4661.

[51] H. Hattori, Y. Ide and T. Sano, *J. Mater. Chem. A,* **2014**, *2*, 16381.

[52] Y. Ide, M. Sadakane, T. Sano and M. Ogawa, *J. Nanosci. Nanotechnol.*, **2014**, *14*, 2135.

Chapter 8

Summery

Chapter 1 is an overview of the entire research. First, the fundamentals of the material focused in this research, TiO_2, was described, especially the short history of photocatalyst and the photocatalytic activity of TiO_2 based catalyst, which are the main features in the thesis. Also, another interest of this research, the UV blocking, was simply reviewed to understand the expected applications of the developed materials.

In chapters 2 and 3, I reported that efficient and/or selective photocatalytic reactions proceed even when using inexpensive catalysts by controlling the reaction environment. Highly efficient and selective sunlight-induced photocatalytic oxidation of cyclohexane on TiO_2 based photocatalyst proceeded under a CO_2 atmosphere. In addition to versatility, this method is also attractive in view of CO_2 reduction and storage. Because it does not require any special equipment, it can be expected as a general-purpose method that can synthesize basic chemicals at low cost and low environmental load. Furthermore, when decomposition of cationic organic dyes in water under sunlight irradiation was conducted under an Ar atmosphere even using pure titanium oxide, it was found that the photocatalytic activity was remarkably improved. Ar is an inert gas widely used in the industry. I anticipate that many known photocatalytic processes are investigated under an Ar atmosphere to improve their photocatalytic activities and fully understand the reaction mechanisms.

In chapters 4 and 5, I investigated design of TiO_2-based photocatalysts by the appropriate surface modification. TiO_2 ternary-modified with Fe^{3+}, Ni^{2+}, and Au nanoparticles exhibited an unprecedentedly high photocatalytic efficiency for selective cyclohexane oxidation under sunlight irradiation. The layered titanate containing immobilized molecular level iron oxide in the interlayer space was found to effectively and selectively catalyze the oxidation of cyclohexane to cyclohexanone and cyclohexanol with molecular O_2 under sunlight irradiation. The photocatalytic activity was also substantially modified by conducting the reaction under a CO_2 atmosphere. These findings strongly indicate that nanostructure design of the hybrid photocatalyst opens up new opportunities for the production of various commodity chemicals in an economically and environmentally favorable fashion.

In chapter 6, I found the positive effects of particle-level mixing of a layered titanate (HTO) and a much smaller amount (~10 wt.%) of various additives, including Pt or Au-loaded TiO_2 (P25), on the photocatalytic activity of the mixtures for the oxidation of formic acid in water under solar light irradiation. The mixture of HTO with Au-loaded P25 showed the best activity, which was 8 times higher than that of P25, a benchmark photocatalyst, and comparable to that of pure Au-loaded P25 (Au loading of 2.0 wt.%), using the same amount of powder. I thus attained largely enhanced activity despite the use of an unusually small amount (0.27 wt.%) of the noble metal. Since a wide variety of advanced TiO_2 materials, including those with precious metal co-catalysts, are available, their use as additives in conventional photocatalytic systems is underway in our laboratory.

In chapter 7, by applying the method used for the synthesis of zeolite to the preparation of titanium oxide type material, I succeeded in synthesizing a new type TiO_2 -based material. A layered titanate $K_2Ti_2O_5$ successfully converted into a new titanate nanostructured material, a microporous titanate nanofiber (MPTNF) having possible onedimensional multi-microchannels. The new material MPTNF exhibited little photocatalytic activity and its refractive index was remarkably small as compared with the conventional titanium oxide based material. By using these remarkable optical properties, MPTNF was efficiently functioned as an ultraviolet light absorbing transparent coating material by dispersing it in a versatile organic polymer.

The results and knowledge of the main features investigated in this thesis will be of use in developing future new photocatalysts and their use in various applications.

List of publications

1. Y. Ide, H. Hattori, M. Sadakane and T. Sano, "Highly efficient and selective sunlight-induced photocatalytic oxidation of cyclohexane on an eco-catalyst under a CO_2 atmosphere"*Green Chem*., **2012**, *14*, 1264.
2. H. Hattori, Y. Ide, S. Ogo, K. Inumaru, M. Sadakane and T. Sano, "Efficient and selective photocatalytic cyclohexane oxidation on a layered titanate modified with iron oxide under sunlight and CO_2 atmosphere", *ACS Catal*., **2012**, *2*, 1910.
3. Y. Ide, N. Kawamoto, Y. Bando, H. Hattori, M. Sadakane and T. Sano, "Ternary modified TiO_2 as simple and efficient photocatalyst for green organic synthesis"*, Chem. Commun.*, **2013**, *49*, 3652.
4. Y. Ide, H. Hattori and T. Sano, "Extraordinary effects of argon atmosphere on TiO_2 photocatalysis", *Phys. Chem. Chem. Phys*., **2014**, *16*, 7913.
5. H. Hattori, Y. Ide and T. Sano, "Microporous titanate nanofibers for highly efficient UV-protective transparent coating", *J. Mater. Chem. A,* **2014**, *2*, 16381.
6. Y. Ide, N. Inami, H. Hattori, K. Saito, M. Sohmiya, N. Tsunoji, K. Komaguchi, T. Sano, Y. Bando, D. Golberg and Y. Sugahara, "Remarkable charge separation and photocatalytic efficiency enhancement through interconnection of TiO_2 nanoparticles by hydrothermal treatment", *Angew. Chem. Int. Ed.*, **2016**, *55*, 3600.
7. H. Hattori, M. Eguchi, Y. Ide and T. Sano, "Enhanced photocatalytic activity of a layered titanate achieved via simple mixing with TiO_2-based photocatalysts as additives", *Bull. Chem. Soc. Jpn.*, **2017**, *90*, 1276.

Acknowledgements

I would like to express my gratitude to all people who have helped me with the preparation of this doctoral thesis. Especially, I am deeply thanked to my supervisor Prof. Dr. Tsuneji Sano for his advice, support, helpful suggestions and continuous encouragement. Without his patient guidance, it is almost impossible to finish my study. I also grateful acknowledge Mr. Yusuke Ide (MANA, NIMS) for teaching me experiments and consideration of experiment results.

I am grateful to all of the members in Cataler for their understanding and cooperation to my work.

Finally, I wish to thank my parents for their understanding and support.

September 2018

Hideya Hattori